

E-16-637

**SYNERGISTIC EFFECTS AND DEFLAGRATION ANALYSIS IN COMPOSITE  
SOLID PROPELLANT COMBUSTION**

**W. C. Strahle  
J. C. Handley**

**November 1, 1975**

**FINAL REPORT – RESEARCH SPONSORED BY  
THE OFFICE OF NAVAL RESEARCH**

**ONR Contract No. N00014-75-C-0332**

**Approved for Public Release; Distribution Unlimited**

**Reproduction in whole or in part is permitted for any  
purpose of the United States Government**

Synergistic Effects and Deflagration Analysis in Composite  
Solid Propellant Combustion

W. C. Strahle

J. C. Handley

November 1, 1975

Final Report - Research Sponsored by  
The Office of Naval Research

ONR Contract No. N00014-75-C-0332

Approved for Public Release; Distribution Unlimited

Reproduction in whole or in part is permitted for any  
purpose of the United States Government

ABSTRACT

Using four common catalysts the existence and magnitude of synergistic effects upon burn rate are studied with HTPB-AP composite solid propellants. The effect under study is one whereby at a fixed total catalyst loading the mixture of two catalysts would be more effective in burn rate augmentation than a single catalyst. At 2000 psia all possible combinations of catalysts showed synergistic effects but the effects are weak and within the reproducibility range of the experiments. Ferric oxide and iron blue showed synergistic effects only at 300 and 2000 psia over the pressure range 300-2000 psia.

Analysis of the effect of binder-oxidizer reactions upon the surface shape of a two-dimensional sandwich has shown that a) the faster are these reactions the more deeply will the sandwich obtain a V-shape and b) these reactions are generally fast enough to indeed affect the surface shape.

## TABLE OF CONTENTS

	Page
Abstract	i
Chapters	
Introduction	1
Fuse Wire Tests	5
Cinephotomacrography	6
Catalyst Loaded into the AP	13
Analysis	15
Conclusions	16
References	17

Appendix A - Solid Propellant Sandwich Deflagration Analysis  
with Binder-Oxidizer Reactions

## INTRODUCTION

The current investigation represents a continuation of the work initiated at the Georgia Institute of Technology, which has been presented in References 1 and 2. In these investigations two-dimensional composite solid propellant sandwiches of polycrystalline ammonium perchlorate (AP) oxidizer and hydroxyl terminated polybutadine (HTPB) binder were used to investigate various modes of catalytic behavior. Four proven burn rate modifiers which behave as catalysts have been used throughout these ongoing investigations. They are Harshaw Catalyst Cu 0202 P, ferric oxide, iron blue and ferrocene.

During the first phase of this investigation<sup>(1)</sup> the catalysts were loaded into either the oxidizer or binder or restricted to the binder-oxidizer interface of two-dimensional sandwiches. Vertical sandwich burn rates and oxidizer normal regression rates were obtained using cinephotomacrography techniques. Details of the surface structure were obtained by using the scanning electron microscope to observe partially burned samples. It was determined that if one effective catalyst was added to the oxidizer and another to the binder, there was a net increase of burn rate over that of the sum of the independent actions of the catalysts. This combined effect was denoted as a positive synergistic effect on sample burn rate. The existence of this synergistic effect for the four catalysts was systematically investigated<sup>(2)</sup> using the two-dimensional sandwiches. The Harshaw catalyst Cu 0202 P - ferric oxide system, Fig. 1, and iron blue-ferric oxide system, Fig. 2, were found to exhibit a positive synergistic effect over the entire pressure range, 600 to 2000 psia and the maximum synergistic effect at 600 psia, respectively. The burn rate ratio on Figs. 1 and 2 is the ratio of the burn rate of the catalyzed sample to the burn rate of a pure AP-HTPB sample.

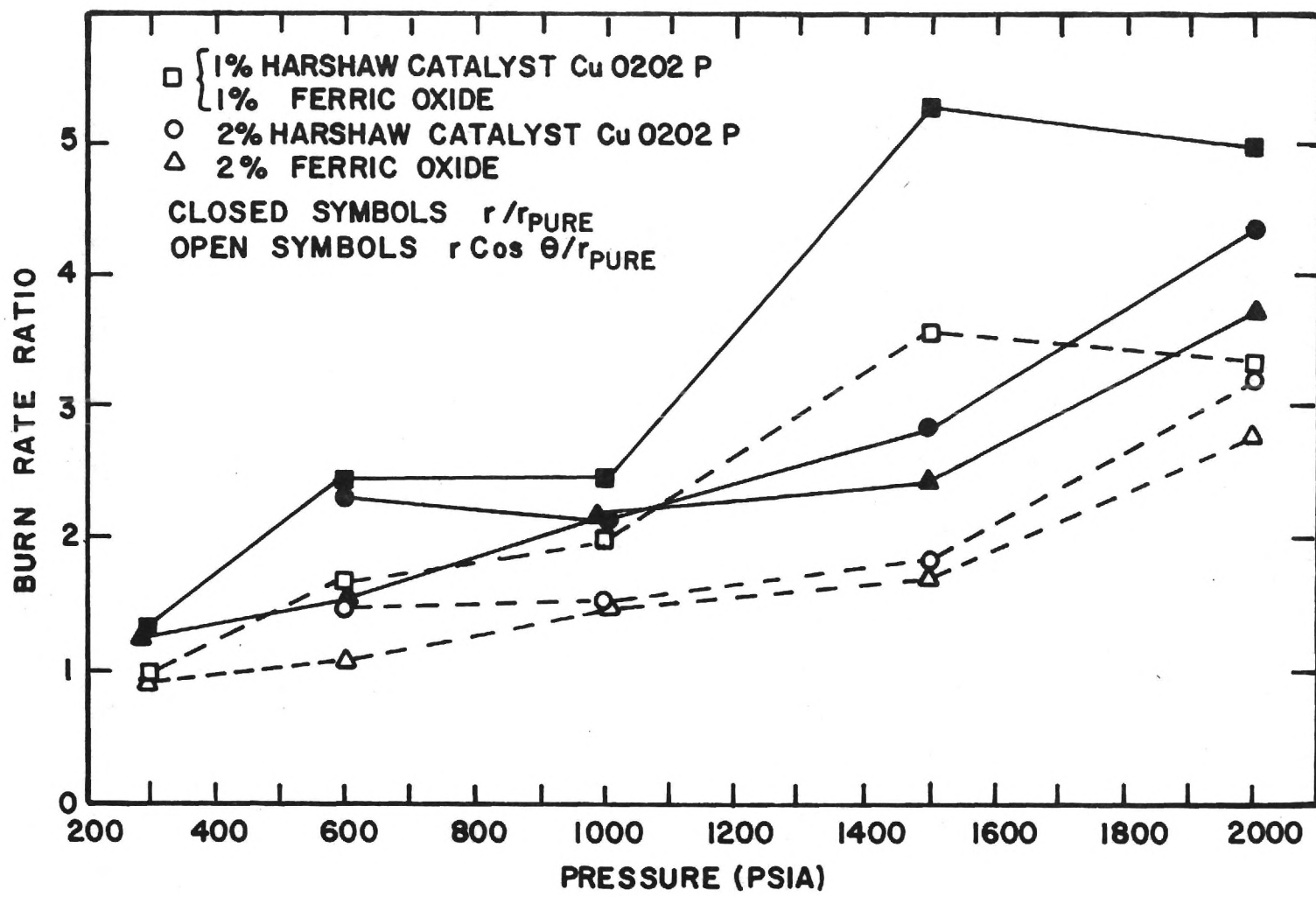


Figure 1. Synergistic Effect on Sandwich Vertical Burn Rate for Harshaw Catalyst Cu 0202 P and Ferric Oxide.

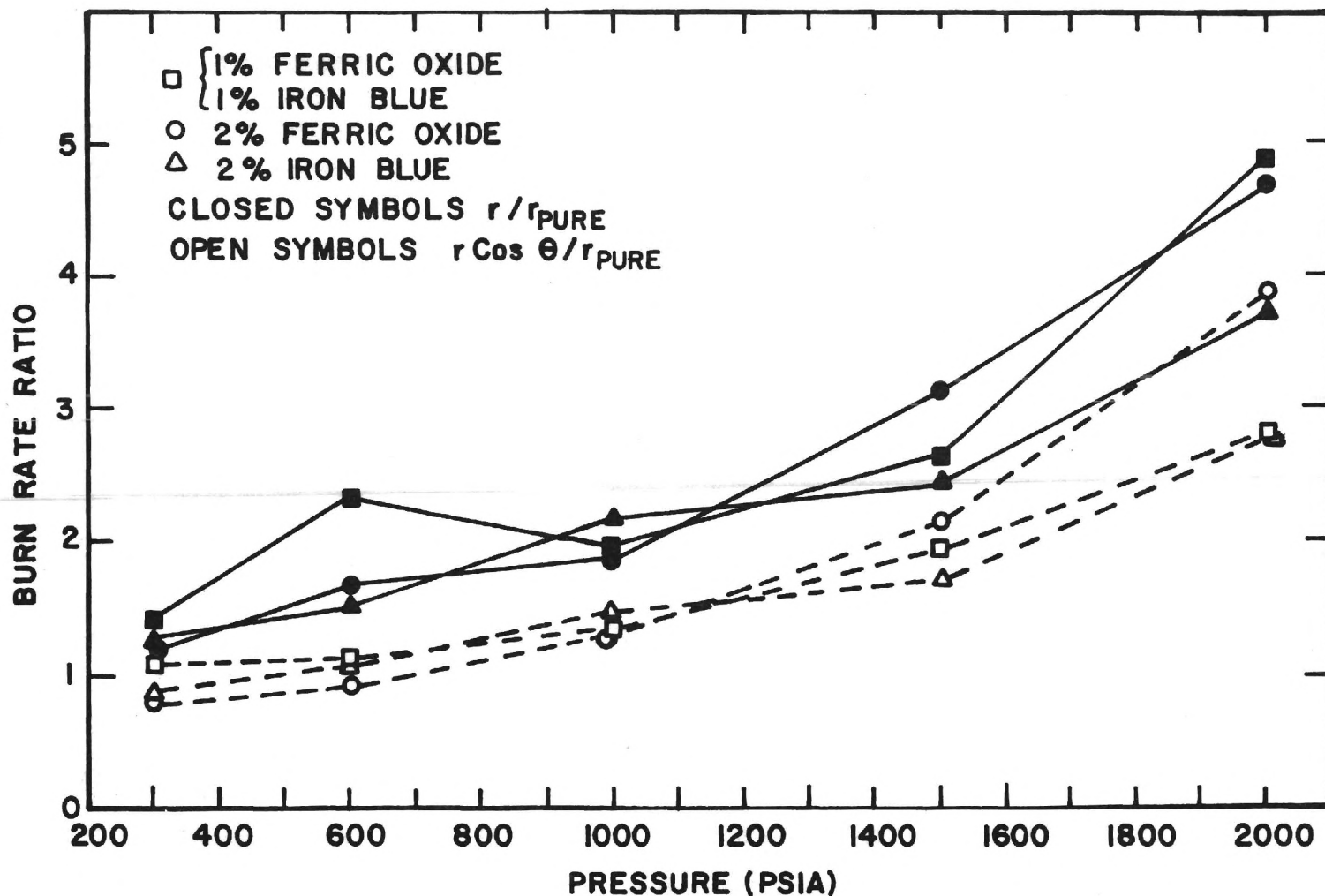


Figure 2. Synergistic Effect on Sandwich Vertical  
Burn Rate for Ferric Oxide and Iron Blue.

These two systems were chosen for further testing in cast propellant configurations. The initial samples were prepared with the same volumetric loading as in the sandwiches. The strands were prepared from a common lot of uncured composite propellant with an 82.7% solids to 17.3% binder loading. The oxidizer particle distribution was:

$$180 \mu\text{m} < 70\% < 212 \mu\text{m}$$

$$37 \mu\text{m} < 30\% < 45 \mu\text{m}.$$

The sample burn rate for the uncatalyzed propellant agreed with the data for propellant # 78 in the Princeton University test series <sup>(3)</sup>. The catalyst was added to the uncured propellant at a weight percent of 2.41. Tests of the Harshaw catalyst Cu O2O2 P - ferric oxide and iron blue-ferric oxide systems showed no positive synergistic effect at 600 psia<sup>(2)</sup>.

These cast propellant samples were initially prepared to contain on average the same volumetric loading of catalyst as the sandwiches. But for the cast propellants all of the catalyst is suspended in the binder matrix, which constitutes 17w% of the sample. Since 2.4w% of catalyst was added to the cast propellant samples, the binder matrix contained 14.2w% of the catalyst. The binder matrix for the sandwiches contained 4.4% of catalyst. This increase of catalyst in the binder affected the cure and the strength of the binder. This high catalyst loading in the binder may be above the amount required for maximum burn rate augmentation. In order to investigate this possibility further, a new set of samples were prepared using a reduced total catalyst loading of 1% catalyst by weight. This reduced the effective binder loading to 5.9%.

The current study has continued the investigation of synergistic effects on sample burn rate in cast composite propellants with 1w% of catalyst. An experimental procedure has been developed to produce a cast propellant that can be used as a con-

venient test vehicle for catalytic effects. An investigation of catalyst loading in the oxidizer of a cast propellant has been performed. Burn rates of these samples have been obtained at 600 and 2000 psia.

#### FUSE WIRE TESTS

Two separate batches of AP and HTPB were prepared for the initial tests of the addition of 1w% catalyst to the uncured propellant. The ratio of 82.7% solids (AP) to 17.3% binder (HTPB) was maintained, consistent with earlier tests<sup>(2)</sup>. The oxidizer particle distribution was maintained at

$$180 \mu\text{m} < 70\% < 212 \mu\text{m}$$

$$37 \mu\text{m} < 30\% < 45 \mu\text{m} .$$

Freon T F was mixed with the first batch of propellant. This decreased the viscosity of the mixture and allowed the propellant to be packed much easier in the teflon strand molds. The Freon T F could be removed by vaporization at room temperature or by vacuum in the curing oven. The samples were not sufficiently fluid to fill the voids as the freon vaporized. This yielded porous cast propellants. All of the oxidizer particles were premixed before the binder and catalyst were added to the second batch of propellant. This propellant was very difficult to mix and pack in the teflon molds. These samples resembled the first batch of samples. They were porous with a grainy appearance.

Thirteen fuse wire tests were conducted using samples from these two batches of propellants. Several variations of sample preparations were used. Different modes of inhibition were tried on the sides of the samples. Coatings of PVC, vaccum grease and epoxy were used along with water leaching of surface AP and increased flushing nitrogen flows. The results for all samples were the same. All fuse wires appeared to break simultaneously. Both batches of propellant

behaved similarly. This had not been encountered with the 2.41w% catalytic samples of Reference 2. There had been fluctuations of burn rates but not consistently high burn rates as indicated by these samples.

High speed motion pictures were taken of four samples from these two batches. Based on a frame rate of 1600 frames per second, the pure AP-HTPB sample and the 1% Harshaw catalyst Cu O2O2 P sample exploded and burned in .015 seconds (24 frames). The 1% ferric oxide sample was completely consumed in .009 seconds (14 frames). The 1% ferric oxide-iron blue sample lasted for .022 seconds (36 frames).

It is believed that during manufacturing too narrow an AP particle size distribution was being employed, preventing binder wetting and good packing. It was decided to broaden the particle size distribution. Based on the length of time that was necessary to prepare fuse wire samples and the possible areas of uncertainty when the sample burns rapidly, it was decided to return to the cine-photomacrography for determination of sample burn rate and uniformity of burn rate. Poor quality propellant samples can be determined immediately from viewing the motion pictures.

## CINEPHOTOMACROGRAPHY

The samples for these tests were prepared from common lots of uncured propellant. The solids to binder ratio was maintained at 82.7% to 17.3%. The bimodal AP particle distribution was broadened to:

$$\left. \begin{array}{l} 180 \text{ } \mu\text{m} < 35\% < 212 \text{ } \mu\text{m} \\ 125 \text{ } \mu\text{m} < 35\% < 180 \text{ } \mu\text{m} \end{array} \right\} 125 \text{ } \mu\text{m} < 70\% < 212 \text{ } \mu\text{m}$$

$$45 \text{ } \mu\text{m} < 10\% < 63 \text{ } \mu\text{m}$$

$$37 \text{ } \mu\text{m} < 10\% < 45 \text{ } \mu\text{m}$$

$$10\% < 37 \text{ } \mu\text{m} \quad \left. \right\} 30\% < 63 \text{ } \mu\text{m}$$

The oxidizer particle size distribution was prepared from ultra-pure ammonium perchlorate supplied by the Naval Weapons Center at China Lake, Calif. It was ground in a 0.3 gallon porcelain mill jar with an assortment of 1.3 and 2.5 cm ( $\frac{1}{2}$ " and 1") diameter balls. A series of seven 20.3 cm (8") diameter U.S.A. standard sieves was used to separate the ground AP. A motor driven sieve shaker was used to vibrate the sieves. The ground and sieved AP was stored in a sealed container and dried for 24 hours at  $70^{\circ}\text{C}$  before mixing with the binder.

The propellant was prepared by mixing all of the ingredients of the hydroxyl terminated polybutadiene with approximately one half of the largest size AP particles. This was mixed thoroughly and all of the AP particles are wetted with binder. This process was repeated with all AP particle sizes adding the finest AP last. This propellant was then divided for catalyst addition. A minimum of 10 grams of propellant was needed for each catalyzed sample. The proper amount of catalyst was added to the propellant and the mixing process repeated. This propellant was cast in 22 mm by 22 mm embedding molds and cured for seven days at  $60^{\circ}\text{C}$ .

The physical properties and appearance of the cured propellant was improved by the increased mixing time of the propellant and the broadened AP particle distribution. All of the oxidizer appeared to be wetted with binder. The cured propellant was cut into convenient sizes (4mm x 6mm x 19mm) for testing in the high pressure combustion apparatus designed by Varney<sup>(4)</sup> and Jones<sup>(5)</sup>.

These samples were similar in size to the two-dimensional sandwiches tested previously. This allowed the same cinephotomacrographic techniques to be used to observe the burning samples. The same nitrogen flows that were determined experi-

mentally for the sandwiches were used for smoke control. The latent image magnification was reduced to slightly less than 1:1 (image: actual). The motion picture speed was maintained at 1600 frames per second. The sample was oriented on the sample holder to allow observation of two sides of the sample. This indicated the uniformity of the burn and any effect of the light source on burn rate.

The sample burn rates and their uniformity were determined by recording sample profiles at 100 frame intervals by tracing the projected burning surface. These could be used to determine a burn rate every .0625 seconds.

The same combination of catalysts, Harshaw catalyst Cu 0202 P - ferric oxide and iron blue - ferric oxide, that were found to exhibit positive synergistic effects on sandwich vertical burn rate, were tested at 1w% addition to cast propellants. These two combinations of catalyst were determined by the two-dimensional screening experiment and were tested at 2.41w% catalyst addition at 600 psia<sup>(2)</sup>.

Initially the six samples were tested at 600 psia. No positive synergism was indicated, so a second set of samples were tested at 2000 psia. The results of both of these tests are shown in Table I.

TABLE I  
Burn Rates for Cast Composite Propellant (11-22-74)

Catalyst	Burn Rate (in/sec)			
	600 psia		2000 psi	
	r	r/r <sub>pure</sub>	r	r/r <sub>pure</sub>
None	.34	1	.66	1
Harshaw Catalyst Cu 0202 P (CC)	.51	1.50	.74	1.12
Ferric Oxide (IO)	.45	1.32	.83	1.26
Iron Blue (IB)	.54	1.59	possible synergism	possible synergism
CC & IO	.48	1.41		
IO & IB	.54	1.59	Yes	Yes

A "positive" synergistic effect on sample burn rate is obtained when the burn rate of the sample with two effective catalysts present exceeds the burn rates of both of the corresponding samples with only one catalyst present. The total catalyst loading is maintained constant for all three samples. A "possible" synergistic effect on sample burn rate is obtained when the burn rate of the sample with two catalysts present is greater than the average of the burn rates for the two samples with only one catalyst present. Consequently, a "positive" synergism is also a "possible" synergism. A "negative" synergistic effect on sample burn rate is obtained when the burn rate of the sample with two catalysts present is less than the burn rates of both of the corresponding samples with only one catalyst present.

The Harshaw catalyst Cu 0202 P - ferric oxide system did not exhibit a positive synergism at either pressure, but there was a possible synergism indicated at 2000 psi. There was a positive synergistic effect on sample burn rate for the ferric oxide - iron blue system at 2000 psi. Because of this the ferric oxide - iron blue samples and their companion samples were tested over the pressure range 300 to 2000 psia. The results are shown in Figure 3. There was a positive synergistic effect at 300 and 2000 psia, a possible synergistic effect at 600 psia, and a negative effect at 1000 and 1500 psia. The positive synergistic effect on sample burn rate at 300 and 2000 psia along with a review of the favorable catalytic effect of ferrocene when it was restrained to the binder-oxidizer interface <sup>(1)</sup> led to a new evaluation of possible synergistic effects for all combinations of catalysts. Five new catalyst configurations were prepared to complete the test matrix. This included a sample with 1% ferrocene added, three samples with  $\frac{1}{2}\%$  of ferrocene and  $\frac{1}{2}\%$  of the other three catalysts and finally a  $\frac{1}{2}\%$  Harshaw catalyst Cu 0202 P and  $\frac{1}{2}\%$  iron blue sample. The results are shown in Table II for 2000 psia.

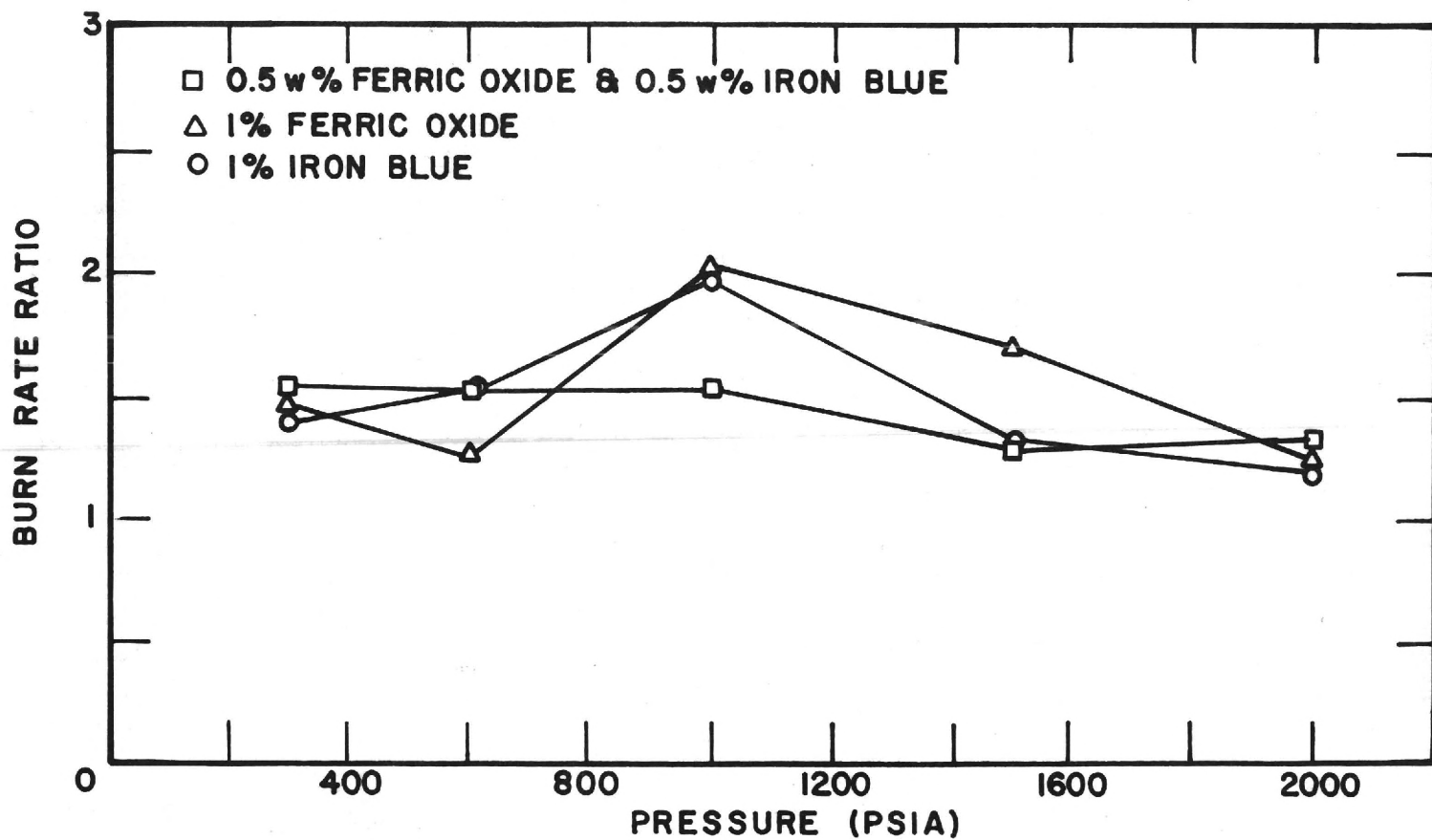


Figure 3. Synergistic Effect for Ferric Oxide-Iron Blue in Cast Composite Propellants.

TABLE II

## Burn Rates for Cast Composite Propellant (5-8-75)

Catalyst	2000 psi Burn Rate (in/sec)	$r/r_{\text{pure}}$
None	.80	1
Ferrocene (F)	.75	.94
CC & IB	1.13	1.41
CC & F	.95	1.19
IO & F	.89	1.11
IB & F	.87	1.09

Initially these burn rates were ratioed with the pure cast propellant burn rate of Table I (11-22-74). These burn rate ratios are shown in the first column of Table III. A positive synergistic effect on sample burn rate was indicated for all new catalyst combinations. This meant that only the Harshaw catalyst Cu 0202 P - ferric oxide system did not yield a positive synergistic effect at 2000 psi. Six separate determinations of sample burn rate yielded a different average burn rate of the pure cast composite propellant (5-8-75). When this new burn rate,  $r_{\text{pure}} = .80$  in/sec was used to ratio the burn rates of samples prepared from the propellant (5-8-75), the second column of burn rate ratios was obtained in Table III. The initial indication of five positive synergisms was reduced to positive synergisms for three systems.

Due to the apparent large difference of burn rate for the pure cast composite propellant samples a third batch of propellant was prepared. All combinations of the four catalysts and their comparison samples were prepared. The burn rates and their ratios are shown in Table IV for 2000 psia. There was a positive synergistic effect indicated for the iron blue - ferrocene system. All indications of synergistic effects were different from the other two batches of propellant. There

TABLE III

Burn Rate Ratios for Cast Composite  
 Propellants (11-22-74) and (5-8-75)  
 at 2000 psia

Catalyst	$r/r_{\text{pure}}$	$r_{\text{pure}} = .66 \text{ in/sec}$	$r/r_{\text{pure}}$	$r_{\text{pure}} = .66 \text{ in/sec}$ or $.80 \text{ in/sec}$
None	1		1	
Harshaw Catalyst Cu O202P(FC)	1.12		1.12	
Ferric Oxide (IO)	1.26		1.26	
Iron Blue (IB)	1.18		1.18	
Ferrocene (F)	1.14	Possible Synergism	.94	Possible Synergism
CC & IO	1.21	Yes	1.21	Yes
CC & IB	1.71	Yes	1.41	Yes
CC & F	1.44	Yes	1.19	Yes
IO & IB	1.33	Yes	1.33	Yes
IO & F	1.35	Yes	1.11	Yes
IB & F	1.32	Yes	1.09	Yes

appears to be a spread of up to .26 in/sec in the burn rate of the pure cast samples. This variation is as large as the burn rate augmentation obtained for most of the catalyzed samples both with single and double catalysts present. It is concluded that reproducibility with these small mixes prevents a conclusive demonstration of synergistic effects.

TABLE IV  
Burn Rates for Cast Composite  
Propellant (8-20-75)

Catalyst	r (in/sec)	r/r <sub>pure</sub>	Possible Synergism
None	.56	1	
Harshaw Catalyst Cu 0202 P (CC)	.78	1.39	
Ferric Oxide (IO)	.85	1.52	
Iron Blue (IB)	.78	1.39	
Ferrocene (F)	.65	1.16	
CC & IO	.77	1.38	No
CC & IB	.78	1.39	?
CC & F	.62	1.11	No
IO & IB	.81	1.45	No
IO & F	.67	1.20	No
IB & F	.92	1.64	Yes

#### CATALYST LOADED INTO AP

Harshaw catalyst Cu 0202 P was selected for tests of loading in the oxidizer polycrystalline structure because of its catalysis of the AP deflagration process<sup>(1)</sup>.

The oxidizer particles for the investigation of catalyst loaded into the oxidizer were prepared from special polycrystalline oxidizer disks. Ultra-pure ammonium perchlorate less than 37  $\mu\text{m}$  in diameter was mixed with 1w% of catalyst and placed in the mold assembly designed by Varney <sup>(4)</sup>. Approximately 5 grams of this fine oxidizer mixture was pressed at one time. The polycrystalline disk was subjected to 30,500 psia for one hour. These disks were reground by hand in a motar and pestle and then sieved. All oxidizer particles less than 37  $\mu\text{m}$  in diameter were discarded. 10% of all remaining sizes was retained for a catalyst loading determination. The remaining oxidizer with catalyst was cast into a solid propellant. The oxidizer particle distribution was:

$$125 \mu\text{m} < 43.7\% < 212 \mu\text{m}$$

$$63 \mu\text{m} < 50.8\% < 125 \mu\text{m}$$

$$37 \mu\text{m} < 5.5\% < 63 \mu\text{m}$$

Comparison samples of pure AP-HTPB and 1w% of catalyst added to the AP-HTPB mixture were prepared with the same oxidizer particle distribution.

These three samples were tested at 600 and 2000 psia. The results are shown in Table V.

TABLE V  
Harshaw Catalyst Cu 0202 P Loaded in AP

Propellant	Burn Rate	(in/sec)
	600 psia	2000 psia
Pure AP-HTPB	.45	.82
1% CC in AP-Pure HTPB	.54	.86
1% CC in HTPB-Pure AP	.69	1.44

The maximum burn rate was obtained for the catalyst added to the AP-HTPB mixture. This is essentially a binder-loaded cast composite propellant.

All three of the special distribution propellants were difficult to mix. The cured propellants were grainy and crumbly in sections. Two separate batches of the pure propellant were prepared and the burn rate varied as  $.82 \pm .05$  in/sec.

A procedure for determining the amount of catalyst remaining in the polycrystalline oxidizer structure was developed. The oxidizer mixture was placed in a 60 ml vacuum funnel with a built-in 40 mm diameter ultra-fine fritted glass filter disk. The ammonium perchlorate was dissolved by repeated washings with distilled water. The washing was continued for three cycles after the liquid showed no perchlorate ions when tested with a methylene blue indicator solution. This solution turns from dark blue to violet in the presence of the perchlorate ions. The material remaining in the filter was dried and weighed. A catalyst determination of the 10% of all size distributions used in the propellant was performed along with the oxidizer with a diameter less than 37  $\mu\text{m}$ . This allowed a catalyst balance to be performed.

Initially 1w% of Harshaw catalyst was added to the AP. The measurement indicated a loading of  $1.6 \pm .3\%$  by weight in the AP which went into the propellant. A catalyst balance was made by determining the amount of catalyst in the sieved polycrystalline oxidizer less than 37  $\mu\text{m}$  in diameter. This balance indicated a possible oxidizer loading of  $.7 \pm .2\%$  by weight. The difference between these two indicated loadings is unresolved.

#### ANALYSIS

The work of Ref. (2) was extended to include the effect of binder-oxidizer reactions on the surface shape attained by a two-dimensional sandwich, assuming there are no melt flows. The work is presented in Appendix A. It is shown that,

indeed, fast binder-oxidizer reactions will force a sandwich to go to a V-shaped structure, as has been suspected from experimental observation and physical reasoning. More importantly, it appears that the oxidizer-binder kinetics are fast enough to influence the sandwich shape at usual deflagration pressures and that the AP flame is not the only heat source which influences the shape attained by the sandwich.

#### CONCLUSIONS

1. Although plagued by reproducibility problems, all possible combinations of the four catalysts investigated exhibited positive or possible synergistic effects on sample burn rate at a pressure of 2000 psia.
2. The synergistic effects are weak and within the range of the reproducibility of the experiments. Consequently, they are of doubtful practical utility with the catalysts investigated in these experiments.
3. The ferric oxide-iron blue system, which was the only system tested over the 300-2000 psia pressure range, exhibited weak positive synergistic effects only at 300 and 2000 psia.
4. The cast propellant samples with Harshaw catalyst Cu O2O2 P loaded in the oxidizer particles did not burn as fast as the binder loaded samples at 600 and 2000 psia. However, difficulties in the experimental determination of the actual catalyst loading in the oxidizer particles render the results inconclusive.
5. Analysis has shown that the faster are the binder-oxidizer reactions the more V-shaped will be a sandwich when deflagrating, reinforcing prior interpretation of sandwich shapes and the effect of catalysis of binder-oxidizer reactions on surface shape.

#### REFERENCES

1. Strahle, W. C., Handley, J. C. and Kumar, N., "Catalytic Behavior in Solid Propellant Combustion," Annual Summary Report for ONR Contract No. N0014-67-A-0159-0016, Georgia Institute of Technology, Atlanta, Georgia.
2. Strahle, W.C. and Handley, J.C., "Synergistic and Novel Effects in Composite Solid Propellant Combustion," Second Annual Summary Report for ONR Contract No. N0014-67-A-0159-0016, Georgia Institute of Technology, Atlanta, Georgia.
3. Steinz, J. A., Stang, P. L. and Summerfield, M., "The Burning Mechanism of Ammonium Perchlorate-Based Composite Solid Propellants," AMS Report No. 830 ONR Contract Nonr 1858 (32), February, 1969.
4. Varney, A. M., "An Experimental Investigation of the Burning Mechanisms of Ammonium Perchlorate Composite Solid Propellants," Ph. D. Dissertation, Georgia Institute of Technology, 1970.
5. Jones, H. E., "An Experimental Investigation Relating to the Combustion Mechanisms of Ammonium Perchlorate Composite Propellants," Ph.D. Dissertation, Georgia Institute of Technology, 1971.

APPENDIX A

Solid Propellant Sandwich  
Deflagration Analysis with  
Binder - Oxidizer Reactions

## NOMENCLATURE

A	constants in the perturbation solution
c	distance above solid surface at which the mass fraction of $\text{HClO}_4$ vanishes
$c_s$	specific heat of solid phase
$c_p$	specific heat at constant pressure
C	deviation of c from the one-dimensional value
E	activation energy
g	dimensionless temperature, $T/T_0$
G	deviation of g from the one-dimensional value
h	specific enthalpy
$\hat{h}_0$	dimensionless specific enthalpy of formation $h_0/c_p T_0$
k	specific reaction rate constant
$\tilde{k}$	$k \rho^2/W^2$
$\hat{k}$	dimensionless preexponential factor
$\ell$	linear transport operator
m	root for exponential solutions
$\dot{m}$	mass flow rate per unit area
q	endothermic heat of gasification
$q_R$	heat of reaction in the gas phase for the pure AP deflagration
r	burn rate
T	temperature
w	production rate, mass/volume/time
$\hat{w}$	dimensionless production rate
W	molecular weight
x	horizontal coordinate
y	vertical coordinate
Y	mass fraction
$\bar{Y}_{s_F}$	mass fraction of $\text{NH}_3$ at solid surface for one dimensional case

$y'$	deviation of $y_s'$ from one dimensional value
$y$	deviation of $Y$ from $\bar{Y}$
$F$	$(1 + y_s'^2)^{1/2}$
$\alpha$	thermal diffusivity or constants in perturbation solution
$\beta$	constants in perturbation solution
$\epsilon$	dimensionless activation energy, $E/RT_0$
$\eta$	$y - y_s$
$\lambda$	thermal conductivity
$\xi$	$c_p \lambda_s / c_s \lambda_g$
$\rho$	density
$\tau_r$	reaction time

#### Subscripts

$o$	cold solid values
$1$	reaction 1 or values at $\eta = c$
$2$	reaction 2
$3$	reaction 3
$4$	reaction 4
$B$	binder
$F_1$	$\text{NH}_3$
$F_2$	$\text{HClO}_4$
$P_1$	products of AP deflagration
$P_2$	products of reaction 2
$P_3$	products of binder-oxidizer reaction
AP	pertaining to one dimensional AP deflagration
$g$	gas phase
$s$	solid phase or at the solid-gas interface
$s^+$	in the gas phase at the solid-gas interface

Superscripts

- \* dimensional quantity
- ' differentiation with respect to x.
- pertaining to one-dimensional deflagration

## INTRODUCTION

In Ref. (A-1) an analysis was conducted of the deflagration of a semi-infinite slab of ammonium perchlorate (AP) adjacent to a semi-infinite slab of binder. It was assumed that the binder was dry and passive so that reactions between the oxidizer and binder were too slow to be effective in driving the deflagration, and there were no melt flows to complicate the binder-oxidizer interface region. The slow reaction assumption required that the AP self-deflagration was the only mechanism responsible for pyrolysing the binder. Accordingly, the analysis could only be valid above the low pressure deflagration limit of the AP. In the current work the assumption of slow binder-oxidizer reactions is relaxed. However, for analytical tractability the no-melt-flow assumption is retained.

It was found in the previous treatment that regardless of binder type the AP would deflagrate with a nearly horizontal surface, far from the binder, and the surface would dip down slightly as the binder was approached. There was then a slope discontinuity at the binder-oxidizer interface and the binder, for usual binder properties, would assume a nearly vertical slope. By relaxation of the zero binder-oxidizer reaction rate assumption it is desired to find a modification to the surface slope that is invariably produced when a catalyst is added experimentally (A-2). That is, the AP assumes a small acute angle with respect to the nearly vertical binder. The reactions between the oxidizer and binder drive the interface region at a faster vertical burn rate than was possible when the AP deflagration above was responsible for the overall sandwich burn rate.

## ANALYSIS

### Reactions Considered

The simplest possible set of gas phase reactions which it appears possible to choose and still show the dominant processes is a set of reactions consistent

with Ref. (A-3). This is



Here  $F_1$  denotes  $\text{NH}_3$  and  $F_2$  denotes  $\text{HClO}_4$  presumed to be the major reactive products liberated from the AP surface. Species B is the binder pyrolysis product and  $P_1$  is some product intermediate.  $P_3$  is the final product of the oxidizer binder reaction. It is to be noted, of course, that these are a simplistic set of global reactions only chosen to describe gross effects.

In order to apply fundamental chemical kinetics to the above reactions it will first be assumed that  $F_1$ ,  $F_2$  and B have identical molecular weight  $w$ . Then  $P_1$  has molecular weight  $2w$ , as does  $P_2$ , and  $P_3$  has molecular weight  $3w$ . Using fundamental kinetics laws (A-4), the production rates of the various species may be written

$$w^* = -\tilde{k}_1^* Y_{F_1} Y_{F_2} - \frac{1}{2} \tilde{k}_4^* Y_{P_2} Y_{F_1}$$

$$w_{P_2}^* = \tilde{k}_1^* Y_{F_1} Y_{F_2} - k_2^* Y_{F_2} Y_B$$

$$w_B^* = \tilde{k}_2^* Y_{F_2} Y_B - \frac{1}{2} \tilde{k}_3^* Y_B Y_{P_1}$$

$$w_{P_1}^* = 2\tilde{k}_1^* Y_{F_1} Y_{F_2} - \tilde{k}_3^* Y_B Y_{P_1}$$

$$w_{P_2}^* = 2\tilde{k}_2^* Y_{F_2} Y_B - \tilde{k}_4^* Y_{P_2} Y_{F_1}$$

$$w_{P_3}^* = \tilde{k}_3^* Y_B Y_{P_1} + \frac{3}{2} \tilde{k}_4^* Y_{P_2} Y_{F_1}$$

(2)

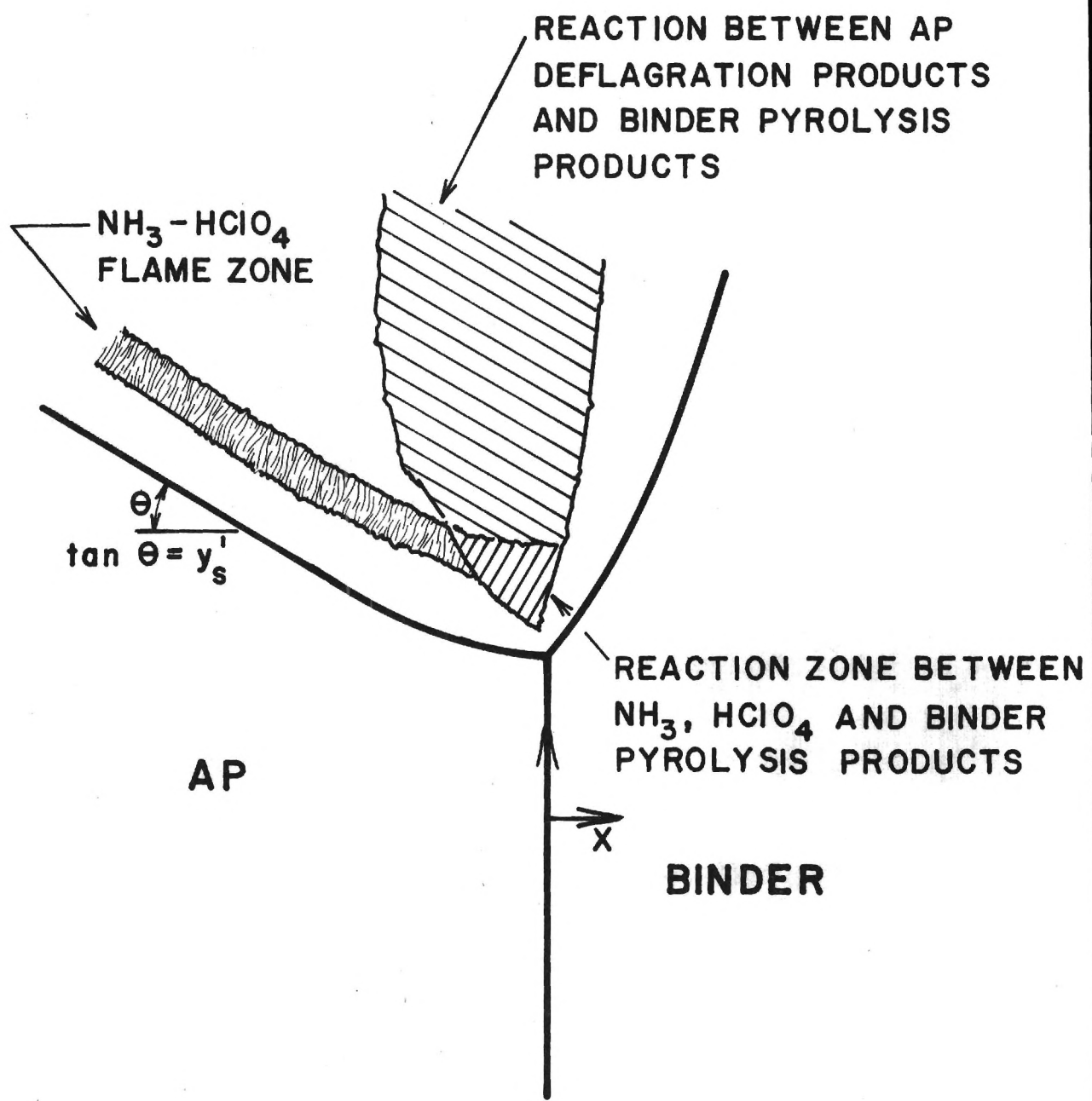


Figure A-1. Sandwich Deflagration Schematic.

These expressions must be used later in the species conservation equations.

Substantial simplification will occur, however, if the boundary conditions on the species are first examined.

### Species Boundary Condition

Making distance dimensionless by  $\alpha_s^*/r^*$  and using Fick's law of diffusion, as in Ref. (A-1), the boundary condition at the gas-solid interface for any species may be written as

$$\frac{\partial Y_i}{\partial n} \Big|_s = -\frac{\xi}{z} \left( Y_{i_s} - \frac{\dot{m}_{i_s}^*}{\dot{m}_{s+}^*} \right) \quad (3)$$

where  $\partial/\partial n = (1/z)(\partial/\partial y) - (y_s'/z)(\partial/\partial x)$ . See Fig. (A-1) for the configuration.

In order to evaluate the derivatives along the surface the same approach as used in Ref. (A-1) will be used. A functional form for  $Y_i$  is chosen as

$$Y_i = Y_{i_s} + (Y_{i_1} - Y_{i_s})(y - y_s)/c \quad (4)$$

with  $Y_{i_s}$ ,  $Y_{i_1}$ ,  $y_s$ , and  $c$  as unknowns to be determined from the conservation equations. All of these unknowns are functions of  $x$ . Note, however, because of the definition of  $c$ ,  $Y_{F_2} = 0$ . Eq. (4) will allow evaluation of the derivative in Eq. (3). First, however, look at the mass flow ratio in Eq. (3). On the binder surface only binder can penetrate so the mass flow ratio is unity if  $i=B$  and is zero for all other species. On the AP surface, consistent with Ref. (A-5),  $P_1$ ,  $F_1$  and  $F_2$  are the species for which the surface is a source. Let  $G$  be the fraction of the surface mass flow which is  $P_1$  and then  $(1-G)/2$  will be the mass flow ratio of  $F_1$  and  $F_2$ . This "dilution coefficient",  $G$ , will be assumed independent of  $x$ , in accord with the independence on surface temperature shown in Ref. (A-5).

Eq. (3) calculated for  $F_1$  as an example yields

$$\frac{-Y_{F_1}}{c} - \frac{y_s'}{z} \left[ \frac{Y_{F_1}}{Y_{i_s}}' \right] = \frac{\xi}{z} \left[ Y_{F_1_s} - \frac{(1-G)}{2} \right] \quad (5)$$

On the other hand, when evaluating Eq. (3) for  $F_1$  on the binder but just at the

interface, more care must be taken. For no mass sources or sinks the  $y_{i_1}$  and  $y_{i_s}$  of Eq. (4) must be continuous at  $x = 0$  and their first derivative must be continuous. However  $y'_s$  undergoes a discontinuity at  $x = 0$ . Therefore, Eq. (3) just to the right of the interface is

$$-\frac{1}{z_B} \frac{y'_{F_1s}}{c} - \frac{y'_{sB}}{z_B} \left[ y'_{F_1s} + \frac{y'_s}{c} y_{F_1s} \right] = \frac{\xi}{z_B} y_{F_1s} \quad (6)$$

where it is understood that Eq. (6) is only good at  $x = 0$ . Eq. (5) is a boundary condition that applies all along  $-\infty \leq x \leq 0$ . The boundary condition on B is

$$\frac{1}{z} \frac{y_{B_1} - y_{B_s}}{c} - \frac{y'_s}{z} \left[ y'_{Bs} - y'_s \left( \frac{y_{B_1} - y_{B_s}}{c} \right) \right] = \frac{\xi}{z} y_{Bs} \quad (7)$$

but right at  $x = 0$

$$\frac{1}{z_B} \frac{y_{B_1} - y_{B_s}}{c} - \frac{y'_{sB}}{z_B} \left[ y'_{Bs} - \frac{y'_s}{c} (y_{B_1} - y_{B_s}) \right] = \frac{\xi}{z_B} (y_{Bs} - 1) \quad (8)$$

Eqs. (6) and (8) may now be investigated concerning orders of magnitude. A perturbation solution will be sought so that at  $x = 0$ , which is the binder-oxidizer interface, only a small perturbation on a one-dimensional AP deflagration will be taking place. That is, the  $P_2$ ,  $P_3$  and B mass fractions will be small compared with unity and the deviations of  $F_1$ ,  $F_2$  and  $P_1$  mass fractions from their one-dimensional deflagration values will be small compared with unity. Guided by Ref. (A-1) it will be assumed that  $y'_{sB}$  is large compared with unity and  $y'_s$  is small but that this product may be of order unity. Derivatives in  $x$  will be of order  $\xi$  compared with unity and  $\xi$  is large. It is assumed that  $y'_{sB}$  is of the order of  $\xi$  or larger and all perturbation quantities are of the order of  $1/\xi$ . From Ref. (A-1),  $c$  is of order  $1/\xi$ . Using these orders of magnitude in Eq. (8), the largest terms, which are of order  $\xi$ , are

$$y'_{sB} y'_{Bs} (0) = \xi \quad (9)$$

Splitting  $y_{F_1s}$  and  $c$  into unperturbed and perturbed parts and using Eq. (6),

the boundary condition is

$$y'_{s_B} - y'_{F_1 s} (0) = - \frac{\bar{Y}_F s}{\bar{c}} (1 + y'_s y'_{s_B}) - \xi \bar{Y}_F s \quad (10)$$

An equation similar to Eq. (10) holds for  $F_2$ . For  $P_1$  the equation is

$$y'_{s_B} - y'_{p_1 s} (0) = - \frac{2\bar{Y}_F s}{\bar{c}} (1 + y'_s y'_{s_B}) - \xi (1 - 2 \bar{Y}_F s) \quad (11)$$

However, investigation of the interface conditions for  $P_2$  and  $P_3$  yield

$$y'_{p_2 s} (0) = 0 = y'_{p_3 s} (0) \quad (12)$$

Equations (9) - (12) hold at  $x = 0$ . The corresponding boundary conditions which hold for the unperturbed and perturbed quantities along the AP surface,  $-\infty \leq x \leq 0$ , are

$$(\xi + \frac{1}{\bar{c}}) \bar{Y}_F s = \frac{\xi(1-G)}{2} \quad (13)$$

for the unperturbed quantity and

$$\begin{aligned} c (\bar{Y}_F / \bar{c}^2) + (\xi + 1/\bar{c}) y'_{F_1 s} &= 0 \\ c (\bar{Y}_F / \bar{c}^2) + (\xi + 1/\bar{c}) y'_{F_2 s} &= 0 \\ (\xi + 1/\bar{c}) y'_{B_s} - y'_{B_1} / \bar{c} &= 0 \\ (\xi + 1/\bar{c}) y'_{p_2 s} - y'_{p_2 l} / \bar{c} &= 0 \\ c (\bar{Y}_{p_1 s} - 1) / \bar{c}^2 - (\xi + 1/\bar{c}) y'_{p_1 s} + y'_{p_1 l} / \bar{c} &= 0 \end{aligned} \quad (14)$$

for the perturbed quantities. In the above, terms of order  $1/\xi$  compared to unity have been dropped.

#### Gas Phase Solution

The conservation equations have been developed in Ref. (A-1), so they will only be stated here. Using the variables  $\eta \equiv y - y_s$ ,  $x$  instead of  $y$ ,  $x$ , the

energy equation is

$$\ell (g) = \sum_{i=1}^6 \hat{w}_i \hat{h}_{i_o}$$

$$\ell \equiv \frac{\partial^2}{\partial x^2} + z^2 \frac{\partial^2}{\partial \eta^2} - 2 y'_s \frac{\partial^2}{\partial \eta \partial x} - y''_s \frac{\partial}{\partial \eta} - \xi \frac{\partial}{\partial \eta} \quad (15)$$

For species  $i$  the conservation equation is

$$\ell (y_i) = \hat{w}_i \equiv - w_i^* \alpha^* c_p^* / (r^* \lambda_g^*) \quad (16)$$

Combination of Eqs. (15) and (16) yields a simple homogeneous equation

$$\ell (g + \sum_{i=1}^6 \hat{h}_{i_o} y_i) = 0 \quad (17)$$

In Eq. (15) the operator  $\ell$  contains  $z^2 = 1 + y'_s^2$ . To the accuracy of the analysis  $y'_s^2$  may be neglected compared to unity. For the unperturbed deflagration of AP, field quantities are functions of  $\eta$  alone. The solution for the AP deflagration has been presented in Ref. (A-1), except for the modification due to the dilution coefficient which is included in this work. The solution is

$$\begin{aligned} \bar{Y}_{F_{1_s}} \left( \frac{1}{c} + \xi \right) &= \xi \left( \frac{1-G}{2} \right) = Q \\ Q &\equiv \hat{k}_1 \frac{Y_{F_{1_s}}^2}{c} \int_0^1 \left( 1 - \frac{\eta}{c} \right)^2 \exp \left\{ - \varepsilon_1 / [\bar{g}_s + (\bar{g}_1 - \bar{g}_s) \frac{\eta}{c}] \right\} d\left(\frac{\eta}{c}\right) \\ \bar{g}_1 - \bar{g}_s &= 2 q_R \bar{Y}_{F_{1_s}} \\ q_R &\equiv \hat{h}_{F_{1_o}} - \hat{h}_{p_{1_o}} \end{aligned} \quad (18)$$

In this work the thermodynamic properties of  $F_1$  and  $F_2$  are assumed identical to each other, for simplicity. All numerical computations have been performed for  $\xi = 9.0$ ,  $\bar{g}_1 = 4.022$ ,  $\bar{g}_s = 2.93$ ,  $G = .75$ ,  $c = .119$  and  $\bar{Y}_{F_{1_s}} = .0634$ . This corresponds to burning at 800 psia, but the dimensionless results are quite insensitive to

pressure, as explained in Ref. (A-1).

The solution of Eqs. (14) and (15) is by an integral technique. Using Eq. (4) as a guessed form for the mass fractions and  $g - g_s = (g_1 - g_s) \eta/c$  for the temperature profile, Eqs. (16) and (17) are integrated in  $\eta$  from 0 to  $c$ . This yields ordinary differential equations in  $x$ . However, appearing in these equations from integration of the second term in  $\ell$  from Eq. (15) is the  $\eta$ -derivative of the appropriate quantity evaluated at  $\eta = c$ . This is an unknown. To eliminate this unknown, as discussed in Ref. (A-1), the parabolic form of Eqs. (14) and (15) are used at  $\eta = c$ . That is, in Eqs. (14).

$$\frac{\partial^2 y_i}{\partial x^2} \Big|_{\eta=c} - \xi \frac{\partial y_i}{\partial \eta} \Big|_{\eta=c} = - \hat{w}_i \Big|_{\eta=c}$$

is used to eliminate  $\partial y_i / \partial \eta \Big|_{\eta=c}$  in favor of the  $x$ -derivative and reaction rate. A similar operation holds for Eq. (17).

The next step in the solution is to let each unknown be represented by its unperturbed, one-dimensional value plus a perturbation component. The equations are then split into unperturbed equations and perturbation equations and the perturbation equations are then linearized. The unperturbed equations have Eqs. (18) as the solution, after using Eq. (13).

It is first instructive to view the solution for the binder mass fraction. The differential equation is

$$\begin{aligned} y''_{B_s} (\bar{c}/2) + y''_{B_1} (\bar{c}/2 + 1/\xi) \\ + (y_{B_s} - y_{B_1})(\xi + 1/\bar{c}) = \hat{k}_2 \left\{ y_{B_s} I_{2_s} + y_{B_1} I_{2_1} \right\} \\ + \frac{1}{2} \hat{k}_3 \left\{ y_{B_s} I_{3_s} + y_{B_1} I_{3_1} \right\} + \frac{1}{2} \hat{k}_3 y_{B_1} e^{-\xi/\bar{g}_1} \end{aligned} \quad (19)$$

where the reaction rate integrals are evaluated from the unperturbed solution

$$I_{2_s} = \int_0^{\bar{c}} \bar{Y}_{F_s} (1 - \eta/\bar{c}) (1 - \eta/\bar{c}) e^{-\mathcal{E}_2/g} d\eta$$

$$I_{2_1} = \int_0^{\bar{c}} \bar{Y}_{F_s} (1 - \eta/\bar{c}) e^{-\mathcal{E}_2/g} d\eta$$

$$I_{3_s} = \int_0^{\bar{c}} \bar{Y}_{p_1}(\eta) (1 - \eta/\bar{c}) e^{-\mathcal{E}_3/g} d\eta$$

$$I_{3_1} = \int_0^{\bar{c}} \bar{Y}_{p_1} e^{-\mathcal{E}_3/g} d\eta$$

Notice that all I's are positive. Now viewing the binder boundary condition in Eqs. (14),  $y_{B_s} \propto y_{B_1}$ . Consequently, Eq. (19) is a homogeneous, linear second order differential equation with the solution

$$y_{B_s} = A_{B_s} e^{m_B x}$$

Making the required substitution  $m_B$  satisfies

$$m_B^2 = \frac{(\xi + 1/\bar{c})(\xi + \gamma) + \mathcal{E}/\bar{c}}{(\xi + 1/\bar{c})(\bar{c}/2 + 1/\xi) + 1/2} \quad (20)$$

where

$$\mathcal{E} = \hat{k}_2 I_{2_s} + \frac{1}{2} \hat{k}_3 I_{3_s}$$

$$\gamma = \hat{k}_2 I_{2_1} + \frac{1}{2} \hat{k}_3 I_{3_1} + \frac{1}{2} \hat{k}_3 e^{-\mathcal{E}_3/g_1}$$

By inspection, therefore,  $m_B^2$  is positive and  $m_B$  has two real, equal roots of opposite signs. The positive sign is accepted so that  $y_B$  will decay to zero at  $x \rightarrow -\infty$ . The constant of integration,  $A_{B_s}$  is determined by application of Eq. (9)

$$A_{B_s} = \xi / (m_B y'_s)$$

The binder solution is therefore completed without knowledge of the behavior of the other mass fractions. Either reaction 2 or reaction 3 will increase  $m_B$  [see Eq. (20)] as the reaction rates increase. This has the effect of lowering

the amount of binder present in the gas phase [Eq. (21)] and of increasing the decay rate of binder as  $x$  proceeds away from zero. These are obvious physical facts since reactions 2 and 3 are disappearance reactions for the binder gases. Also note from Eq. (20) that  $m_B$  is indeed order  $\xi$ , if  $\xi$  is less than or equal to order unity. As a consequence  $y'_B$  is of the order of  $\xi y_B$ , as asserted above. For  $\xi = \gamma = 0$ ,  $m = 6.73$ . Note furthermore that  $m_B$  is independent of  $\bar{y}'_s$ , under the restriction already imposed that  $\bar{y}'_s$  is of order  $1/\xi$ .

All other mass fractions do not behave in an autonomous manner, however. The differential equation derived from continuity of the  $P_2$  species, for example, yields

$$\begin{aligned} & y_{P_2s}'' (\bar{c}/2) + y_{P_2l}'' (\bar{c}/2 + 1/\xi) \\ & + (y_{P_2s} - y_{P_2l}) (\xi + 1/\bar{c}) = -2 \hat{k}_2 \left\{ y_{B_s} I_{2s} + y_{B_l} I_{2l} \right\} \\ & + \hat{k}_4 \left\{ y_{P_2s} I_{4s} + y_{P_2l} I_{4l} \right\} \end{aligned} \quad (22)$$

where, as before,

$$I_{is} = \int_0^{\bar{c}} \bar{Y}_F(\eta) (1 - \eta/\bar{c}) e^{-\xi_i/\bar{g}} d\eta$$

$$I_{il} = \int_0^{\bar{c}} \bar{Y}_F(\eta) e^{-\xi_i/\bar{g}} d\eta$$

Considering that  $y_{P_2s} \propto y_{P_2l}$  from Eqs. (14), Eq. (22) is a linear, second order equation in, say,  $P_2s$ , but it is inhomogeneous because of the appearance of the binder mass fractions. It follows, therefore that  $y_{P_2s}$  will have a solution of the form

$$y_{P_2s} = A_{P_2s} e^{m_{P_2} x} + \alpha_{P_2s} e^{m_B x}$$

It may be verified by substitution that the root to the homogeneous equation,  $m_{P_2}$ , increases with an increase in rate of the destruction reaction, reaction 4.

Application of Eq. (12) yields

$$A_{p_2_s} = -\alpha_{p_2_s} \frac{m_B/m}{p_2}$$

Continuing for  $P_3$ , the solution would look like

$$y_{p_3_s} = A_{p_3_s} e^{\frac{m}{p_3}x} + \alpha_{p_3_s} e^{\frac{m}{p_2}x} + \beta_{p_3_s} e^{\frac{m}{B}x}$$

since the production of  $P_3$  depends upon both  $B$  and  $P_2$ . However, since  $P_3$  is never destroyed  $m_{p_3}$  is determined by Eq. (20), setting  $\epsilon = \gamma = 0$ .

Here  $m_{p_3} = m = 6.73$  and all decay scales other than a fixed  $m$  are set by  $m_{p_2}$  and  $m_B$ .

The situation with  $F_1, F_2$  and  $P_1$  are more complex, however, since they contain unperturbed as well as perturbed components. Only two of them need be considered, however, since

$$y_{F_1} + y_{F_2} + y_{P_1} + y_{P_2} + y_{P_3} = 0$$

Here  $y_{P_1}$  will be eliminated and only  $F_1$  and  $F_2$  are considered. Furthermore, consider now the case where  $k_2$  and  $k_4$  are zero (only a diffusion flame between the binder and AP deflagration products exists). In this case the equations for  $F_1$  and  $F_2$  are the same, as are the boundary conditions.

Consequently  $y_{F_1} = y_{F_2}$ , as is obvious since there are no chemical reactions that prefer one over the other.

The differential equation for conservation of  $F_1$  (or  $F_2$ ) is

$$\begin{aligned} c''(\bar{Y}_{F_s}/2) + y_{F_1_s}''(\bar{c}/2) + \frac{y_{F_1_s}'}{\bar{c}} - c \bar{Y}_{F_s}'/\bar{c}^2 \\ + y_{F_1_s}''' \bar{Y}_{F_s} + \xi \frac{y_{F_1_s}}{\bar{c}} = (\partial Q / \partial Y_{F_1_s}) y_{F_1_s} + (\partial Q / \partial c) c \\ + (\partial Q / \partial y_{F_1_s}) G_1 + (\partial Q / \partial g_s) G_s \end{aligned} \quad (23)$$

where the derivatives of  $Q$  may be evaluated from Eq. (18). The unknowns are now  $c, y_{F_1_s}, y', G_1$  and  $G_s$ . The boundary condition of Eqs. (14) provides an algebraic

relation between  $C$  and  $y_{F_1}$ , A second algebraic condition comes from the assumption of an equilibrium gas-solid interface (A-5, A-1), whereby

$$y_{F_1} = \tilde{b}_F e^{-\frac{E_B}{g_s}}, \quad y_{F_1} = \frac{G_s \frac{E_B}{g_s^2}}{\bar{g}_s^2} \bar{Y}_s F \quad (24)$$

A fourth equation in the five unknowns is obtained by integrating Eq. (15) and applying the perturbation procedure

$$\begin{aligned} & (G_1'' + G_s'') (\bar{c}/2) + (G_s - G_1) (\xi + 1/\bar{c}) \\ & + G_1'''/\xi + \sum_{F_1, F_2, P_3, B} (\hat{h}_{i_o} - \hat{h}_{p_{i_o}}) \left\{ (y_{i_1}'' + y_{i_s}'') (\bar{c}/2) \right. \\ & \left. + y_{i_1}'''/\xi + (y_{i_s} - y_{i_1}) (\xi + 1/\bar{c}) \right\} = 0 \end{aligned} \quad (25)$$

Equation (25) is not a homogeneous equation in the five unknowns because underneath the summation sign sit  $y_{p_s}$  and  $y_B$ , whose solutions are now known.

In the current case the operation on  $P_3$  in Eq. (25) is the homogeneous operator  $e^{m_p x_3} = e^{m_x}$  which wipes out the  $e^{m_p x_3} = e^{m_x}$  solutions. One is therefore left with only  $e^{m_B x}$  type of behavior. The only way for the four equations in five unknowns to have a solution and still satisfy the boundary condition of Eq. (10) is to let

$$\begin{aligned} G_1 &= A_{g_1} e^{m_B x}, \quad C = A_c e^{m_B x} \\ Y' &= A'_Y e^{m_B x}, \quad G_s = A_{g_s} e^{m_B x} \\ y_{F_1} &= y_{F_2} = A_F e^{m_B x} \end{aligned}$$

and use the boundary condition as an additional equation. It is to be noted that this procedure also holds if  $\hat{k}_3 = 0$ , the case of a purely inert binder. This latter case is the one treated by Ref. (A-1), but the solution there did not involve Eq. (9). It is now believed that Ref. (A-1) is in error since Eq. (9) must be satisfied for consistency. In any event, following the solution procedure, eliminating  $C$  and  $G_s$  and recalling that in Eq. (10)  $y'_s(0) = \bar{y}'_s + A'_Y$ , there result three equations

in three unknowns of the form

$$\begin{aligned}
 A_{11} A_{g_1} + A_{12} A_{Y_F} &= 3 y_B (h_{p_{30}} - h_{p_{10}}) [\varepsilon + (1 + c \xi) \gamma] \\
 A_{21} A_{g_1} + A_{22} A_{Y_F} + A_{23} A_{Y'} &= 0 \\
 A_{32} A_{Y_F} + A_{33} A_{Y'} &= - \frac{\bar{y}_F [ \xi + (1 + \bar{y}'_s y'_B) / c ]}{m_B y'_B}
 \end{aligned} \tag{26}$$

It may be verified in Eq. (26) that  $A_{11} < 0$  and for exothermic reaction between B and  $P_1$ , the heat of formation difference in the first of Eq. (26) is negative. Since  $\varepsilon$  and  $\gamma$  are positive, the first of Eq. (26) clearly shows that the reaction tends to elevate  $g_1$ .

### RESULTS

Consider first the solution for no reactions,  $\varepsilon = \Gamma = 0$ . For various  $y'_s$  and  $\bar{y}'_s$  values the solutions to Eq. (26) are shown on Fig. A-2 as  $A_{g_1}$  vs  $y'_s(0) = \bar{y}'_s + A_{Y'}$ . The values for  $y'_s$  increase as one moves to the right along any curve of fixed  $\bar{y}'_s$ . It is seen first of all that there are no solutions for which  $y'_s(0) > 0$ . Furthermore, in regimes where  $g_1 - \bar{g}_1$  are less than zero, which is the only physically reasonable regime, since the binder is a heat sink,  $y'_s < \bar{y}'_s$ . This means that the AP surface turns down to attempt to intersect the binder at an acute angle, rather than an obtuse angle. This is demanded by the gas phase solution alone and does not depend upon binder or AP properties in the solid phase. This character of the solution is somewhat counter to the author's intuition. It was expected that the AP would curve upward as the binder is approached.

For the case with reaction consider a high activation energy case so that  $\gamma$  is dominated by the last term and  $\varepsilon \ll \gamma$ . As an example take  $\gamma = 0.15$  and

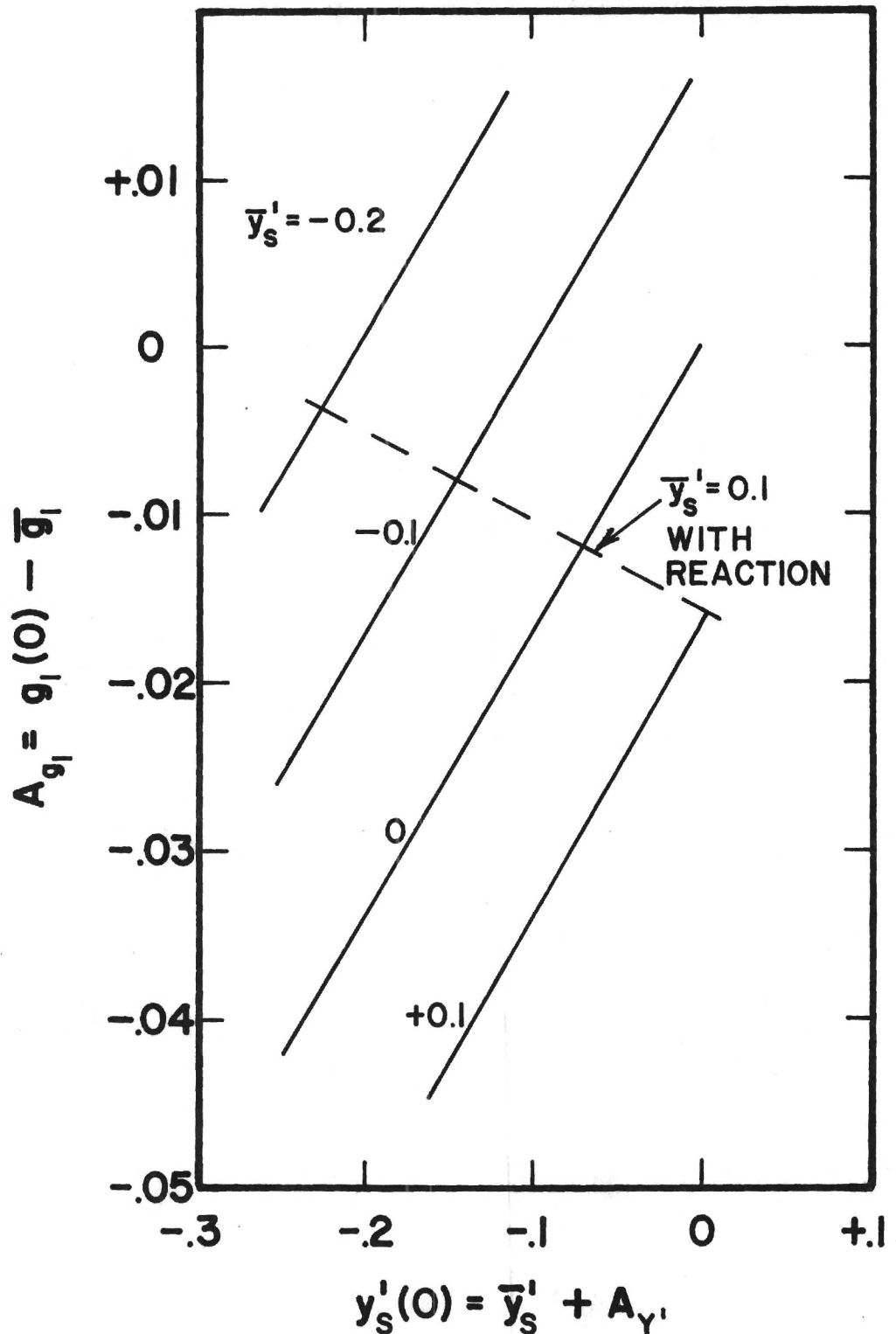


Figure A-2. Temperature at the Edge of the AP Flame as a Function of the Surface Slope at the Binder-Oxidizer Interface.

$\hat{h}_p - \hat{h}_{p_1} = -10$ . On Fig. A-2 the dashed line shows the solution for  $\bar{y}'_s = 0.1$ .  
 $_{30}^{\circ}$  The temperature is, of course, elevated as compared with the no reaction case.

Here there is no good physical argument to reject solutions for  $A_{g_1} > 0$ . However, only one solution curve is shown and for  $\bar{y}'_s = 0.1$ ,  $A_{g_1} < 0$ .

In order to show which binder properties belong to each point on the curves of Fig. A-2 one must consider first the solution for the solid phase heat transfer. This solution was obtained in Ref. (A-1). By inspection of that solution, invoking the continuity of the heat transfer vectors in the solid and gas phases at the intersection of the binder and oxidizer, and applying the order of magnitude arguments, the solution for the binder heat of gasification is

$$q_B = m_B A_{g_s} y'_{s_B} + \left[ 1 + y'_{s_B} y'_s(0) \right] \left[ \frac{\bar{g}_1 - \bar{g}_s}{\bar{g} \bar{c}} + 1 - \bar{g}_s \right] \quad (27)$$

It turns out, therefore, that the result is independent of the solid phase solution. This is a remarkable property of the problem. The final link to the binder is the pyrolysis law. As stated in Ref. (A-1) this is

$$\frac{1}{(1 + y'_{s_B}^2)} = \frac{b_B}{r} e^{-E_B/\bar{g}_s} \quad (28)$$

Given the activation energy,  $b_B$  is directly determined by  $y'_{s_B}$ , since  $r = r_{A_P}$  consistent with the orders of magnitudes considered here. Then Eq. (27) determines the allowable  $q_B$  for any given  $\bar{y}'_s$ , which is the eigenvalue of the problem.

The results of this calculation are plotted for the no reaction case in Fig. A-3. Given a set of binder properties determines the eigenvalue  $y'_s$  on this plot. The disappointing result is that within the solution constraint that  $\bar{y}'_s$  is small there are no solutions for binder properties of interest. Shown, for example, are the CTPB and HTPB points for properties taken from Ref. (A-6). There simply are no solutions to the problem for which  $A_{g_1} < 0$  at large positive  $q_B$ . What

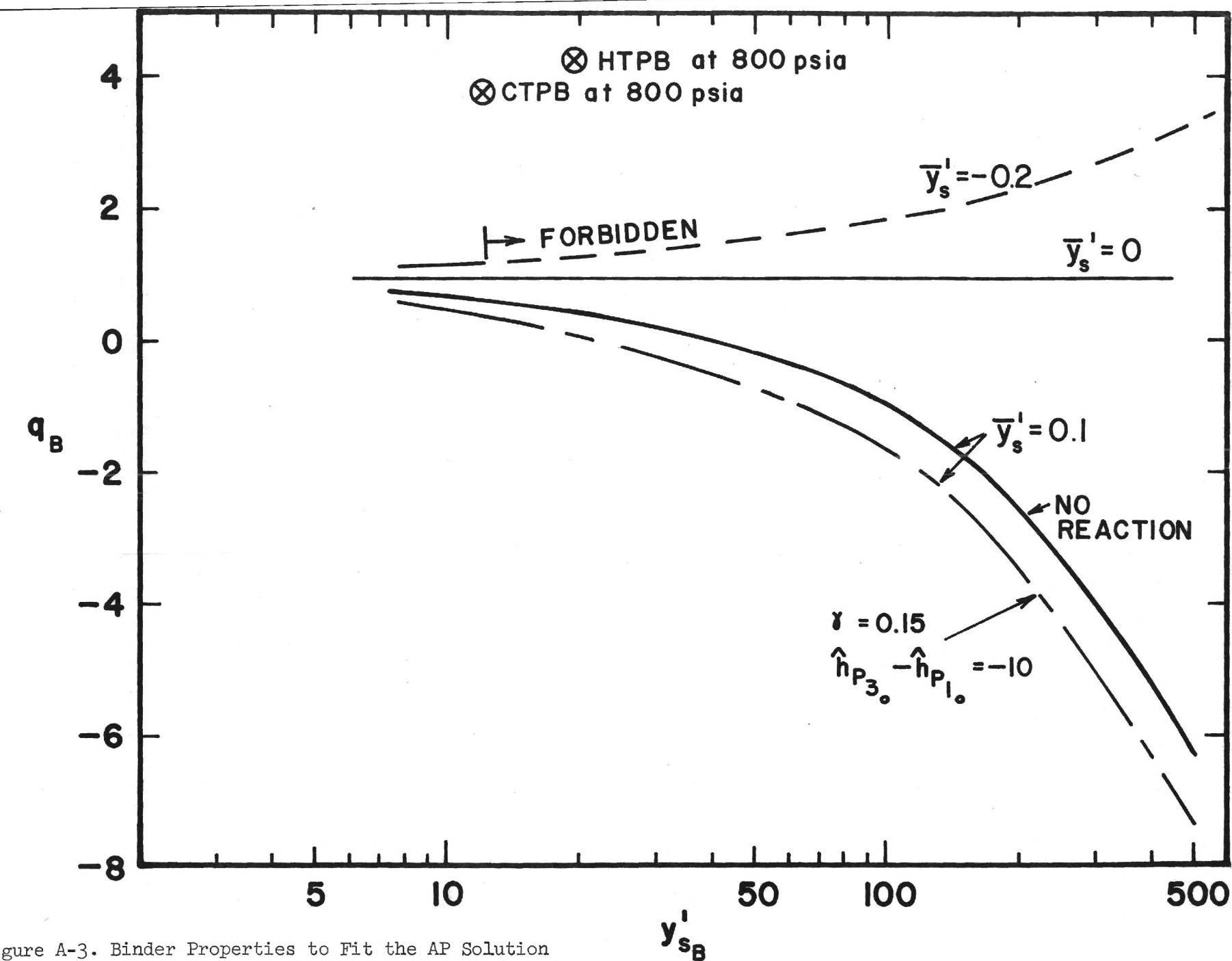


Figure A-3. Binder Properties to Fit the AP Solution  
 with Surface Slope Far from the Binder as  
 a Parameter; Reaction and No-Reaction Cases.

must occur for binders of interest is one must consider the fully nonlinear set of equations. Nevertheless, this solution may be used as a guide to investigate the qualitative effect of parameter changes.

Within the regime of allowable solutions, which basically limits the solution to small positive or negative  $q_B$  and  $\bar{y}'_s > 0$ , an increase in pyrolysis rate at fixed  $q_B$  increases  $\bar{y}'_s$ . An increase in heat of gasification at fixed pyrolysis rate ( $y'_{s_B}$  fixed) decreases the slope of the AP far from the interface ( $\bar{y}'_s$  decreases).

For the case with reaction, considered above, the solution for  $\bar{y}'_s = 0.1$  is shown on Fig. A-3. Exothermic reaction shifts all of the curves to lower  $q_B$  for fixed  $y'_{s_B}$ . Therefore, for a fixed set of binder properties the exothermic reactions decrease  $\bar{y}'_s$ . That is, the solution says that reactions tend to promote an acute angle between the oxidizer and binder, as is experimentally observed.

Tracing through the nondimensionalization procedure and for the numbers used here a characteristic reaction time is given by  $1/\tau_r^* = k_3^* e^{-\mathcal{E}_3/\bar{g}_1} \gamma_{B_s}^* \rho^*/W^*$ , and  $\tau_r^* \approx 10^{-4}$  sec at 800 psia for  $\gamma_{B_s}^* = 0.1$  (which depends on  $y'_{s_B}$  through Eq. (9)). From Ref. (A-7) a typical reaction time under these conditions may be computed to be  $10^{-5}$  sec. Therefore, typical reaction times are well within the range that a significant impact would be made on the sandwich shape by the binder-oxidizer reactions. Furthermore, for completeness reactions 2 and 4 should be considered. However, because of the limited applicability of this solution together with the qualitative information already gleaned from the solution, no further computations will be made.

#### CONCLUSIONS

1. A linearized solution using an integral technique has been found to the problem

of a deflagrating semi-infinite slab of AP adjacent to a semi-infinite slab of binder which is capable of reaction with the AP in the gas phase. The solution was found to only be valid for binders which are difficult to gasify (low pyrolysis rates) and with low or negative (exothermic) heats of gasification. A further restriction to the solution is that there are no melt flows.

2. For typical reaction times the binder-oxidizer reactions are fast enough to substantially affect the deflagration rate. The effect is to make the slab of AP intersect the binder at an acute angle, giving the appearance that the interface region is driving the deflagration rate, which it is.
3. The solution predicts that as one approaches the binder along the AP surface the AP surface becomes convex from above, which is somewhat counter to physical intuition.

REFERENCES

- A-1. Strahle, W. C., "Solid Propellant Sandwich Deflagration Analysis," AIAA J., Vol. 13, May 1975, pp. 640-646.
- A-2. Strahle, W. C., "Catalytic Effects in the Combustion of AP-HIPB Sandwiches to 3200 psia," Combustion Science and Technology, Vol. 8, Sept.-Dec., 1974, pp. 297-304.
- A-3. Beckstead, M. W., Derr, R. L. and Price, C. F., "A Model of Composite Solid Propellant Combustion Based on Multiple Flames," AIAA J., Vol. 8, Dec. 1970, pp. 2200-2207
- A-4. Williams, F. A., Combustion Theory, Addison-Wesley, Reading, 1965, p. 4.
- A-5. Guirao, C. and Williams, F. A., "A Model for Ammonium Perchlorate Deflagration between 20 and 100 atm," AIAA J., Vol. 9, July 1971, pp. 1345-1356.
- A-6. Cohen, N.S., Fleming, R. W. and Derr, R. L., "Role of Binder in Solid Propellant Combustion," AIAA Paper 72-1121, New Orleans, La. 1972.
- A-7. Myers, B. F. and Bartle, E. R., "Reaction and Ignition Delay Times in the Oxidation of Propane," AIAA J., Vol. 7, Oct. 1969, pp. 1862-1869.

**FINAL REPORT**

**COMBUSTION MECHANISMS  
OF SOLID PROPELLANTS**

**By**

**E. W. Price, J. C. Handley, W. C. Strahle,  
T. S. Sheshadri, R. K. Sigman, Ashoke Ghosh**

**Prepared for**

**OFFICE OF NAVAL RESEARCH  
ARLINGTON, VIRGINIA 22217**

**Under**

**Contract N00014-75-C-0332 Mod. P00005**

**September 1980**

**Approved for public release; distribution unlimited**

**GEORGIA INSTITUTE OF TECHNOLOGY**  
**SCHOOL OF AEROSPACE ENGINEERING**  
**ATLANTA, GEORGIA 30332**

**1980**



COMBUSTION MECHANISMS  
OF SOLID PROPELLANTS

Prepared for

Office of Naval Research  
Arlington, Virginia 22217

by

E. W. Price, J. C. Handley, W. C. Strahle  
T. S. Sheshadri, R. K. Sigman, Ashoke Ghosh

School of Aerospace Engineering  
Georgia Institute of Technology  
Atlanta, Georgia 30332

Approved for public release; distribution unlimited

ONR Contract N00014-75-C-0332 Mod. P00005

September 1980

Conditions of Reproduction

Reproduction, translation, publication, use and disposal in whole or in part by or for the United States Government is permitted.

## Unclassified

SECURITY CLASSIFICATION OF THIS PAGE (When Data Entered)

REPORT DOCUMENTATION PAGE		READ INSTRUCTIONS BEFORE COMPLETING FORM
1. REPORT NUMBER	2. GOVT ACCESSION NO.	3. RECIPIENT'S CATALOG NUMBER
4. TITLE (and Subtitle) COMBUSTION MECHANIS OF SOLID PROPELLANTS		5. TYPE OF REPORT & PERIOD COVERED FINAL TECHNICAL REPORT 1 Dec. 1976 - 31 July 1979
		6. PERFORMING ORG. REPORT NUMBER
7. AUTHOR(s) E. W. PRICE, J. C. HANDLEY, W. C. STRAHLE T. S. SHESHADRI, R. K. SIGMAN, ASHOKE GHOSH		8. CONTRACT OR GRANT NUMBER(s) ONR Contract No. N00014-75-C-0332, Mod. P00005 NR# 092-543/6-20-79(473)
9. PERFORMING ORGANIZATION NAME AND ADDRESS GEORGIA INSTITUTE OF TECHNOLOGY SCHOOL OF AEROSPACE ENGINEERING ATLANTA, GEORGIA 30332		10. PROGRAM ELEMENT, PROJECT, TASK AREA & WORK UNIT NUMBERS
11. CONTROLLING OFFICE NAME AND ADDRESS OFFICE OF NAVAL RESEARCH ARLINGTON, VIRGINIA 22217		12. REPORT DATE September 1, 1980
		13. NUMBER OF PAGES
14. MONITORING AGENCY NAME & ADDRESS(if different from Controlling Office) POWER PROGRAM OFFICE OF NAVAL RESEARCH ARLINGTON, VIRGINIA 22217		15. SECURITY CLASS. (of this report) UNCLASSIFIED
		15a. DECLASSIFICATION/DOWNGRADING SCHEDULE
16. DISTRIBUTION STATEMENT (of this Report)  Approved for public release; distribution unlimited.		
17. DISTRIBUTION STATEMENT (of the abstract entered in Block 20, if different from Report)  Approved for public release; distribution unlimited.		
18. SUPPLEMENTARY NOTES		
19. KEY WORDS (Continue on reverse side if necessary and identify by block number) COMBUSTION, PROPELLANT, HETEROGENEOUS, ROCKET, PROPULSION, EXPERIMENTAL, THEORETICAL		
20. ABSTRACT (Continue on reverse side if necessary and identify by block number)  See next page.		

#### ACKNOWLEDGEMENTS

This research has been sponsored by the Power Program of the Office of Naval Research, Arlington, Virginia, under the Contract No. N00014-75-C-0332. Dr. Richard S. Miller served as the technical monitor and program manager for this contract. His support of this research investigation is greatly appreciated.

## TABLE OF CONTENTS

Section	Page
1.0 Introduction .....	1
1.1 General Objectives .....	1
1.2 Historical Background .....	1
1.3 Current Situation .....	5
1.4 Approach to Present Investigation .....	14
2.0 Thermal Degradation of Propellant Binders .....	15
3.0 Sandwich Burning .....	19
3.1 Introduction .....	19
3.2 Combustion Zone of AP/HC Sandwiches .....	19
3.3 Classification of Sandwiches and Expected Behavior .....	21
3.4 Scope of Current Investigation .....	26
3.5 Interface Profile and Melt Flows .....	28
3.6 Binder Thickness .....	34
3.7 Comparison of Binders .....	36
3.8 Diffusion Flame .....	42
3.9 Discussion of Sandwich Burning Results .....	45
4.0 Tests on Other Ordered Microstructures .....	53
4.1 Philosophy of Tests .....	53
4.2 Combustion Behavior .....	53
4.3 Fuel Strands - Beaded Sandwiches .....	56
4.4 Fuel Strands - Fuel Filaments .....	62
4.5 Ordered Arrays of Spherical Oxidizer Particles .....	67
4.6 Stacked Cylinder Configuration .....	68
4.7 Discussion .....	69
5.0 Surface Characteristics of Quenched Propellants .....	74
5.1 Philosophy of Tests .....	74
5.2 Test Design .....	74
5.3 Results .....	75
5.4 Discussion .....	79
6.0 Least Time Path for Burning Rate .....	81
7.0 Stability Analysis of Diffusion Flames .....	82
7.1 Introduction .....	82
7.2 Posing the Analytical Problem .....	82
7.3 Analysis .....	83
7.4 Results .....	84
8.0 Statistical Modeling of the Combustion Zone .....	85
8.1 Introduction .....	85
8.2 Critique of Statistical Models .....	86
8.3 Surface Statistics Model .....	91
8.3.1 The Burning Surface of a Propellant .....	91
8.3.2 Mass Flow from the Burning Surface .....	97
8.3.3 Application of Equations .....	100
8.3.4 Assumptions in the Surface Statistics Model .....	101
References .....	105
Appendix A .....	A1

## INTRODUCTION

### 1.1 General Objectives

Research on combustion of solid rocket propellants is typically motivated by practical needs of the solid rocket business, as perceived by propellant chemists, propulsion engineers, and by combustion scientists. Direction and level of effort are usually determined by current applied problem areas such as need for large changes in burning rate or specific impulse, encounters with unstable combustion in development programs, need for smokeless exhaust plumes, etc. However, there has always been a modest level of more fundamental research aimed at understanding the underlying details of the combustion process. It is this kind of research that provides the physical insight and factual base on which more applied efforts are built and evaluated. Typical of such research, it is fundamental in its objective of seeking understanding, but applied in the sense that physically and chemically complex problems are accepted in order to preserve relevance to the practical problem. The present program has been designed to help serve this need for "fundamental" research. The scope has been limited for practical reasons to combustion of heterogeneous systems, without powdered metal fuel ingredients. Objectives are to determine the structure of the combustion zone, the behavior of the individual ingredients in the combustion zone, and the relative importance of competing processes. As a means of controlling variables, combustion experiments have until recently used ordered microstructure (e.g., oxidizer-binder sandwiches). From a practical viewpoint, the objectives are to assist in selection and control of ingredient characteristics, design of propellants, prediction of steady and unsteady combustion, and in troubleshooting for systems that are not meeting specifications.

### 1.2 Historical Background

Combustion of solid rocket propellants is an applied science that has its origins in the science of internal ballistics of guns. Indeed, the propellant charges used in the early days of the modern era of rocketry

(1937 - 1944) were made from gun propellants and trench mortar sheet propellant. These propellants consisted primarily of nitrocellulose, with various amounts of plasticizer (often including nitroglycerin). The propellants were colloidal in nature, virtually homogeneous. Rocket applications called for predictable, smooth surface burning of relatively large pieces of propellant, at pressures much lower than in guns. Because of urgent need, development of such propellant charges proceeded on a substantially trial-and-error basis, while a science of internal ballistics of rockets was developed as the needs of the immediate situation dictated. Progress of the 1940's is typified by the book "Internal Ballistics of Solid-Fueled Rockets" by Wimpress (Reference 1), and by a collection of papers on theory of combustion of solid propellants, in the Journal of Physical and Colloid Chemistry, Volume 54, of 1950 (Reference 2). It is worthy note that the science of propellant combustion remained substantially empirical, with heavy reliance on laboratory tests to determine burning rates of modified propellants; and with little or no capability to describe or anticipate such all-too-common, unwanted behavior as spontaneous oscillatory combustion.

By 1950, significant progress had been made in development of propellants made from hydrocarbon fuel and inorganic crystalline oxidizers. In such propellants, the granular oxidizer was contained in a matrix of rubber-like fuel. The theoretical science of propellant combustion was hardly prepared to deal with the new complexity of a heterogeneous propellant, and the progress of the 1950's was largely dependent on the empirical methods and such physical insight as could be developed from experimental research. It didn't take too much physical insight to recognize that a propellant that consisted of a near stoichiometric ratio of oxidizer and fuel would burn faster than the usual fuel-rich mixture, or that fine oxidizer size yielded higher burning rate. It took more effort to determine the effects of such propellant variables on the sensitivity of burning rate to pressure, temperature and flow environment in the rocket motor. But laboratory tests could be run, and motor firings could be made until the propellant developers got what they wanted. Financial support for

research aimed at principles of combustion languished. In an American Rocket Society Meeting in the late 1950's, a panel of propellant developers was asked what help research had been to them, and they said, "none" (probably not entirely accurate, but compatible with the relative amount of past effort devoted to trial and error development vis-a-vis research).

In 1959, the role of research was drastically changed by the increasing cost of motor testing associated with development of larger and more sophisticated motors and new propellants. A Defense Department Ad Hoc Committee (Reference 3) studied the risks to large motor programs posed by the problem of combustion instability, and recommended an aggressive combustion research effort, to provide a more fundamental basis for anticipating and correcting problems in development programs. Combustion instability was used in Congressional briefing by liquid propellant proponents as an argument against use of solid rockets in ballistic missile programs (even though combustion instability was a proven problem in liquid rockets, an unknown in large solid rockets).

By this time a much wider range of composite propellants came into consideration or use, further complicating the problem of predicting combustion behavior. The years 1958 - 1970 were extremely productive years from the standpoint of increased understanding of propellant combustion. The role of research was particularly evident in the problem of combustion instability, primarily because it involved a complex transient interaction of combustion, gas dynamics of the combustor, and geometry of the combustor. Propellant developers were not equipped to deal with such a problem, and motor designers could not solve the problems by trial-and-error firings of motors because of the costly motor firings involved. While laboratory scale burners could be used to advantage they had to be developed by research teams. Only limited aspects of the problem could be tested this way, and considerable advance in understanding was required even to understand the laboratory burner behavior (Reference 4). This situation has led to a much more conspicuous role for research, the benefits of which were not limited to solving combustor stability problems. A panel of propellant developers might today grudgingly concede that combustion research

has provided improved laboratory test methods, better interpretation of test results, better advance identification of key problems, and even helped bring desirable new propellant formulations to successful application.

Recent trends in propellants and applications continue to produce new needs for understanding. Interest has grown in propellants that produce no optically visible exhaust trail from the missile, a trend that poses combustion stability problems associated with exclusion of aluminum from the formulation. In these applications, even the traditional oxidizer (ammonium perchlorate) is undesirable because of its tendency to give a water condensation trail due to the HCl in the reaction products. Efforts to change to nitramines (e.g., HMX) have posed difficulties over the whole spectrum of combustion problems. Another general problem in modern propellants comes from the ever-present desire to increase the energy content of the propellant (particularly important in upper stage and space motors, and in volume-limited missile systems). The ingredients of such propellants (e.g., nitrocellulose, nitroglycerin, HMX) are individually and collectively detonable. The processing industry has worked the miracle of learning how to produce motors with these dangerous ingredients (which are considerably less delicate once they are manufactured into a propellant), but they still represent a serious hazard if the combustion does not proceed as planned. As a result there has been increased research on combustion as it relates to transition to detonation.

In the face of changing military and space program needs, the problems emphasized in propellant combustion research have shifted on a time scale of from one to five years, with the most fundamental efforts traditionally facing a struggle for survival because of lesser apparent relevance to solution of "today's" problem. No matter that the fundamental knowledge contributes to all problems, it is not identified easily enough with today's problem to compete for support. Unlike low support in the 1950's, there is considerable support for scientific work on propellant combustion in the 1970's (albeit less than in the 1960's), a result of increased complexity of problems and of increased cost of "solving" them by empirical means. But the problem-oriented nature of the motivation for support tends to

obscure the fact that science and scientists are not produced by solving practical problems, but rather by study of the underlying principles and by advancement of understanding and methods. For this reason, a modest level of research on combustion mechanisms has continued for the last 30 years, as an essential part of capability to deal with "today's" problems. Such "fundamental" research is only fundamental in the context of an applied science such as propellant combustion, and in the context of its motivation, which is to understand. In this sense, the work described in this report is fundamental.

### 1.3 Current Situation

One may examine the current situation in two ways (a) What kind of practical combustion problems do we have?, or (b) What aspects of the combustion mechanisms do we understand, what do we not understand? These questions are addressed here.

Of course, one would ideally like to be able to predict in advance all combustion characteristics of a given propellant, and even calculate modifications in propellant to produce desired effects in combustion characteristics. However, such a capability is not likely to be achieved, primarily because of the complexity of propellants and of their combustion. It has been suggested that such goals might be achieved by a massive systematic experimental investigation of the effect of propellant and environmental variables and suitable correlation of test results and test variables. However, the scope of such an effort is almost boundless, and the cost prohibitive unless restricted to a very limited set of variables. Thus it appears to be preferable to seek the capability to predict trends, and leave the "fine tuning" of propellant formulation to the time when the application has established constraints such as the domains of accessible propellant variables, expected environmental variables, and acceptable combustion behavior. This is, in fact, the strategy that has been followed, although probably more out of expediency than logical choice.

The classical list of practical combustion problems and research objectives will probably always be relevant to some degree. The objectives

include assurance of the following:

1. Desired burning rates, uniformity of rate.
2. Desired (usually minimal) dependence of burning rate on variables of the combustor environment (pressure, temperature, etc.).
3. High combustion efficiency.
4. Stable combustion (non-oscillatory).
5. Adequate ignition properties, quenching properties in some applications.
6. Low smoke in combustion products (some applications).
7. Low susceptibility to detonation.
8. Physical and chemical stability in storage.
9. Minimum toxicity of combustion products.

Unfortunately, resolution of combustion problems is never absolute, because the problems are not independent of each other; resolution of one problem often worsens others. This is the very reason that purely empirical fixes of problems have such limited applicability. New applications demand new trade-offs, and there is no substitute for "mechanistic understanding" in design of the trade-off.

An illustration of strengths and weaknesses in our present knowledge, and of the impact of demands by new applications, is provided by the trend to low smoke motors in recent years. This trend has had two major impacts on propellants, with companion combustion problems. Powdered metal ingredients are eliminated, and efforts are being made to avoid use of ammonium perchlorate. The metals yield condensed oxide smoke in the exhaust; and AP yields HCl, which causes water condensation in the exhaust trail. But the oxide smoke from metals had virtually eliminated oscillatory combustion in earlier motors, and now the problem is back "full force". The proposed abandonment of AP is causing consideration of a new spectrum of ingredients such as nitramines, which have very different combustion characteristics that are only poorly understood. These are driving forces in a large part of today's propellant combustion research, some of which was abandoned years before because of apparent decline of need at that time.

Another need that has heavily affected recent research is the hazard of very high energy propellants selected for those applications where viability of the weapon system is dependent on attaining high specific impulse. This has necessitated better understanding of detonation hazards, a situation that has led to research on both mechanical and combustion behavior of heterogeneous solids.

Both the oscillatory combustion and the detonation hazards problems are made relatively intractable by the necessity to embrace the complexities of transient nonlinear processes, in heterogeneous systems.

In science, problems involving complex systems are necessarily approached by a great deal of observation, ordering of observations, recognition of critical features of behavior, construction of hypotheses and analytical models to explain and exhibit the observed features of behavior, followed by cycles of refinement through experiments and analysis (a somewhat grand example is the entire science of cosmology). Success, however viewed, quite often depends on understanding of processes originating at the microscopic level (in the case of cosmology, understanding at the atomic and nuclear level), and this is true of propellant combustion, where reaction zones and thermal layers that control the macroscopic burning are of the same dimensional order as the granularity of the propellant ingredients. Unfortunately, observational methods generally do not have adequate spatial resolution at those dimensions. In spite of this difficulty, it is necessary to obtain knowledge regarding the combustion zone structure in order to recognize critical features of behavior and construct relevant models.

The present state of theory of propellant combustion is somewhat like that of cosmology in 1938. Many observations of the macroscopic aspects of combustion and a bountiful and growing array of hypotheses and analytical models are in hand, but there is only minimal information on the microscopic processes that drive the overall phenomenon (nuclear processes in cosmology, molecular and microflame processes in propellant combustion). This difficulty has not been too serious in developing an understanding of steady state combustion, because only a time-wise average of the micro-

processes is important. In transient processes, the time constants of the micro processes (mixing times, flame transit times, collision times) become important aspects of the macroscopic behavior, and the knowledge to deal with this fact is largely lacking. A classic example is the inability to explain the dynamic response of combustion to pressure waves in high frequency oscillatory burning (i.e., explain the effect of mean pressure, oxidizer particle size, and ballistic modifiers on dynamic combustion response). Another example is the response of a burning porous bed to the penetration of hot gases ahead of the reaction wave (an element of the deflagration-to-detonation transition process). There is no way these processes can be correctly explained without looking at the situation on a three-dimensional microscopic scale and describing the transient processes on that basis.

One might summarize the present situation in combustion science of propellants by the following:

1. The response of propellant ingredients to controlled heating has been studied by a variety of processes in the hopes that response in the propellant combustion zone can be learned under less difficult conditions. Tests have never been standardized, results have not been catalogued, and the various studies have not used the same ranges or increments of control variables. Many ingredients have been tested only superficially. For some ingredients (e.g., ammonium perchlorate) the test temperatures have remained too low to simulate combustion zone behavior. Very little of this work is being done in the U.S.A. anymore. The results remain fragmentary.

2. Deflagration and combustion of ingredients under controlled conditions is often done as a means of overcoming the limitations of relevance of thermal response tests, while avoiding the difficulties of observation with propellants. These studies are often a source of embarrassment to modelers because they reveal complex behavior not included in analytical models. They eventually lead to better models, and more realistic mech-

anistic insight (deflagration of ammonium perchlorate crystals is the most conspicuous example of this kind of study). At present almost no work of this kind is going on in the U.S.A. except with HMX.

3. The steady state, one dimensional representation of propellant burning can be coded for computers and solutions in principle can be obtained if suitable reaction kinetics can be established. However such models have not to date provided for the phenomenon of selective concentration of stable ingredients or reaction intermediates on the burning surface, a process usually observed in experiments. Further, the reaction kinetics are still undetermined for most ingredients. Although propellant combustion calculations can sometimes be technically justified from one-dimensional models, such calculations are not used much because they are not relevant to heterogeneous propellants. Of course burning rates can be measured by a variety of methods.

4. The present modeling of transient combustion (one-dimensional) is essentially the same as it was ten years ago. Improvements are probably needed in modeling the high frequency response, as problems exist with combustion instability in low-smoke tactical rockets. However improvements have been slow because of lack of kinetic data on surface and gas phase reactions, inapplicability of 1-D models to heterogeneous propellants, and mistrust of experimental data available to evaluate models. On the other hand, the experimental results from T-Burner tests are widely used as a basis for combustor stability calculations.

5. Steady state burning of heterogeneous propellants has been a continuing topic of study, both experimental and analytical approaches being used. Most of the experimental work has been aimed at determining burning rates, and the effects of propellant and environmental variables on burning rates. Analytical models are based on the calculation of heat transfer rates from reaction zones back to the propellant surface (a one-dimensional representation). The propellant heterogeneity enters in through the calculation

of the effective distances of various exothermic reaction steps from the surface, a calculation based on assumptions and calculations of the microstructure of the combustion zone. Analytical modeling work has been at a relatively high level for several years. Recent advances in theory have mostly been concerned with "liberalizing" the assumptions about microstructure, primarily by inclusion of more versatile descriptions of particle size distribution. However these changes do not include much improvement in description of the state or configuration of the propellant burning surface and the real three-dimensionally complex interaction of gas phase flames and heat transfer with the surface. Further, experimental studies of these processes are also minimal. The vigorous modeling activities, lacking new experimental inputs, tend to become preoccupied with details and speculations.

6. Erosive burning is a phenomenon that has resisted decisive measurement and modeling, probably partly because engineering schemes for prediction have been good enough to invalidate the need for a more decisive attack on the problem. However the low level of progress in this area is also attributable to lack of sufficient knowledge of combustion zone microstructure, difficulty in laboratory scale simulation of the motor flow environment, difficulty in measuring burning rate under such conditions, and intractability of relevant analytical models of the combined combustion-flow process. Recently increased efforts have made significant progress in modeling the effect of flow field on combustion zone and microstructure. The models are necessarily less rigorous representations of combustion zone microstructures than the no-flow models because of the necessity to incorporate the complication of the flow field. Such experimental work as has been conducted is aimed at determining erosive burning rate itself, rather than at obtaining the information on combustion zone structure needed to improve the model. As always, experiments in laboratory scale apparatus raise doubts about adequacy of simulation of the rocket motor flow field.

7. Oscillatory combustion of heterogeneous propellants is a matter of great practical concern, and a logical extension of topic #4, with the added complication of a three-dimensionally complex combustion zone. It is helpful to discuss the topic in 2 parts, because the status differs markedly relative to them. The first part is called pressure-coupling, i.e., the dynamic response of the combustion to pressure oscillations. The other part is called velocity coupling, i.e., the dynamic response of the combustion to gases oscillating parallel to the burning surface. As one might anticipate by analogy with steady state burning, the state of knowledge of pressure coupling (analogous to pressure dependence of steady state rate) is much more advanced than the state of knowledge of velocity coupling (analogous to "erosive" burning). If for no other reason, this is due to the macroscopically one dimensional nature of the process in pressure coupling, as compared to the necessarily two dimensional nature of the process in velocity coupling.

Experimental methods and analytical models of pressure coupled oscillatory combustion have evolved continuously since 1956, with modern developments mainly extending the range of frequency and types of propellants whose behavior can be described. Measurements are costly and only semi-quantitative, being better for nonaluminized propellants than for aluminized ones. Analytical models have until recently been purely one-dimensional. The most recent efforts using statistical description of the combustion zone rely on one-dimensionalizations and steady state calculations at various points in the computational sequence, while failing to describe the transient three-dimensional behavior at the microscopic level. This latter aspect of the problem has thus far escaped experimental study as well. In general, experimental results at all levels have been from programs of limited scope in many laboratories without benefit of any standardized increments of propellant or test variables, so few generalizations can be made from experimental results (a JANNAF committee to establish standards was unable to gain acceptance). However results have been useful in selection of propellants for development motors that were expected or known to have combustor stability problems, and the test methods and services

were the product of combustion research teams.

The state of knowledge of velocity coupled combustion response is very poor indeed, although a matter of particular concern due to experiences in development programs. Valid analytical modeling is even more difficult than in the case of erosive burning, and the results of a valid model are in a form that is difficult to apply to motors (in effect, the model calculation has to be repeated at time intervals during burning in every motor, in combination with the charge geometry and internal ballistic equations of the motor) (see Appendix A). Models to date are few, complex, unevaluated, but clearly naive as far as relevance to behavior of ingredients of heterogeneous propellants and combustion zone microstructure are concerned. Further, velocity-coupled combustor instability has certain nonlinear characteristics that have proven to be very much a part of the difficulty in development programs, but singularly intractable in analytical modeling and in design of laboratory-scale simulation of motors. As in the case of erosive burning, the problem is to produce a flow field adjacent to the burning surface that simulates that in the rocket motor, except that in the velocity coupled instability experiment one must also simulate correctly the gas oscillations, and measure the effect of the combustion response on the oscillations. The so-called velocity-coupled T-Burner apparently does exhibit velocity coupled response, and can probably distinguish between propellants with high and low velocity-coupled response. However simulations of motor flow fields is very superficial, interpretation of test results is speculative, results are not very reproducible, and the method is currently usable only over a limited range of test variables. No serious effort has been made to explore experimentally the primary source of nonlinear behavior, which relates to the superposition of mean flow field and parallel-acoustic oscillations. An independent approach to measurement of velocity-coupled response, using a system with driven oscillations, is under development at one laboratory, and has some potential for better measurements in the frequency range where the T-Burner is least satisfactory (low frequency).

8. Transition from Deflagration-to-Detonation is the combustion topic under most intensive study, and the most complex one. The phenomenon involves dynamic mechanical failure of the propellant as much as it involves combustion. In addition, it involves extremely high pressures and short times, so that it is not clear what chemical steps actually have time to participate in transition. Analytical modelers are confronted with analysis that bridges the domain from classical diffusion-controlled combustion to shock propagated detonation; an analysis that is almost prohibitively difficult for a pure detonable liquid or pre-mixed gas. Given the added complications of a heterogeneous, chemically complex solid with possible porosity, it seems unlikely that any comprehensive solution of the problem will be achieved. Under these conditions the analytical modelers can run wild solving dozens of simplified models, while critics can show that the models are patently naive. Ultimately, an integrated program of analysis and experiments must emerge, that establishes and models the key aspects of the phenomenon and identifies what properties of practical propellants prevent an accelerating reaction front. Progress in research is limited not only by the difficulty of identifying the key processes to study and model, but also by the difficulty of designing and conducting corresponding experiments (complicated further by hazardous materials and the risk of, or need for detonations).

It is not intended to summarize here the status of research and knowledge on the topic of DDT, which is still somewhat primitive. However some points merit particular note:

- a) To the extent that mechanical degradation of the solid propellant under dynamic loading is involved, the theory is in very bad shape for heterogeneous materials (put more charitably, a relevant theory is incredibly complex).
- b) The high temperatures and rapid changes involved during the accelerating and "shock building" phase of transition probably invalidate the use of conventional combustion concepts such as "ignition" and "burning rate", which are still used by modelers.
- c) It is not clear what chemical reactions actually have time to

contribute to the acceleration of reaction (a more fundamental statement of (b)).

d) It is not yet clear whether transition can occur in a practical propellant without prior mechanical degradation, leaving unclear the issue of the kind of processes to include in design of experiments and analyses.

#### 1.4 Approach in Present Investigations

In the present program, propellant combustion has been studied by examination of:

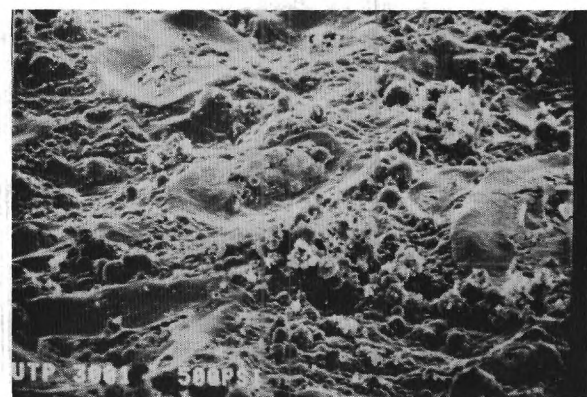
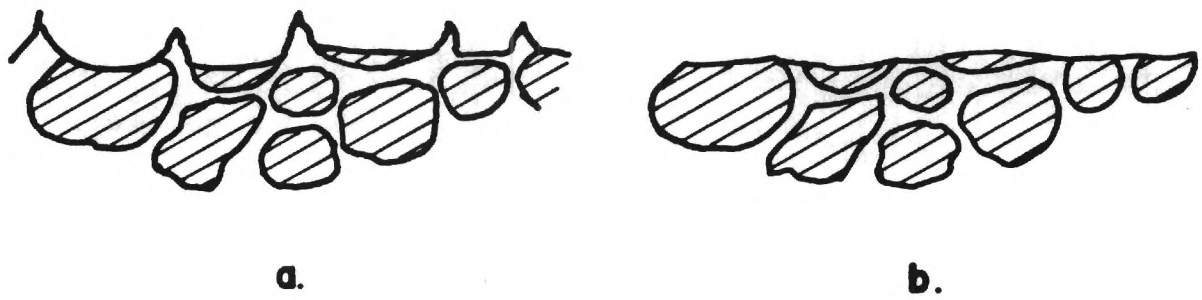
1. Physical, chemical and combustion behavior of propellant ingredients at elevated temperatures.
2. Similar behavioral studies of ingredient combinations.
3. Suitable means to describe the microstructure of a heterogeneous propellant and its burning surface.
4. Structure of the combustion zone of heterogeneous systems.
5. Analytical modeling of ideal systems.
6. Combination of the results in models most appropriate for their application (e.g., representation of perturbation response to pressure, velocity; erosive burning; role of ballistic modifiers; a context for description of surface accumulation as with aluminum).

There is nothing particularly novel about this strategy, but in many critical respects past work has been indecisive, leaving the objectives of understanding and valid description of propellant combustion in a speculative state. The investigations reported here were designed to answer outstanding questions of understanding or of validity of modeling. While gravely constrained by the difficulties of designing relevant and tractable experiments and analytical models, some progress in development of experimental methods is reported, and results of experiments and analysis show some microscopic and transient aspects of the combustion process that are important in propellant combustion but neglected in past work.

## THERMAL DEGRADATION OF PROPELLANT BINDERS

In most models of the combustion of heterogeneous propellants, it is assumed that the binder is degraded from a solid to a gas in place, with the geometry of its exposed surface regressing in accordance with the local heat transfer to produce gasification temperatures (Figure 1a). The heat to the complex array of binder is supplied by a coupled, complex combination of exothermic reactions in the oxidizer and/or gas phase. In analytical models, the geometrical details of this coupled process are ignored, and the binder surface is assumed to be flat, with a regression rate of the propellant (Figure 1b) (without any argument as to why the surface would be flat). In practice, burned surfaces of propellants (quenched by various means) exhibit complicated surface configurations, with the details depending on the types of binder and oxidizer, combustion pressure, nature of gas flow adjoining the burning surface (e.g., Figure 1c). These details of the combustion process have not been determined systematically, and their importance is unknown (omission from combustion models is more a matter of simplification of mathematics and ignorance of details than physical justification).

In order to better anticipate or explain the role of binder in the combustion zone process, it is natural to explore the response of the pure binder material to heating in the temperature range characteristic of the propellant burning surface (up to several hundred degrees C). Such experiments have been done in the past, using combustion of samples, pyrolysis by radiant energy, and electrical heating of samples. Observations included photography, thermal-gravemetric measurements, differential scanning calorimetry, etc. Prior experience in the present program had indicated that "melting" and flow of the binder might play an important role in propellant combustion (the term is used to refer to a state of the binder and/or intermediate decomposition products that will flow). Accordingly it was decided to use a hot stage microscope to observe the physical state and activity of binder samples during heat-up to  $1200^{\circ}$  C. Tests were done at atmospheric pressure in air, oxygen and argon atmospheres with vapor



(c)

Figure 1. Burning surface profiles.

- (a) Typical profile at pressures above 6 MPa (AP-HC propellants)
- (b) Surface profile typical of analytical models
- (c) Burning surface after quench by rapid depressurization  
(UTP 3001 propellant, AP-HC-A1)

products flushed by the control gas flow. Visual observations were recorded. Five different hydrocarbon binders were used.

A typical test required about 60 seconds to reach 600° C and was continued to 1000 to 1400° C. All binders showed some degree of internal gasification with a boiling-like behavior indicative of fluidity. With increasing temperature, this evolves into a tar-like (usually discolored) substance of less volume than the original sample, which vaporizes as temperature increases further, leaving a modest residue of char-like material. In an oxygen atmosphere the gasifying tar ordinarily ignited at about 600° C, while the one binder that gasified at lower temperature did not ignite. In the fluid stage, the different binders showed significantly different degrees of fluidity. Two binders yielded a small amount of thermally stable, clear liquid at 1000° C, but only when heated in oxygen. Details of the results were reported in Reference 5, and are summarized in Figure 2. The binders used in these tests were used also in other experiments summarized in later parts of this report, and imply that surface temperatures of the rapidly heated binder in the propellant combustion zone may be as high as 600+ degrees C, with gas evolution and melt properties at much lower temperatures. Polysulfide binder decomposed at the lowest temperature with the least melt; polyurethane produced the most melt; PBAN and HTPB binders produced the most extensive melts, with PBAN melt being the most fluid. The clear liquid residue formed by HTPB and CTPB in oxygen atmospheres still persisted (although in diminished amount) at 1400°C. Collectively, the results suggest that the fluid state of the binder or its intermediate products will ordinarily be present on the propellant burning surface to high temperatures, with polysulfide being an exception.

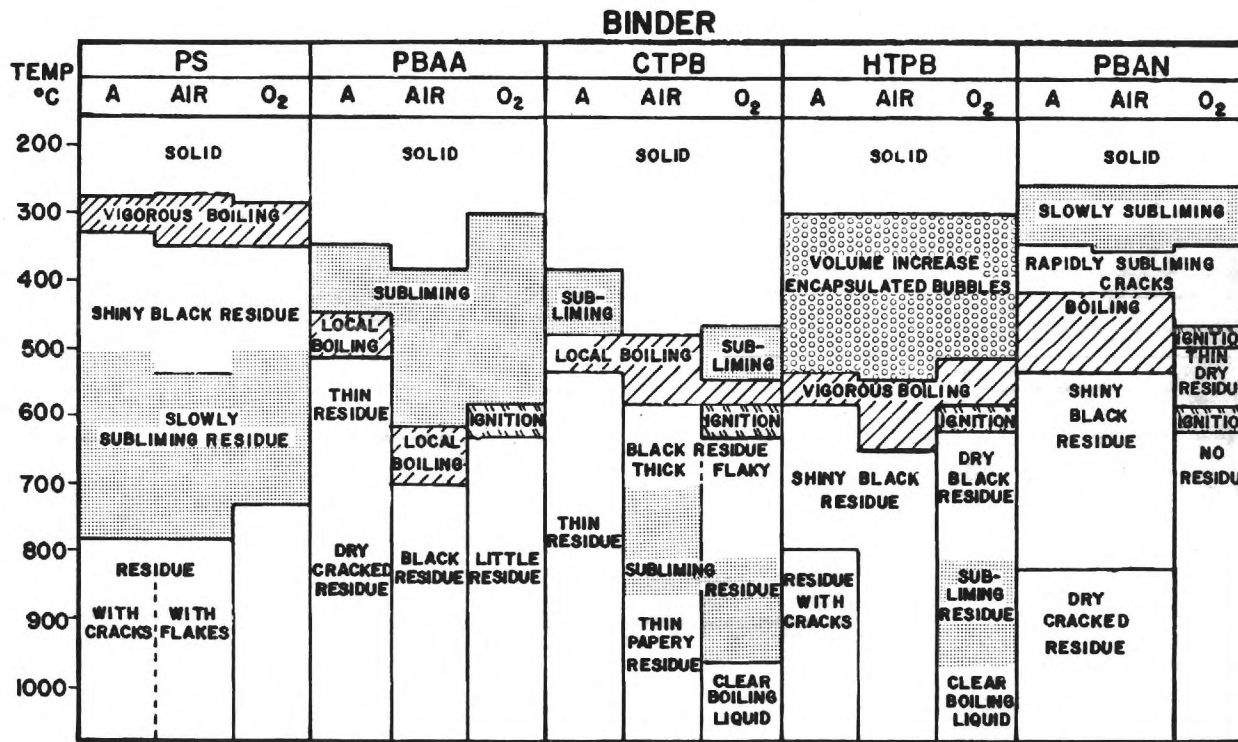


Figure 2. Thermal decomposition of binders. Summary of results from hot stage microscope tests.

## SANDWICH BURNING

### 3.1 Introduction

If one is seeking understanding of combustion or a comprehensive basis for its control, a composite propellant is a remarkably difficult object for study. Not only is it very costly to make up samples with systematic changes in relevant variables, but the resulting samples are of chaotic character on a microscopic (<1 mm) scale. Given the unavoidable difficulties of producing, and making time-resolved observations of a microscopic subject in a hostile environment, the added problems of sample preparation and characterization have severely limited progress in research, and it is not surprising that investigators have resorted to other, more controllable and/or inexpensive schemes for preparing test samples. One of these is the ingredient "sandwich" illustrated in Figure 3. Alternate sheets of propellant ingredients are laminated together, and burned edgewise. Such a configuration has the advantages of

1. Low cost
2. Control over microstructure and placement of ingredients
3. Relative ease of observation during burning
4. Ordered structure that qualitatively establishes the structure of the combustion zone
5. Relative amenability of processes to analytical modeling (2-dimensional steady state behavior)

It is these attributes that have motivated the use of sandwiches in past and present investigations of propellant combustion mechanisms.

### 3.2 Combustion Zone of AP/HC Sandwiches

The details of sandwich combustion are suggested by Figure 4. Sandwiches are ordinarily ignited on the top edge, and side burning is avoided by a modest flow of nitrogen, which also minimizes recirculation of combustion products in the line of sight of combustion photography. Above its self-deflagration pressure limit, AP has an exothermic decomposition flame (②, in Figure 4), and a thick AP lamina will burn independently

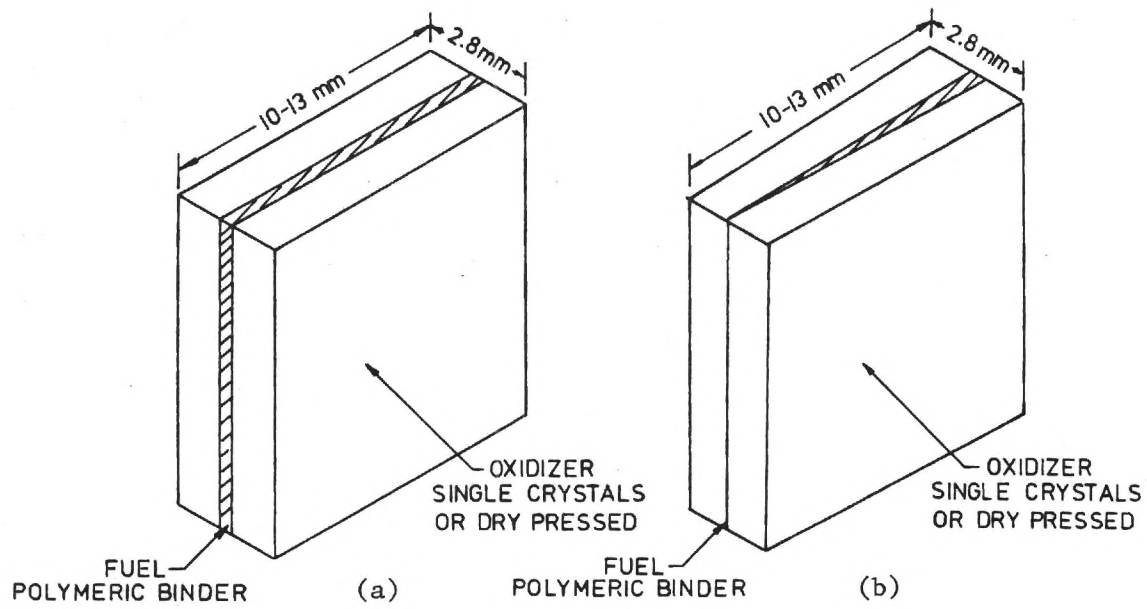


Figure 3. Sketch of AP-binder-AP sandwiches  
 (a) Conventional  
 (b) Tapered

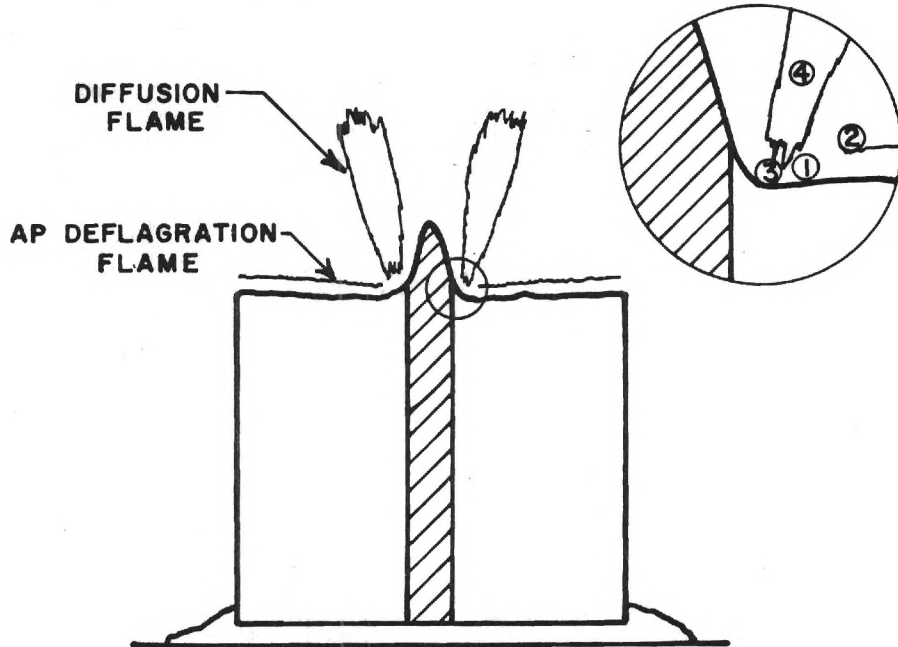


Figure 4. The combustion zone structure of an AP-HC sandwich  
 (profile typical of pressure 5-10 MPa).

of the binder (Figure 5a). Near the binder-AP interface, a diffusion flame occurs between oxidizer and binder vapors (③, ④ in Figure 4). The binder lamina, which decomposes endothermally under the influence of the diffusion flame, tends to protrude and may even divide the combustion region into two halves (especially if conditions are unfavorable for pyrolysis of the binder). Anything that selectively enhances the rate of the AP-binder reaction tends to accelerate the surface regression in the vicinity of the interface, giving a profile like that in Figure 5b. At pressure below the AP deflagration limit, the AP pyrolysis, like the binder, is supported by the diffusion flame. In this case the AP burning surface lags the interfacial region just as the binder does (Figure 5c). Depending on details of the situation, the burning may simply proceed down and leave a slot, or the surface will develop into a deep V-shaped contour (see later).

This simplistic description of sandwich burning is consistent with current understanding of the decomposition-deflagration characteristics of the binder and AP, and with most of the current literature. However, there are difficulties on both the microscopic and macroscopic scale that must be resolved to fully understand sandwich burning and its relation to combustion of solid propellants. These difficulties are addressed in the following.

### 3.3 Classification of Sandwiches and Expected Behavior

As one may observe in Figure 4, sandwich burning is characterized by several exothermic reaction steps that "drive" the combustion. AP oxidizer burns as a monopropellant (above about 20 atm), with exothermic reaction at the surface, and in a decomposition flame in the gas phase. These heat sources are augmented by the diffusion flame between binder and oxidizer vapors. The locations of these heat sources were denoted in Figure 4 by the number inserts 1-4. The way the sample burns is determined by the return of heat to the solid surface to support continued pyrolysis. This in turn depends upon the location of the exothermic reaction sites, the relative amount of heat release in each, and the overall stoichiometry of the sample (amount of heat release compared to amount

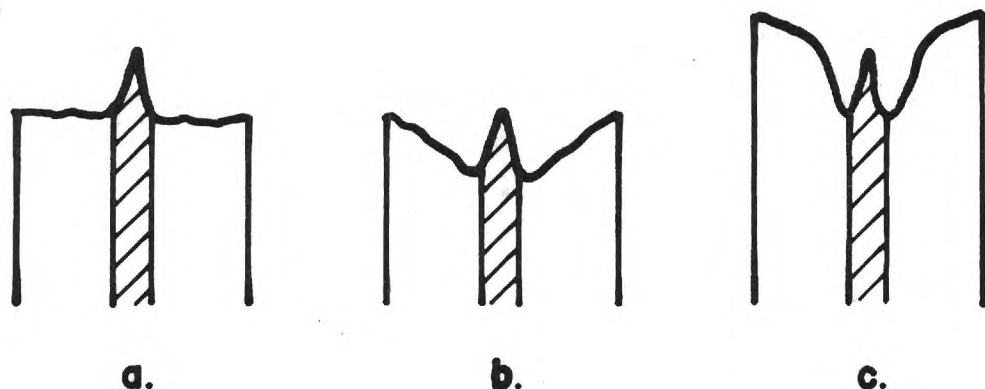
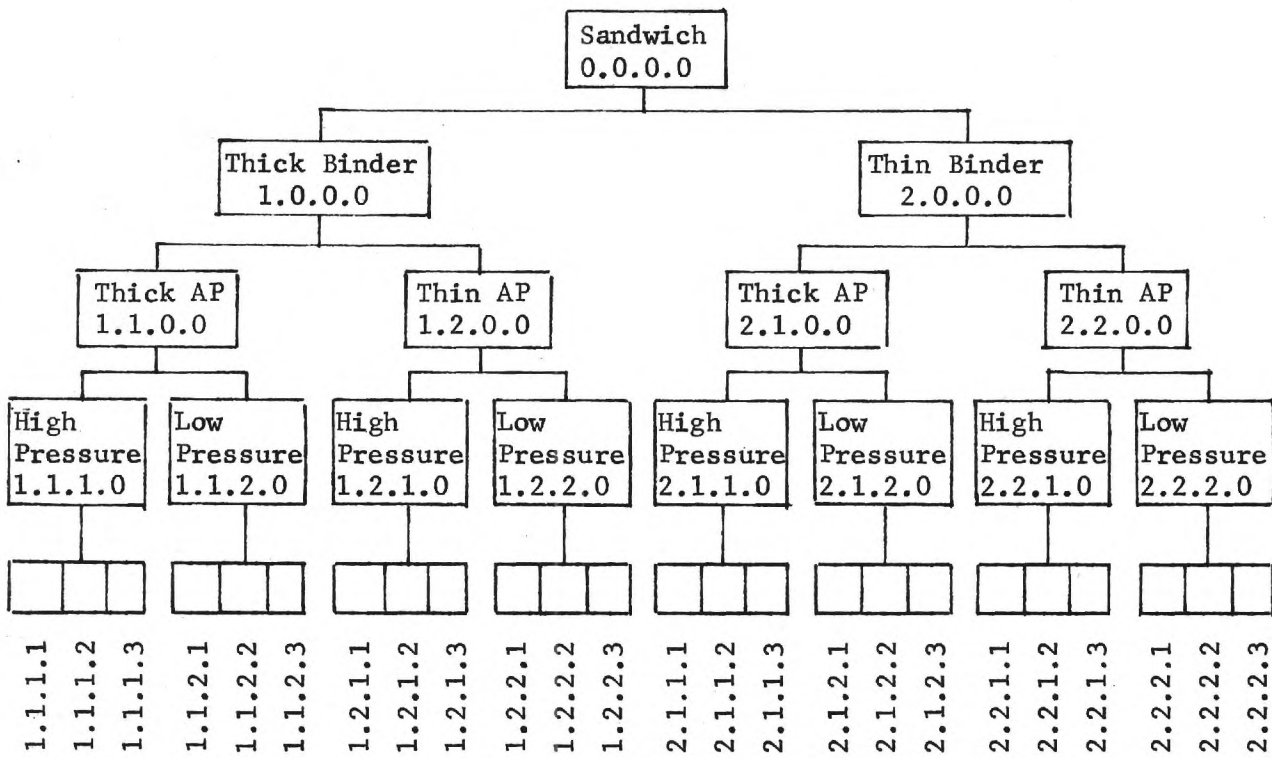


Figure 5. Surface profiles of burning sandwiches of AP and HC binders.  
 (a) AP deflagration dominating deflagration (typical of elevated pressure, e.g. 10 MPa)  
 (b) AP deflagrating, but regression rate enhanced by diffusion flame contribution (typical of medium pressures, e.g. 4 MPa)  
 (c) AP won't deflagrate without heat input from the diffusion flame (typical of low pressure, e.g. < 2 MPa)

of heat required for heat-up and pyrolysis of the solid).

The configuration of the burning surface of sandwiches has been somewhat stereotyped in the past according to Figure 5a or Figure 5c, where 5a is typical for self-deflagrating oxidizers and Figure 5c is for oxidizers that require heat from the diffusion flame to maintain gasification (this includes AP at low pressures). In terms of propellant combustion, these classifications are superfluous, because they refer to samples with thick binder and oxidizer layers that are not typical of propellants, and they describe the overall appearance of those samples. At the very least, consideration should be directed to the details of surface geometry near the oxidizer-binder interface, and in that region, consideration needs to be given to whether a thick binder layer is causing flooding by molten binder, and to the localized effect of the diffusion flame near the interface.

In the interest of more objective observation and reporting of present and future results, a scheme of classification of sandwiches is proposed in Figure 6. In this categorization, all samples are first divided into two groups according to whether the binder is thick or thin, where "thin"



n.0.0.0 Binder Thickness

0.n.0.0 AP Thickness

0.0.n.0 Pressure (relative to AP deflagration limit)

0.0.0.n Binder Pyrolysis Characteristics

0.0.0.1 Heat resistant, nonmelting binder

0.0.0.2 Binder with thermally stable melt

0.0.0.3 Easily gasified binder, minimal melt

Figure 6. Classification of sandwich burning experiments.

Chart designed for self-deflagrating oxidizer, with "low pressure" referring to below the self-deflagration pressure and "high pressure" to conditions above the limit. For the time being, "thick" binder refers to thickness compared to that region of the surface in which presence of the binder affects the regression front of the oxidizer at pressures above the deflagration limit of the oxidizer.

means comparable to structural elements of binder in propellants (e.g., 2-20  $\mu\text{m}$ ). These categories 1 and 2 are each divided into two more depending on whether the oxidizer layer is thick (1.1 and 2.1) or thin (1.2 and 2.2). In the present work, the terms "thick" and "thin" oxidizer refer to overall sample stoichiometry, with thick oxidizer meaning oxidizer-rich. The third categorization (third digit of the classification number) refers to whether the oxidizer self-deflagrates or not (In the classification diagram this is referred to as high and low pressure, because we were concerned with AP oxidizer). The fourth categorization (see diagram and 4th digit) refers to the melt-gasification characteristics of the binder. Using this categorization of sandwiches, their burning behavior can be more comprehensively categorized as in the following.

Looking first at sandwiches with thick binder (categories 1.0.0.0, Figure 7, top), the binder tends to protrude and divide the primary part of the diffusion flame into two flames that proceed relatively independently of each other. These flames will extend beyond the binder and merge if the overall stoichiometry of the sample is not too fuel-rich (thick AP, case 1.1.0.0). If the stoichiometry is fuel-rich, (case 1.2.0.0), the flames will not merge and the fuel protrusion will increase progressively during burning. If the pressure is high (1.1.0.0, 1.2.1.0), the oxidizer will recede ahead of the fuel protrusion (Figure 7), while low pressure (1.1.2.0, 1.2.2.0) will lead to protrusion of the oxidizer as well as the fuel. The extent of the AP protrusion will be less with thin AP (fuel-rich stoichiometry, 1.2.2.0).

When the binder is thin (lower row, Figure 7), it does not protrude because it is so easily pyrolyzed. Accordingly the two diffusion flames are not distinguishable (most work reported in previous literature does not correspond to this thin binder situation, although propellant combustion does along most of the exposed oxidizer-binder interfaces on the burning surface). At high pressure (2.1.1.0 and 2.2.1.0) the AP recedes with the binder, but at low pressure the AP recedes less rapidly and protrudes (2.1.2.0 and 2.2.2.0). In the thick oxidizer case (2.1.2.0), the oxidizer-binder interface region burns down to form a groove, the fuel being insufficient to react with the oxidizer excess (samples of this type often will

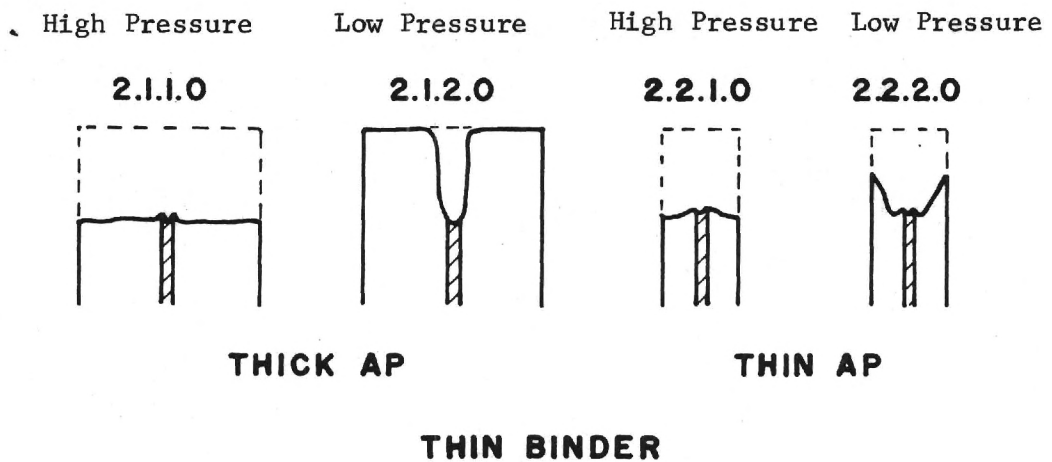
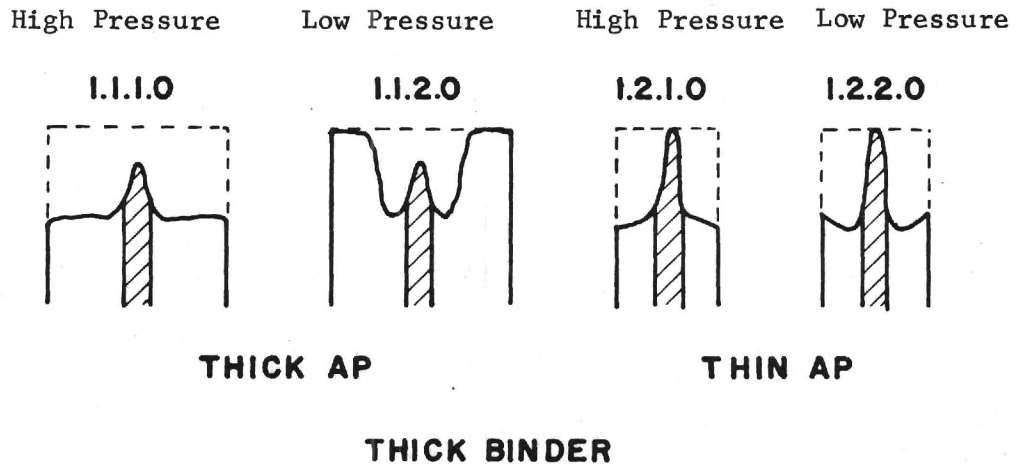


Figure 7. Burning surface profiles corresponding to the classes of sandwiches in Figure 6.

not sustain burning). With thinner oxidizer and low pressure (2.2.2.0), the oxidizer protrusion is present but not so conspicuous because the sample is nearer to stoichiometric overall.

Much of the results of early work on sandwich burning (of AP/HC samples) can be anticipated on the basis of the foregoing classification scheme, and some apparent contradictions can be rationalized in that framework. As experimental methods are improved, many more detailed aspects of combustion behavior become evident, such as the observation of characteristic surface patterns on the AP with evidence of reacting surface melts; flow of binder melt onto the AP surface; accumulation of ballistic modifiers on the AP surface; and non-stationary (intermittent) behavior of the diffusion flames. Perhaps most significant, the behavior in the vicinity of thin binder laminae ( $< 50 \mu\text{m}$ ) has proven to be very complex. Since this is the dimensional domain relevant to propellant combustion, the present research has gradually turned to that domain. This has proven to be a much more difficult domain to study.

### 3.4 Scope of Current Investigations

The objective of sandwich burning in the present research was to determine the effect of binder thickness, type of binder, and pressure on the details of combustion zone behavior. In addition to determining burning surface profiles, the investigations sought to determine the effect of binder melt flow, and the unsteady nature of the diffusion flame. Experimental methods consisted primarily of high speed motion picture photography, and interrupted burns followed by microscopic examination. Binder thickness effects were investigated by burning the tapered edge of "tapered sandwiches," in which the thickness of the binder (as viewed on the burning edge) was graduated from about  $10 \mu\text{m}$  at one edge to about  $150 \mu\text{m}$  on the opposite edge (all samples were of this form unless otherwise specified). The combinations of kind of binder and combustion pressure are shown by the test matrix in Table 1. The shaded boxes in the matrix indicate quench tests in which results were not obtained or were compromised by experimental difficulties. The cross-hatched boxes indicate conditions that were not

Table 1. Tests on Tapered Sandwiches

	1.38 MPa		4.14 MPa		6.89 MPa		13.8 MPa	
	QUENCH	MOVIE	QUENCH	MOVIE	QUENCH	MOVIE	QUENCH	MOVIE
PS	1	2/2	1	2/2	2	1/2	1	0/3
PBAN	1	3/4	1	2/3	1	3/4	3	1/3
CTPB	1	1/1	1	1/1	1	1/1	1	0/1
HTPB	2	4/4	2	3/3	3	3/3	4	0/1
PBAA	1	1/1	1	0/1	1	0/1	1	1/1
Mica								

tested. For each pressure there is a column for indicating quench tests and a column for indicating photographic tests. From the test results, observations were made on a number of basic aspects of the combustion zone. The results are described in the context of these details.

### 3.5 Interface Profile and Melt Flows

Sandwich burning studies reported in the early 1960's stated that the leading edge of the burning front was at the binder-oxidizer interface (Figure 8a), a result that was used by some investigators to support an argument that burning rate was dominated by heterogeneous reactions at the interface. However more careful experiments showed (Reference 6) that the leading edge was never at the interface (AP oxidizer), but was usually on the oxidizer surface not far from the interface (e.g. 50-500  $\mu\text{m}$ ) (Figure 8b). It was assumed that the binder, being a heat sink, lowered the temperature of the AP near the interface enough to retard its deflagration. However the diffusion flame preferentially heats this same region, so that no presumption can be made about dominance of these two opposing effects.

An analytical model of combustion in the interface region (Reference 7) indicated that the oxidizer surface should regress uniformly to within a few microns of the interface, at which point the AP surface would lead slightly due to heat transfer from the diffusion flame via the binder (Figure 8c). Since this was contrary to the observed results, it was speculated that the binder melt flow (observed in many quench tests) was retarding the AP deflagration at the interface. Accordingly, samples were made in which the oxidizer lamina was formed by dry-pressing AP powder on sheets of concrete and of mica. The samples were burned and quenched (Table 1) at burning pressures high enough to burn without fuel (6.9 MPa, 1000 psi). The quenched samples with concrete sheets in place of binder crumbled during burning; the samples with mica sheets burned normally and gave good quench samples (except for some delamination within the mica). The quenched samples exhibited surface profiles that were flat all the way to the interface, except for the usual formation of surface patterns over the entire AP surface (Figure 9). Since the typical dimension of irregularity

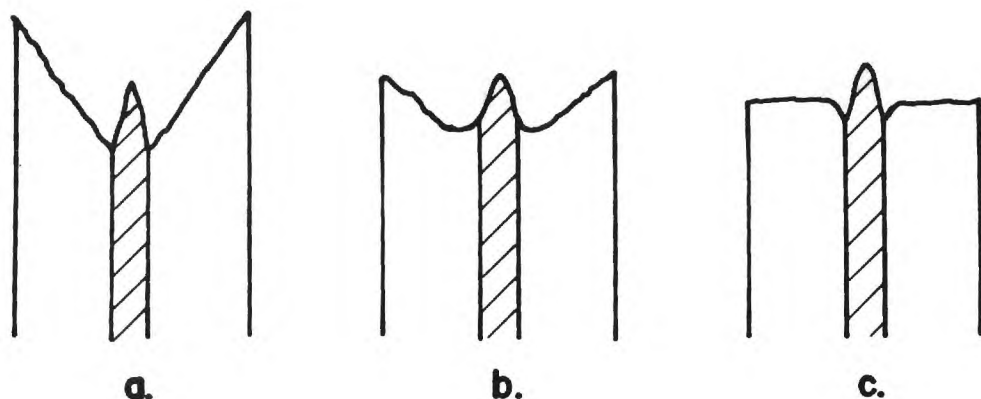


Figure 8. Different leading edge-interface profiles postulated in earlier work.

- (a) Early descriptions of profile, probably relevant with endothermic oxidizers (e.g., KP)
- (b) Generally accepted (1979) profile for AP
- (c) Prediction of 2-D model without binder encroachment on AP surface

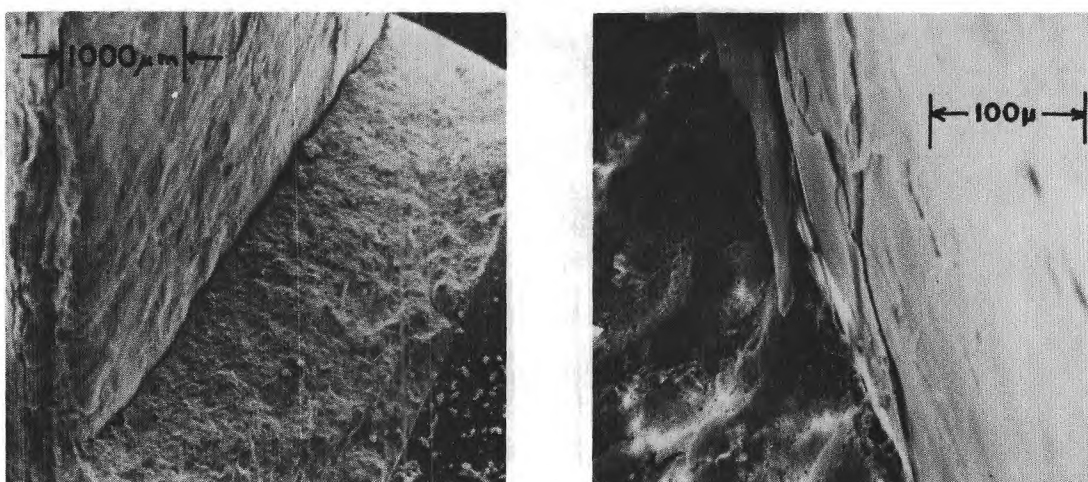


Figure 9. Surface of quenched AP-mica sandwich burned at 6.9 MPa. Note AP surface detail remains typical all the way to the mica interface (a delaminated flake of mica obstructs the interface at upper end).

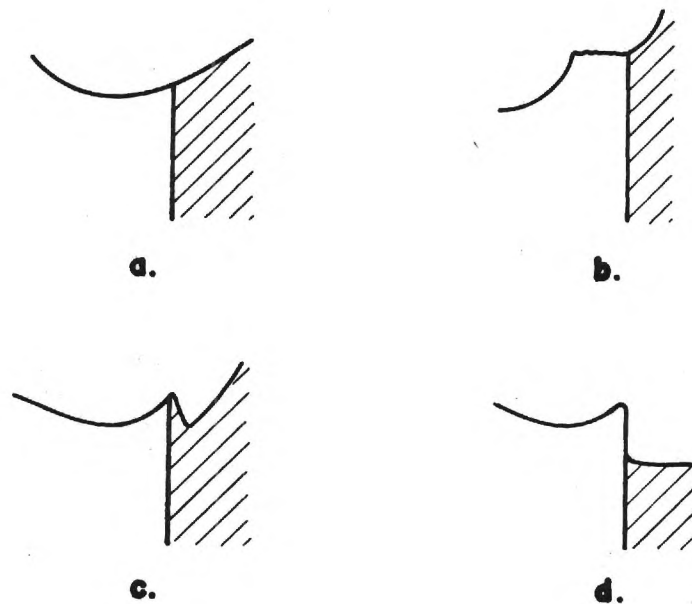


Figure 10. Profiles of quenched surfaces of sandwiches, illustrating details near the interface.

- (a) Typical of AP-HTPB at 4.1 MPa (binder thickness  $> 70 \mu\text{m}$ )
- (b) Typical of AP-PBAN binder at 13.8 MPa (binder thickness  $> 70 \mu\text{m}$ )
- (c) Typical of AP-HTPB binder at 4.1 MPa (binder thickness  $\sim 50 \mu\text{m}$ )
- (d) Typical of AP-all binders at 1.4 MPa (binder thickness  $< 25 \mu\text{m}$ )

of the surface patterns is comparable to the dip in the AP surface at the interface predicted by the two-dimensional model, it was not possible to verify this prediction of the model. However both this result and the model imply that the typical retarded regression near the interface in AP-binder sandwiches is due to binder melt flow or other influence of the binder. It should be noted that melt flow (as judged from quenched samples) occurs on a dimensional scale of the same order as oxidizer particle sizes in propellants, raising the question of the possible importance of melt flows in propellant combustion. Accordingly, it also suggests that the melt characteristics of the binder are important. Investigation of these questions is continuing.

Recent results with tapered, thin-binder sandwiches have revealed a variety of profiles adjoining the interface (illustrated by sketch in Figure 10). These will be discussed in appropriate context in following

sections. However, the following generalizations can be made:

1. With the relatively thick AP laminae used in the present work, most of the quenched AP surface looks like that of AP samples tested without binder laminae (i.e., above the AP low pressure deflagration limit). The surface exhibits characteristic undulations, and froth-like residue (reported in many references, e.g. Reference 8).
2. There is always a region of the AP surface adjoining the interface where the surface is relatively smooth (Figure 11, 12; see also later figures).
3. The smooth surface often exhibits obvious flow patterns, especially near and across the interface (See later figures.).
4. The surface effects extend for 10-200  $\mu\text{m}$  from the interface, sometimes further.
5. Regression of the AP surface is retarded in the smooth-surface region (Figure 10, 11). As a corollary, the surface regression in the AP is higher in the region just beyond the smooth region. The regression is usually highest there,\* suggesting the importance of the AP-binder flame on burning rate (below about 6.9 MPa, 1000 psi).
6. The surface effects 2-5 are absent when the binder is replaced by mica (Figure 9).

It is premature to say whether the smooth-surface band adjoining the interface is due simply to melt flow, although the evidence is very strong that part of the band nearest the binder lamina originates as flow from the binder. The outer portion of the band may reflect the (as yet undetermined) process by which binder-coated AP decomposes, or may reflect AP decomposition modified by diffusion of gaseous species from the binder or the leading edge of the diffusion flame. Given the fact that the leading edge of the AP deflagration front is apparently caused by the added heating resulting from thermal diffusion from the oxidizer-binder gas flame, it is reasonable to postulate that chemical species from that flame can also diffuse a comparable distance and modify surface processes.

---

\* The meaning of "highest" becomes unclear in profiles such as Figure 10 c, d.

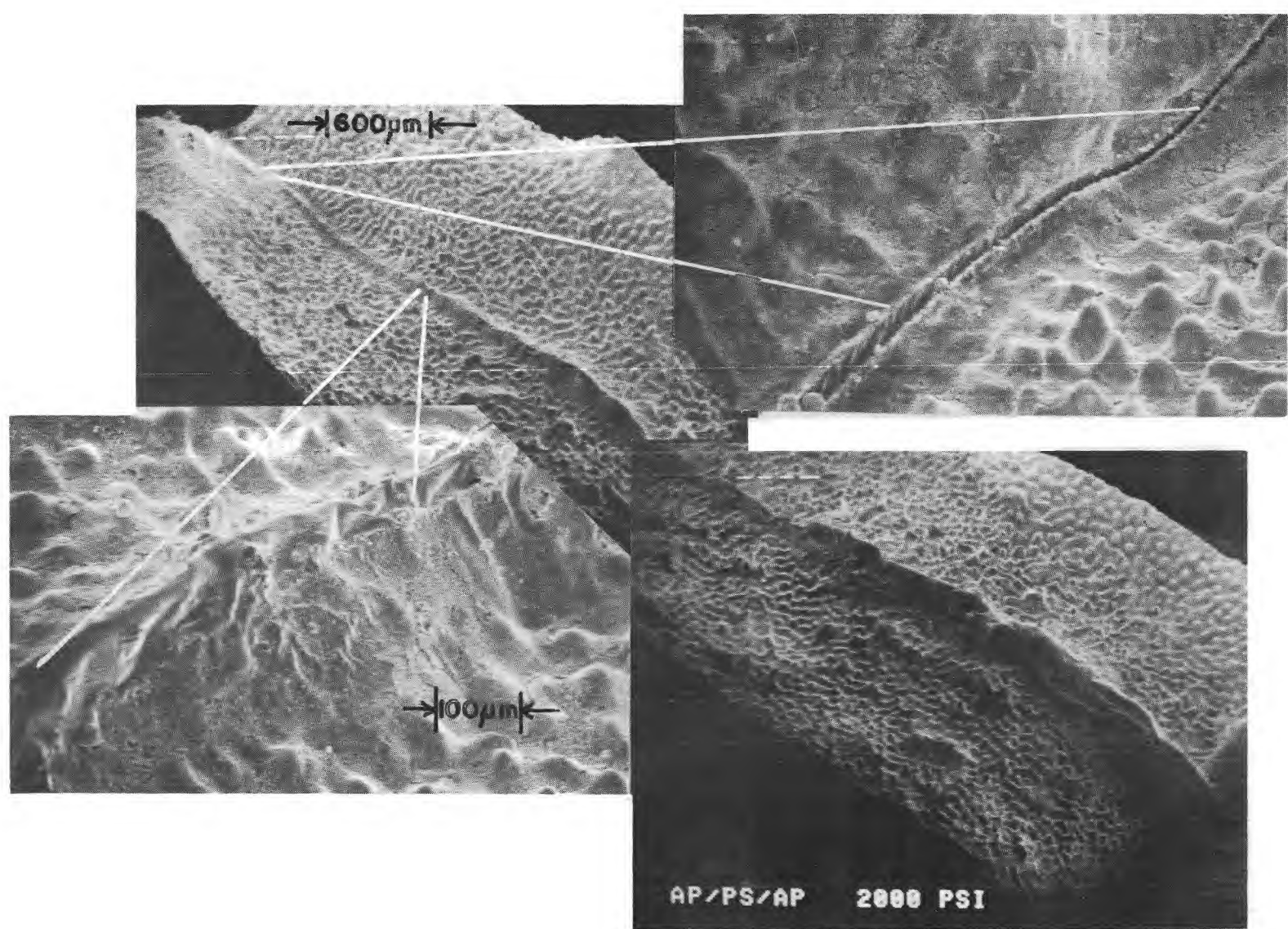


Figure 11. Surface of a quenched tapered sandwich, showing burning surface detail and profile. Sandwich was AP-PS binder, burned at 13.8 MPa. Thick binder at lower right.

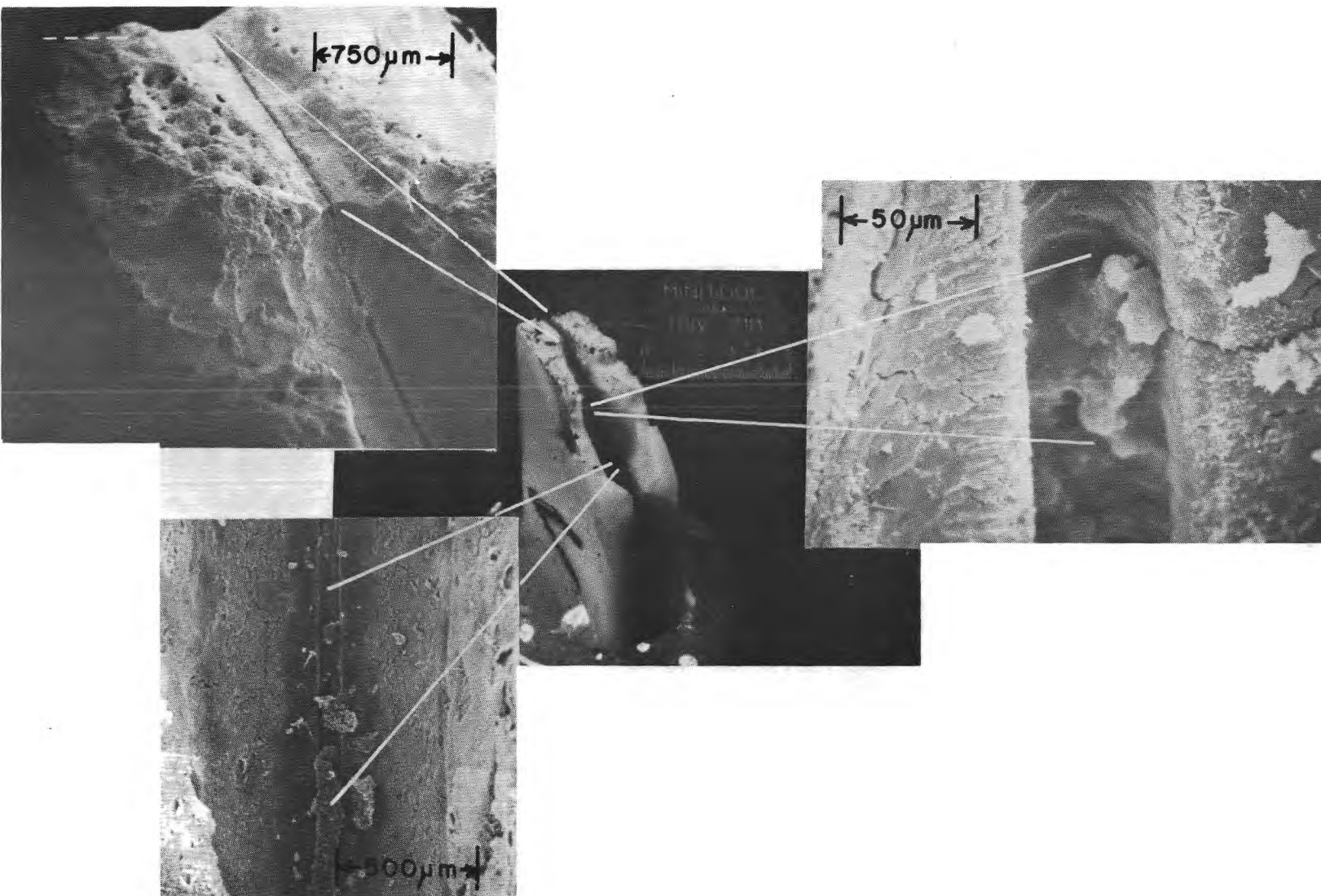


Figure 12. Surface of quenched sandwich showing effect of low pressure and binder thickness on the burning surface profile. This is an example of an AP-PS sandwich partially burned at 1.4 MPa.

Perhaps the most important point merits repetition, i.e., that relative to real rocket propellants, the surface distances involved in the smooth-band phenomenon are of the same order as oxidizer particle size in propellants. This implies that deflagration of oxidizer particles may be materially affected by binder behavior and diffusion flames, and in a way dependent on distance from the particle periphery and possibly in a fluctuating, time dependent way. The implication of these observations relative to effects of particle size on steady and oscillatory burning should be noted. It is also worthy of note that the retardation effect on burning rate can be quite large at high pressure (Section 3.7, with profiles as in Figure 10b).

### 3.6 Binder Thickness

As suggested in the earlier classification system for sandwiches (Figure 6), binder thickness is an important factor in how sandwiches burn. Most investigators have used thicknesses that are an order of magnitude larger than the thicknesses in high-solids heterogeneous propellants. This has the effect of placing most of the diffusion flame at a relatively large distance from the burning surface, excepting that region close to the oxidizer-binder interface. Accordingly, it is probably worth repeating that only that region of the surface located near the interface experiences propellant-like conditions. Further, even that region may be influenced by behavior further out from the interface that is not typical of propellants (for example, by abnormally large melt flow from a thick binder layer).

In the present work, the effect of binder thickness was investigated by testing "tapered" sandwiches (Figure 3) under the conditions in the test matrix of Table 1. The general trend of behavior is in accordance with class 1.1.1.0 and 1.1.2.0 samples (Figure 6, 7: thick binder-thick AP-high and low pressure), with a transition to class 2.1.1.0 and 2.1.2.0 samples (thin binder-thick AP-high and low pressure) towards the thin-binder end of the sample.

The thick binder ( $100-150 \mu\text{m}$ ) end of the samples yielded nearly flat AP with binder protruding in varying degree with evidence of binder melt

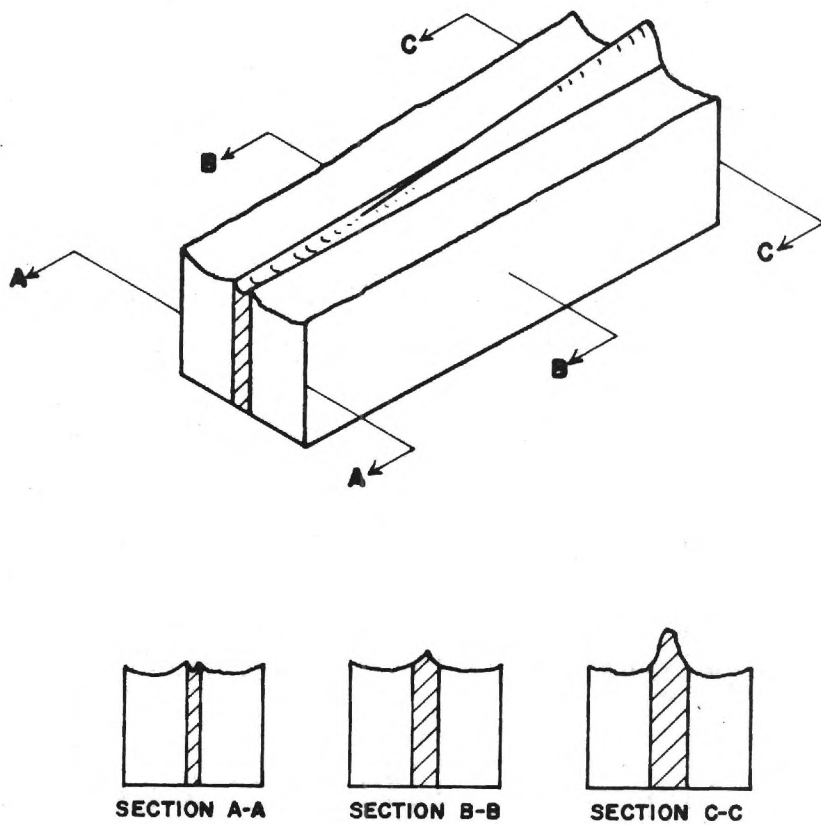


Figure 13. General trend of surface profile with binder thickness.

flow (high pressure tests, e.g., Figure 11c, category as in Figure 7 - 1.1.1.0); or burning into a deep, relatively flat bottom groove in the AP with minimal binder projection (low pressure tests, e.g., Figure 12, category as in Figures 6 and 7, 1.1.2.2, 1.1.2.3).

The thin binder (10-15  $\mu\text{m}$ ) end of the samples yielded nearly flat AP with binder flat or recessed (high pressure tests, e.g., Figure 11, category as in Figures 6, 7 - 2.1.1.0); or burning into a deep groove in the AP with binder recessed sharply below the AP (low pressure tests, e.g., Figure 12, category as in Figures 6, 7 - 2.1.2.0, and Figure 10d). Burning would not sustain at low pressure with very thin binder.

To the extent that generalizations can be made, the trends with binder thickness are summarized by the sketch in Figure 13 (which is drawn to correspond to a pressure of 4-5 MPa). "Thick" binder tends to protrude

and give a melt flow across the binder/AP interface, the extent of these features depending on binder characteristics and pressure. As one proceeds to thinner binder, the protrusion and flow are less conspicuous, and regions of the binder profile sometimes extend below the interface AP. With binder thickness less than about 30  $\mu\text{m}$  (or greater thickness at low pressures), the binder is completely recessed below the adjoining AP. As noted in Section 3.5, the AP profile is inclined upward toward the interface plane, and this was true at all binder thicknesses and pressures tested. This up-sloping surface always exhibited relative freedom from the frothy characteristic of the rest of the AP surface (Figures 11, 12, 14-17), often showing initial markings suggestive of melt flow from the binder.

The general trends with lamina dimensions and pressure were in accord with the arguments leading to Figure 7, provided one makes allowances for the binder properties (the fourth digit in the sandwich categorization scheme in Figure 6). However, there are some features of the behavior that go beyond the basis of Figures 6 and 7. Most notable was the demonstration of a binder thickness-dependent low pressure deflagration limit (Figures 12, 14). At 1.4 MPa, sandwiches were difficult to ignite, and did not burn the thin-binder end of the sample (that portion with binder thickness less than 25  $\mu\text{m}$ ). This pressure is below the deflagration limit of the AP alone, and the diffusion flame apparently cannot supply enough heat to sustain losses and pyrolysis of the AP and binder. Interpreted in the context of a propellant surface, this result provides some understanding of the typically high dependence of burning rate on pressure and particle size at low pressure, and the high dynamic response during oscillatory flow.

The flamelets are not only unstable individually, but also collectively.

### 3.7 Comparison of Binders

As noted in Section 2, the propellant binders used in this program have observable differences in thermal decomposition behavior, with the polysulfide binder being most distinctive because of its low decomposition temperature (approximately 200° C lower than the others, Figure 2). As noted in the test matrix, tapered sandwich tests were run with these binders at several pressures. The collected test results show significant differences.

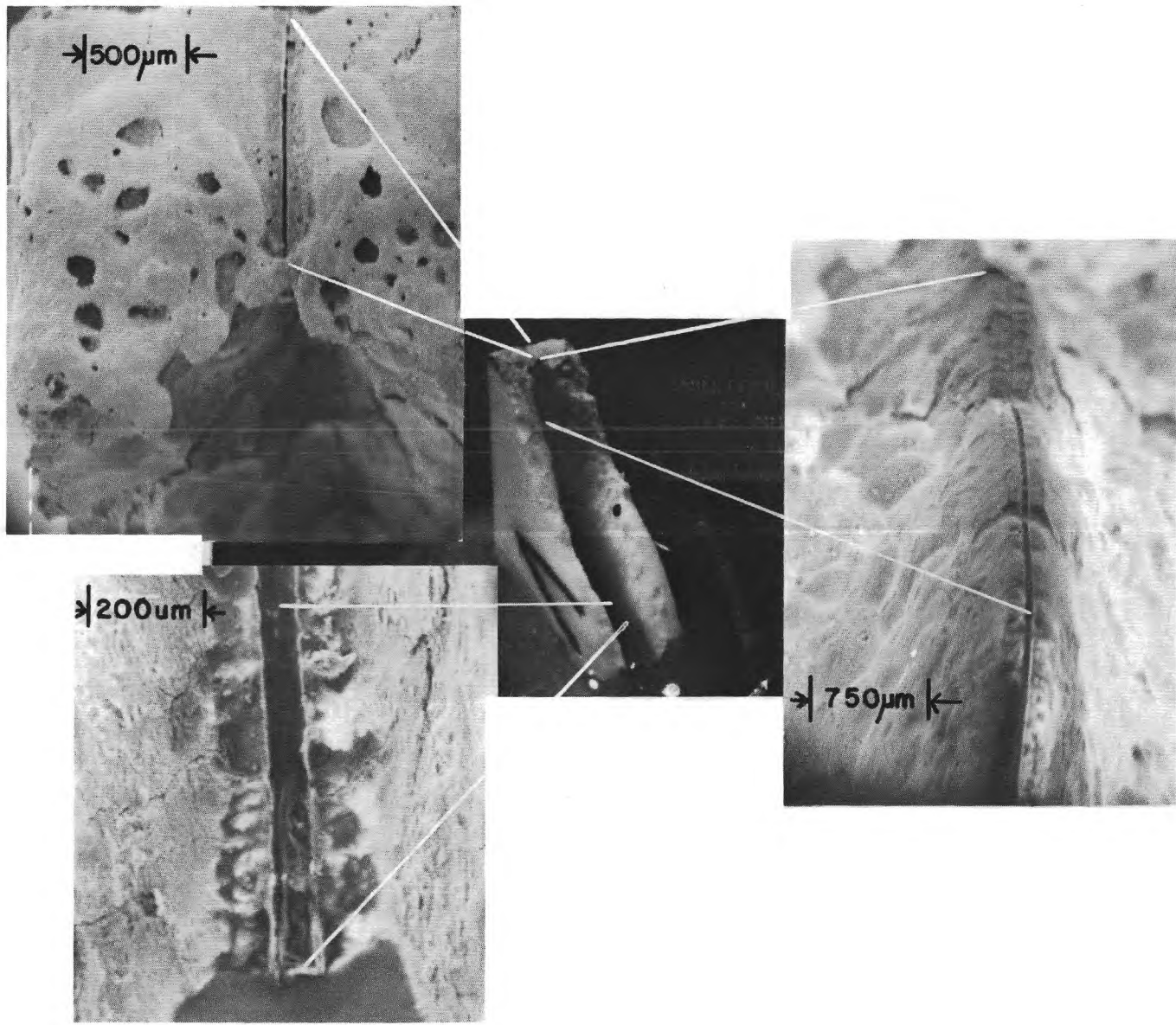


Figure 14. Surface of quenched sandwich illustrating limitation of flammability at low pressure. The thin-binder end has not sustained burning (HTPB binder, test at 1.4 MPa).

Figure 15a and b compare the quench surface of a sandwich with PS binder and one with HTPB binder (both were burned at 4.1 MPa, 600 psi). The figure illustrates the pervasive effect of the binder on the surface of the adjoining AP, an effect that is present with all binders and all binder thicknesses tested (although less pronounced with thin binder). There is less appearance of melt flow in the case of PS binder, less total protrusion of the binder at the thick end of the lamina, and the binder is more deeply recessed in the groove at the thin end.

A singular behavior observed with PBAN binder (and superficially with HTPB) only at high pressure (13.8 MPa, 2000 psi) is shown in Figure 16 and corresponds to the sketch in Figure 10b. The binder appears to severely retard or arrest the AP deflagration in the "smooth" band out to about 100 m from the interface. At this pressure the balance of the AP surface regresses ahead of the retarded surface, leaving a plateau-like raised section of AP and binder. This raised section apparently becomes undercut by lateral AP deflagration, as the plateau is discontinuous along the interface in an irregular manner. The occurrence of this behavior was not conspicuously dependent on binder thickness, except that with thin binder the regarded regions of the AP adjoining the binder simply slope away from the interfaces, with the resulting ridge of AP being topped by a binder recess (profile category 2.2.1 of Figure 7). One may speculate that binder melt flow formed a stable residue when it decomposed, one that protects the underlying AP from heat and chemical attack. It's not clear why this occurs only in high pressure tests, and only with selected binders (generalizations made hesitantly because of limited testing), but it may be significant that AP itself experiences a transition in mode of deflagration in the 12.4-15.1 MPa (1800-2200 psi) pressure range (Reference 9,10). The retarded region, as at all pressures, is also coincident with the smooth band.

Differences in binder behavior were most conspicuous in the low pressure tests (1.4 MPa; 200 psi). In all cases there appeared to be a threshold binder thickness for the binder below which burning would not self-sustain. This was illustrated by Figure 13, which shows the quench surface of

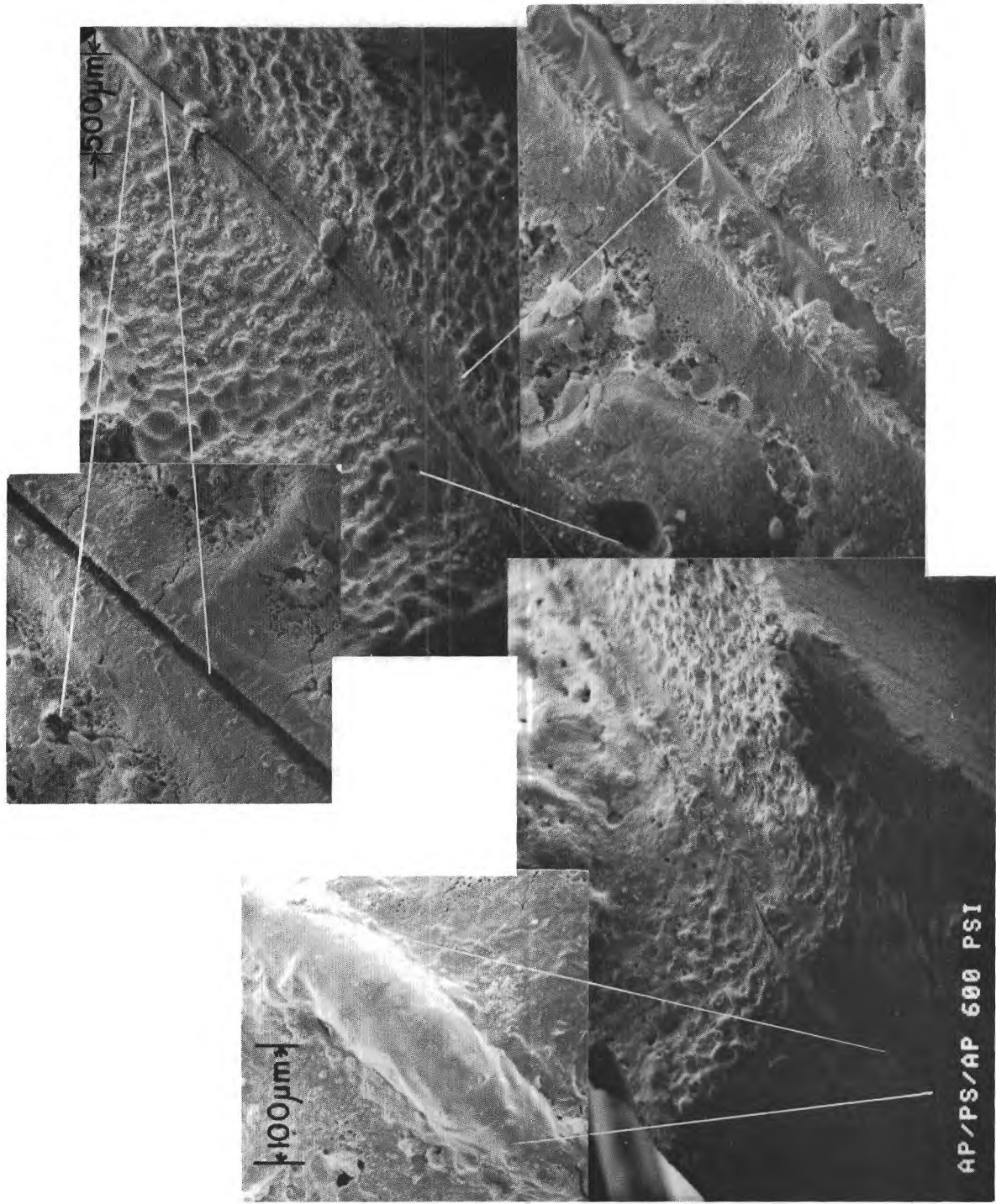


Figure 15. Comparison of surfaces with PS and HTPB binders (4.1 MPa). (a) Polysulfide binder.

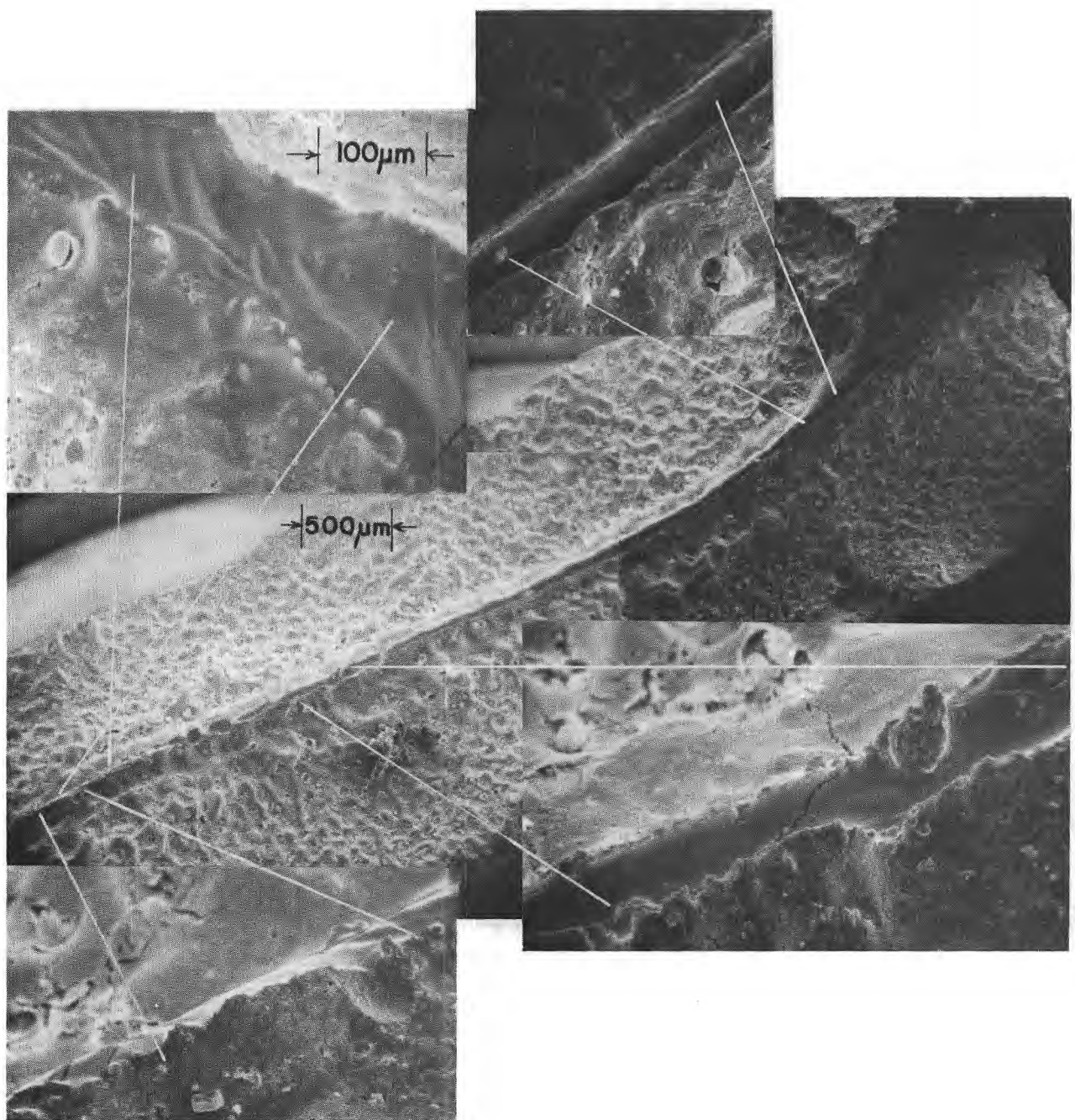


Figure 15. (Continued) Comparison of surfaces with PS and HTPB binders (4.1 MPa). (b) HTPB binder.

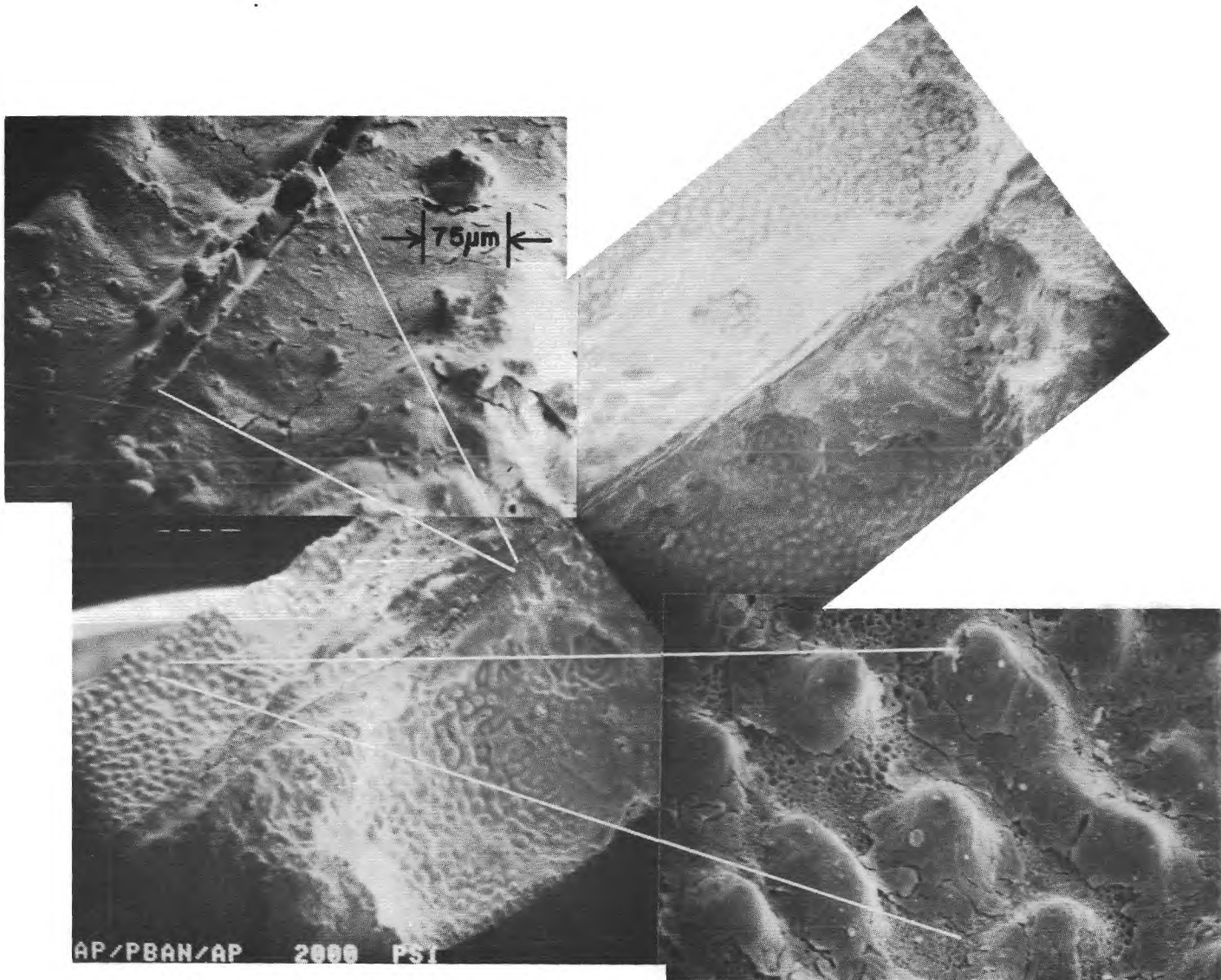


Figure 16. Plateau profile suggestive of arrested burning near interface. PBAN binder at 13.8 MPa.

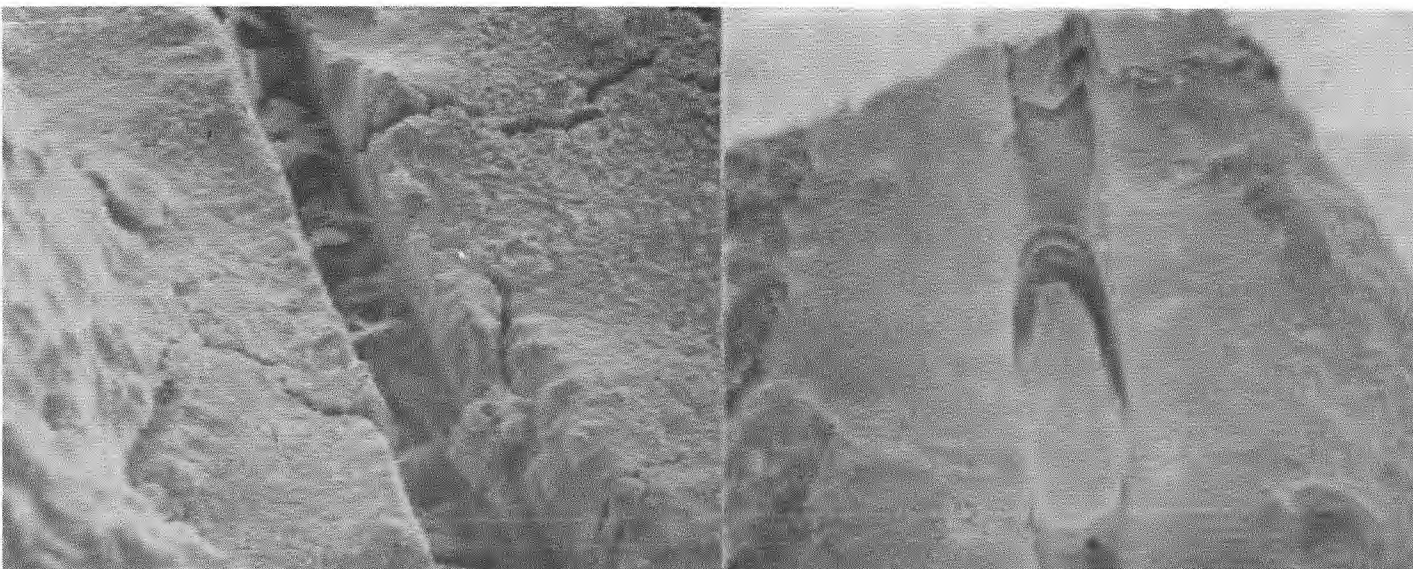
a tapered sandwich that burned normally on the thick end. In that portion of the sample that burned, the appearance of the various binders differed. PS binder was most deeply recessed and showed a residue of unidentified flakey material (Figure 17a). HTPB and CTPB binders formed miniscus-like profiles in the recess, with some visible flow marks (Figure 17b). PBAN binder showed a complex stringy structure in the recess (Figure 17c) suggestive of viscous properties (it's not clear what process caused formation of the structure, but it may be the result of subsurface bubbling during burning or during the quench depressurization). It is a little surprising that, even with the recessed binder situation, all the binders produced the smooth band on the adjoining AP surface outside the recess, and the point of maximum regression of AP is always at the outer edge of the smooth band. Conditions for melt flow over the AP surface appear to be very unfavorable in the recessed, thin binder situation, suggesting that binder effects on the AP surface are not necessarily due only to melt flow.

### 3.8 Diffusion Flame

High speed combustion photography shows luminous flames originating near the oxidizer-binder interfaces. These flames are orange in color and very likely are plumes of radiating hot carbon in the diffusion flame. The nature of these flames has been noted before (References 11, 12), earlier observations having usually been made by viewing end-on to the sample so as to see in between the walls of AP that occur in low pressure tests. The flame seen from this orientation was referred to as "brushy" (Reference 11).

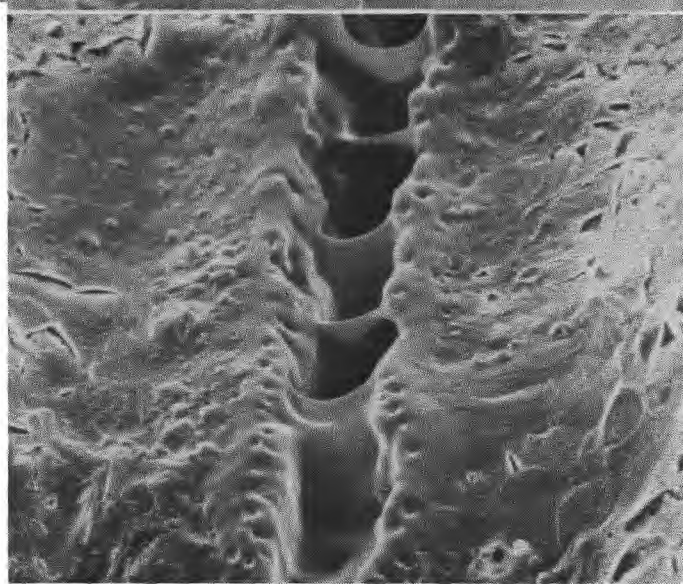
With tapered sandwiches, there is a motivation to view the diffusion flame sheet side-on, so as to resolve the flame behavior as a function of binder thickness. Initial tests showed that this arrangement was feasible, and that significant differences in flame behavior did indeed occur as a function of binder thickness. However the diffusion flame is obscured from side viewing in low pressure tests by the protruding wall of slower-burning oxidizer, limiting useful results to tests above 4.1 MPa (600 psi) or so.

Figure 18 shows a frame of a side-view motion picture of an HTPB sandwich



a

b



c

Figure 17. Singular features of three binders at 1.4 MPa.

(a) Polysulfide binder, thickness 22  $\mu\text{m}$  (b) HTPB binder, thickness 29  $\mu\text{m}$   
(c) PBAN binder, thickness 26  $\mu\text{m}$



Figure 18. Diffusion flamelets on a burning sandwich. Binder thickness decreases to the right. HTPB binder, test pressure 6.9 MPa. Picture shows full width of the sample, about 1 cm.

while burning at 6.89 MPa (1000 psi). This corresponds to an exposure time of about 1/3000 sec, and shows the diffusion flame to be a line array of separate flamelets. These flamelets appear to be transitory in nature, on a very short time scale. Most are not identifiable in successive frames of motion pictures taken at 2500 frames per second (a few flamelets at the thick-binder end of the interface are recognizable for 2 or 3 frames). Many motion pictures were made of sandwiches (Table 1) and examined for flamelet behavior. The transient behavior does not appear to be an oscillation in position, but rather a truly transitory existence. The average distance between flamelets is greater in the thick-binder end of the interface as is the size of the flamelet. With HTPB binder there were usually two rows of flamelets, one for each interface. Indeed, there is some indication that the distinctness of the two rows of flamelets with HTPB binder resulted from a tendency for the two interfaces to regress one ahead of the other with that particular binder. Resolution in pictures does not establish whether the two rows remain identifiably different at the thin-binder end of the burning surface, although it seems likely that they will not. It should be noted that, while the side-view pictures seem to show

a line of vertical flamelets, end view pictures reported in the past show the flamelets are at various angles to the mean burning surface, giving the "brushy" appearance.

Partial results from the photographic test series in Table 1 show that a transitory flamelet array is common to all the binders tested, over all the pressures that yielded a view of the relevant region of the combustion zone (in the tests at 1.4 MPa, 200 psi, the view was obscured by the wall of unburned AP; in 4.1 MPa tests the view was partially obscured). The sandwiches with PS binder gave such low flame luminosity that this behavior could not be determined, or included in the description of flamelet behavior.

The transitory nature of the diffusion flamelets led to the speculation that a continuous flame sheet might not be dynamically stable, a speculation that motivated the analysis in Section 7. Another speculation about the transitory flamelet field stems from the fact that the flamelets originate in the region where the AP surface processes appear to be influenced by the binder (region of the "smooth band"). The nature of this surface is unknown, but it is reasonable to speculate that the nature is locally intermittent, (an example of intermittent behavior would be emergence of oxidizer vapors through a thin binder melt overlay by bubble blowing).

Whatever the cause of the evident instability of individual flamelets, the resulting nature of the flamelet field is a matter of considerable practical importance in that it may play a critical role in the response of combustion to flow disturbances that lead to combustion instability. Of course understanding of the cause of the flamelet response will suggest means to change it.

### 3.9 Discussion of Sandwich Burning Results

3.9.1 Results of the present investigation are similar to those of earlier investigations in some respects, different in others. The differences are most conspicuous in the thin-binder geometry, which also is the configuration least investigated by others but most closely simulating propellant

combustion conditions. The similarities with previous studies (i.e., arising from tests of similar geometry and test conditions) include:

1. Consistency with the general classification system in Figures 6 and 7.
2. A characteristic (pressure dependent) pattern of depressions and evidence of a frothy melt on the AP surface.
3. Presence of a leading "edge" of the burning surface of the AP near, but not at, the AP-binder interface.
4. Anomalous smooth surface quality of the AP between the leading "edge" and the interface.
5. Width of the band of modified surface in 4 comparable to the particle diameter of AP in propellants.
6. Evidence of melt flow over the interface (not certain at low pressure or with thin binder).
7. A tendency for protrusion of the binder lamina to disappear as the binder thickness is reduced.
8. Diffusion flames that are "brushy" when viewed in line with the sandwich lamina.

Novel results in the present investigations include:

1. Minimal protrusion of binder with thin binder lamina, recessed in low pressure tests (possibly all pressures).
2. Persistence of the anomalous "smooth" band of AP surface adjoining the interface, even with low binder thicknesses not previously studied.
3. Apparent retardation of AP regression rate in the "smooth band", leading to the presence of a leading edge of the AP front outside the smooth band, even with thin binder at low pressure, where the binder is recessed (Figure 12, 14, 15, 17).
4. Retardation of the smooth band so extreme at high pressure that the unaffected AP surface apparently regresses laterally under the retarded smooth-band surface (PBAN binder, Figure 16).
5. Substantial difference in state of binder surface (e.g., fluidity, residue) as a function of kind of binder. Specifically, HTPB and PBAN binders showed the most evidence of molten state, and CTPB binder showed a relatively less viscous melt. HTPB

and CTPB binders tended to show more char than the others. PS binder showed the least evidence of melt state (these judgements are somewhat subjective, based on evidence of melt flow and/or bubbles from quenched samples and observations by combustion photography).

6. Unsteadiness of the diffusion flame, that leads to intermittent flamelets with size, spacing and duration being larger for thick binder, smaller for thin binder.
7. A low pressure limit for sustained burning of thin-binder sandwiches (1.4 MPa for 30  $\mu\text{m}$  binder).
8. Several detailed differences in combustion behavior according to binders used.
9. Non-reproducible combustion behavior with thin-binder sandwiches that was apparently due to locally intermittent behavior, and sometimes to proximity to the deflagration limit.

3.9.2 The "smooth band" on the AP surface adjoining the interface appears to be a major factor in behavior on the dimensional scale of propellant microstructure, but the nature or cause of this band is still unknown. It has been attributed in the past to binder melt flow. This argument was based on results with thick-binder sandwiches, where the flow pattern over the interface is visible (References 11, 12) and the binder film is visible in profile of sectioned samples (Reference 6). This argument is less convincing with thin-binder sandwiches where a "deficiency" of binder leads to recessed binder surfaces, but does not eliminate the smooth band. Since the leading edge in the AP surface is at the outer edge of the smooth band, the diffusion flame is exerting some effect at least that far out. Thus the smooth band is probably on the fuel-rich side of the diffusion flame mean position. However, this flame may actually consist of an array of transitory flamelets issuing from the smooth band--possibly at the sites of more or less randomly bursting bubbles in the smooth band. Existing observational methods have not thus far provided adequate resolution to determine the actual details, but the combustion photography establishes the short duration of the flamelets (of order  $10^{-4}$  to  $10^{-3}$  sec).

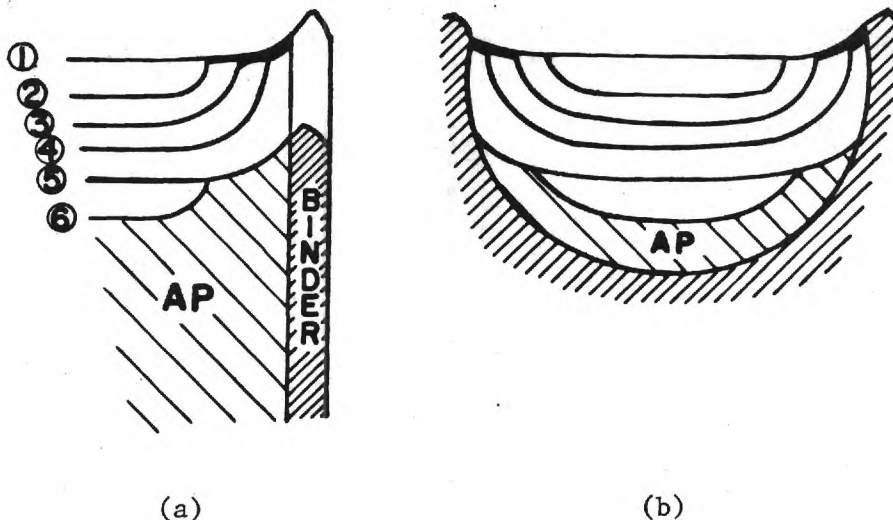


Figure 19. Successive burning surfaces reflecting retardation of the AP burning surface near binder.  
 (a) Sandwich    (b) Particle

While the microscopic and chemical details of the smooth band and diffusion flamelets are still unresolved, it seems clear that the band is a region of retarded regression of the AP (relative to the flame-assisted leading edge). In the high pressure tests this retardation is so great that the unassisted AP deflagration undercuts the surface of the band (PBAN binder). These effects are on an easily resolvable scale, the same scale as AP particle size in propellants. Thus the results raise profound questions about how AP particles burn in propellants, and what constitute valid models for propellant combustion. This is suggested by the sketch of successive burning surface profiles in Figure 19, where part a is the interpretation of results of 13.8 MPa sandwich burning tests, and part b is a corresponding speculation about particle burning in propellants. Not only does this type of particle burning raise difficulties with existing analytical models of propellant burning rate, but adds features to the combustion zone structure that are likely to be important in the dynamic response that drives combustion instabilities.

3.9.3 As with any simplified model of a complex system, the sandwich model must fail to simulate some important aspects of propellant combustion,

and may also produce some effects that are of only secondary importance with propellants. These are the prices that must be paid for the benefits of controlled variables, and simplicity of interpretation of test results.

Perhaps of first importance to relevance is the distance of things on the propellant burning surface. Oxidizer particles in propellant ordinarily have an effective radius in the range of 2 - 200 micrometers, so that distances from oxidizer binder interfaces are in that range, and the flame environment occurring in that range is the one relevant to propellant surfaces. A relevant theory or experiment is one that correctly describes conditions or processes in the 200  $\mu\text{m}$  range from the interface. This implies that relevant experimental observations of sandwich burning must pertain to the 200  $\mu\text{m}$  range relative to the interface, and the experiment must simulate propellant behavior in that region.

Past work pertaining to sandwich burning, both analytical and experimental, has not been too faithful to the above test of relevance to propellant burning, a point that will not be belabored here except to point out that increasing emphasis has been placed in the present work on details close to the binder interface, and on use of binder thicknesses comparable to binder structural elements in the matrix of propellants.

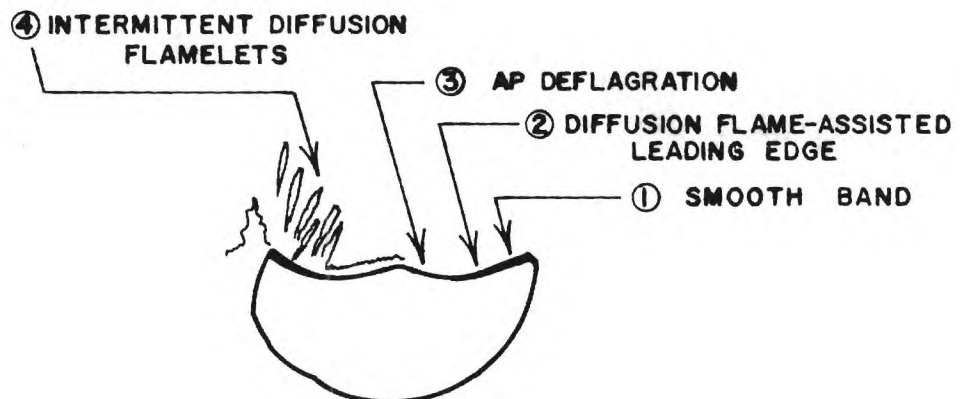
A second basic concern regarding relevance of sandwich burning to propellants is the relatively steady state nature of burning in sandwiches. Being made primarily of particulate ingredients, the combustion of heterogeneous propellants is locally intermittent (on a time scale corresponding to the burning time of the ingredient particles). Thus any condition on the burning surface of a sandwich that requires a generation time longer than the propellant particle burning time will not be fully developed on the propellant surface because of the interruption at particle burnout. An example of this is the "needle" structure reported (Reference 9) on the deflagration surface of AP at high pressure, which involves a layer of thickness about the same as the diameter of AP particles in propellants. This does not mean that the phenomena observed during more nearly steady burning are not relevant, but rather that those resulting from slow processes will not become fully developed in particle burning.

A third basic concern regarding relevance of sandwich burning has

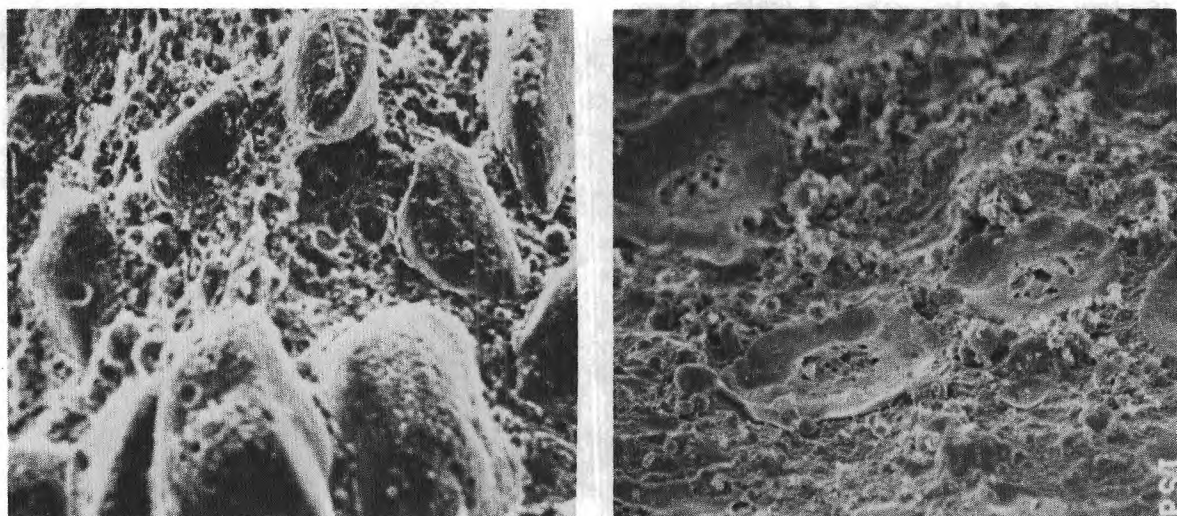
to do with the "edgewise burning" of the interface. In the sandwich, the geometry constrains the burning front to proceed in the direction of the interface. Because of the granular nature of ingredients in propellants, the interfaces are not only discontinuous, but inclined in varying degree to the mean burning surface regression. There may be a significant portion of the particle burning in which edge burning is approximated, but it is not presently established what contribution each part of the particle burning history makes to the overall burning rate, or to the structure of the burning surface and gas phase combustion zone. These questions cannot be answered by sandwich burning, but are probably important issues in determining steady and oscillatory burning characteristics and proper mechanistic models thereof.

3.9.4 From the results of the sandwich burning tests and the foregoing considerations, it is concluded that the principal results of value to propellant applications come from examination of the surface behavior within about 200 micrometers of the binder-oxidizer interface and the diffusion flames issuing from that region. Further, it appears that results relevant to propellants can be obscured if thick binder laminae are used. In addition unless caution in interpretation is exercised, one may draw conclusions from results of sandwich burning experiments that are not relevant to propellants because of the quasi-steady nature of sandwich burning (as opposed to the intermittency induced by the granular nature of the propellant microstructure).

In the present work, the "novel results" in 3.9.1 above are believed to all be relevant to propellants, and pose a rather different picture of propellant combustion zone behavior than that generally described in the past. This is illustrated by the somewhat speculative picture of the combustion zone microstructure in Figure 20. The accompanying photomicrographs of quenched burning surfaces attest to the complexity of the real combustion zone structure on a microscopic scale and illustrate details similar to the sketch, as modified by the expected trends in the features of the combustion zone as discussed in the following.



(a)



(b)

Figure 20. Combustion zone microstructure.

(a) Sketch--mid pressure range ( $\sim 7$  MPa)

(b) Quenched burning surface, 0.1 MPa (left) and 6.9 MPa (right), both UTP 3001 propellant

The sketch in Figure 20a is based on behavior at about 3.5 MPa (~ 500 psi), corresponding to the second part of Figure 20b. The sketch is also based on an AP particle diameter of about 300-400  $\mu\text{m}$ . The features of the combustion zone would be expected to vary with particle size, pressure, time during burning, etc., in the following manner.

1. SMOOTH BAND, present at all pressures, retards surface regression. May cover whole particle when particles are small. May have progressive effect with time during burning of each particle. May provide anchor sites of diffusion flamelets.
2. LEADING EDGE OF AP surface, caused by diffusion-flame<sup>\*</sup> augmented AP deflagration. Contribution of the flame to regression rate at high pressure (e.g., 10-15 MPa) is minor, contribution at low pressure (<2 MPa) is dominant. Effect may be washed out by smooth-band effect with small particles.
3. AP DEFLAGRATION dominates AP surface in the central area of the particle surface, especially with large particles and at higher pressures. At lower pressures this area is raised because its regression is not effectively assisted by the diffusion flame (large particles).
4. DIFFUSION FLAMELETS occur in the vicinity of the oxidizer-binder interface, and are intermittent and localized on a time scale of about 1 millisecond. The causes of this behavior are not determined by the experiments. However, it is significant that the flamelets apparently originate over the smooth band rather than the interface, implying that their singular behavior may be related to the nature of the smooth band. Since the "root" of the diffusion flame dominates the overall flame behavior and its contribution to burning rate and dynamic behavior, it seems crucial that the nature and role of the smooth band be further clarified.

---

\* In this report the "diffusion flame" is used to designate the AP binder flame, regardless of whether its rate is "diffusion limited" or "kinetically

## TESTS ON OTHER ORDERED MICROSTRUCTURES

### 4.1 Philosophy of Tests

Use of simple microstructures such as sandwiches is helpful in understanding tests results, but any such configuration necessarily fails to exhibit faithfully all aspects of propellant combustion behavior. In the following, some examples of this are described, along with some ideas about ordered microstructures that might serve well to demonstrate aspects of combustion behavior not exhibited by sandwiches. Following this discussion, some exploratory tests will be described, tests designed to supplement the results obtained in sandwich burning tests. These tests are catalogued in Table 2.

### 4.2 Combustion Behavior and Test Design

In combustion of real propellants, there are aspects of behavior that depend on the smallness of distances in the propellant microstructure, the interaction of neighboring flames, and intermittency of composition

Table 2. Tests on Ordered Structures \*

	4.14 MPa		6.89 MPa	
	Quench	Movie	Quench	Movie
Check on burning rate of pressed AP alone				8/9
Beaded Sandwiches			5/8 2/5	4/4 1/1
Nylon threads in AP HTPB threads in AP	1/2 0/3		1/6 5/5	3/3 3/3
Sandwich with 600 $\mu\text{m}$ spheres			1/3	
Stacked Cylinders				5/6

\* Table entries indicate number of tests run, and number with useful test results (i.e., apparatus function OK and sample burn regular).

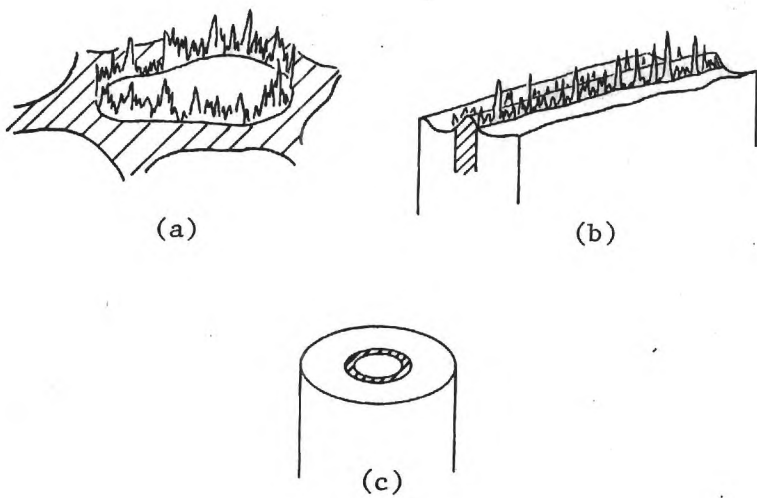


Figure 21. Nature of flame sheets.

- (a) Closed interface line typical of oxidizer particles in propellants
- (b) Open interface line typical of sandwiches
- (c) Experimental arrangement for studying behavior of a closed-interface counterpart of a sandwich (fuel coated oxidizer rod in oxidizer)

in any line of progression of the burning surface (due to heterogeneity). These are typical propellant-dependent differences from the edge-burning sandwich model, and these differences are known to be important to steady state and/or oscillatory combustion of propellants.

The foregoing is illustrated by the following example. One might reasonably question to what extent the surface and flame behavior observed in sandwich burning would occur if the diffusion flame and interface-related effects issued from a small closed interface curve such as the border of a partly burned AP particle in a propellant burning surface, instead of the linear interface of a sandwich (Figure 21). At what diameter of a closed interface do the adjoining and opposite elements of the flame surface (flamelets) or the "smooth band" start interacting with each other, and what is the effect on propellant burning rate or combustion stability? Presumably these issues would be clarified by studying combustion of rods of AP coated with binder and surrounded by more AP (Figure 21c). End-burning behavior as a function of rod diameter would give some clues to

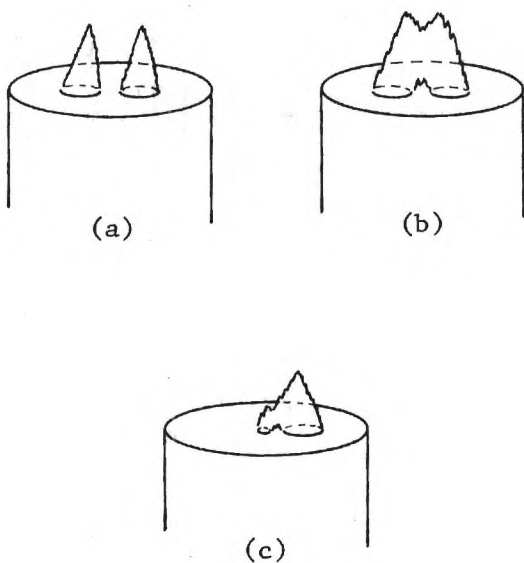


Figure 22. Arrangements of fuel filaments in oxidizer.

- (a) Two filaments, far enough apart for separate flames
- (b) Two filaments, interacting flames
- (c) Two filaments, different size, interacting flames

the real propellant effects posed by the initial question.

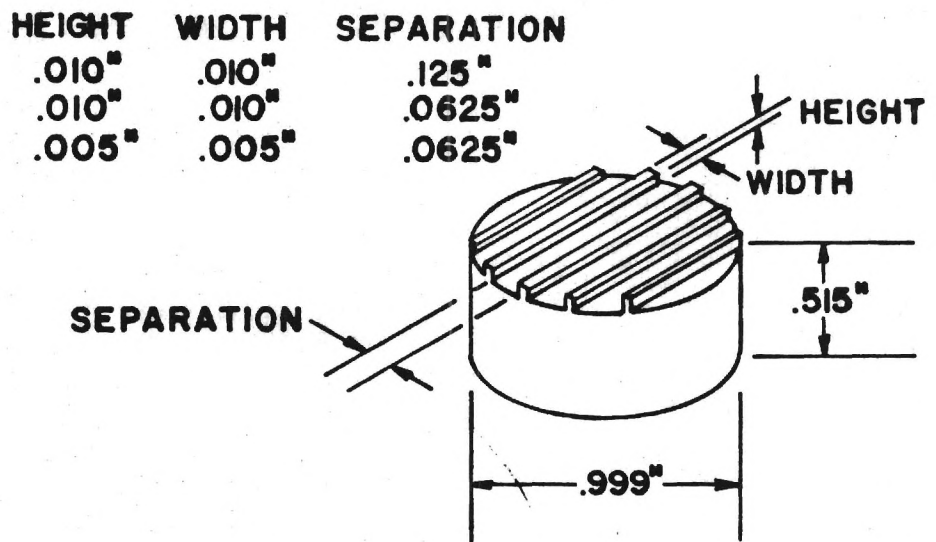
A second fundamental question of composite propellant burning is the interaction of diffusion flamelets from adjoining oxidizer particles (Figure 22). Do flamelets from neighboring particles tend to support each other (possibly suppressing flickering), or "repel" each other (by consuming each other's local fuel supply)? Does the behavior of a big flame envelope of a large oxidizer particle modify the smaller envelopes of smaller neighboring oxidizer particles (or vice versa)? If adjoining envelopes flicker, do they flicker together? Do such interaction effects possibly develop only in oscillatory environments, and if so at what frequency? Some of these questions reflect mechanistic issues currently being considered in computer modeling of the combustion, but the factual information on real behavior is lacking. The real combustion behavior could be studied in a controlled laboratory experiment in which the oxidizer particles are replaced by oxidizer rods, packed in varying degrees of proximity. However, such a configuration is difficult to produce, and in the present

work, the experiment is "inverted" by using small binder rods pressed in an AP test sample.

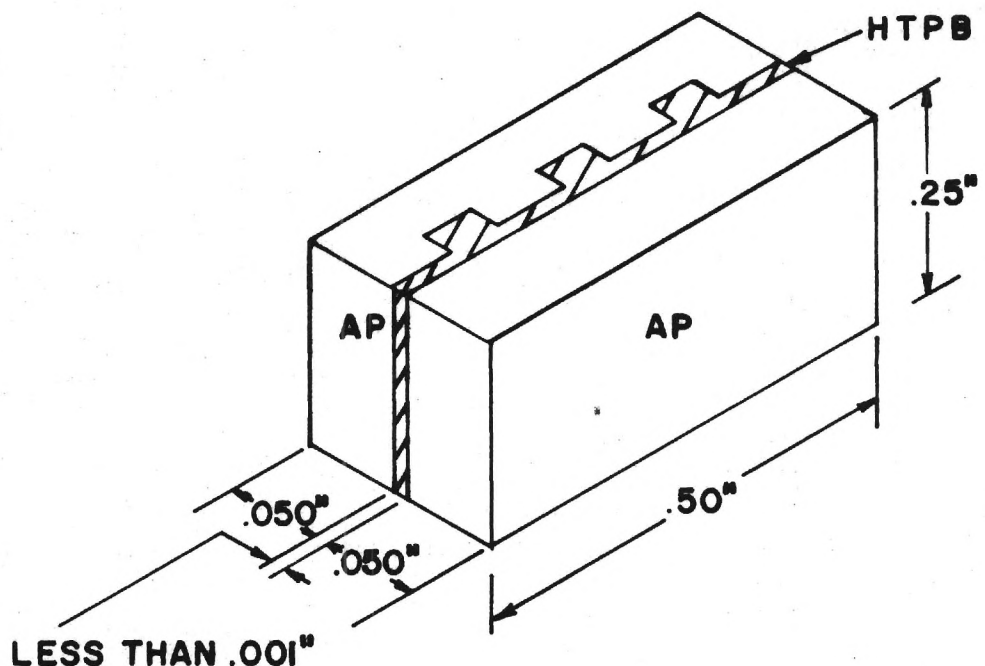
The third fundamental aspect of composite propellant combustion that is not addressed by sandwich models (or analytical models) is the local intermittency of the microstructure, i.e., the structural and chemical discontinuities corresponding to particulate ingredients. In an ideal experiment, it would be desirable to start with intermittency while retaining an ordered microstructure, thus avoiding those complications in characterization of combustion that are due to the difficulty of characterizing the original sample microstructure in the first place. Some efforts were made in the present program to achieve this goal, without much success to date.

#### 4.3 Fuel Strands - Beaded Sandwiches

In an effort to produce diffusion flame arrays that are more localized than conventional sandwiches provide, tests were run on the configuration shown in Figure 23b. The configuration in part b of the figure was produced by modification of the sandwich fabrication. The die used in pressing the AP sheets was milled so that its face had a series of small parallel ridges (Figure 23a), which produced small parallel grooves in the pressed surface. Sandwiches were made by pairing these special sheets with flat ones, and using minimal HTPB binder in the flat interface (20-25  $\mu\text{m}$ ). Excess binder filled the grooves, giving binder "beads" or "filaments" roughly 160  $\mu\text{m}$  square and 80  $\mu\text{m}$  square (two different pressing dies). Tests were made on those samples by edge burning, with combustion photography and rapid depressurization quench (Table 2). Tests on the "Beaded Sandwiches" were not particularly rewarding, but results are worth recording. Combustion photography showed a luminous flame from each binder "bead", very little flame elsewhere. Figure 24 shows three typical sequences of frames from motion pictures taken at 1000 frames per second (the first sequence is taken without external illumination). The pictures show an irregular flame envelope above a 160  $\mu\text{m}$  binder bead, which changes only slowly with time compared to the flamelets seen in flat sandwiches.



a) MOLD FOR GROOVED AP DISKS



b) AP-HTPB SANDWICH WITH GROOVES

Figure 23. Arrangement for sandwiches with beaded binder lamina.

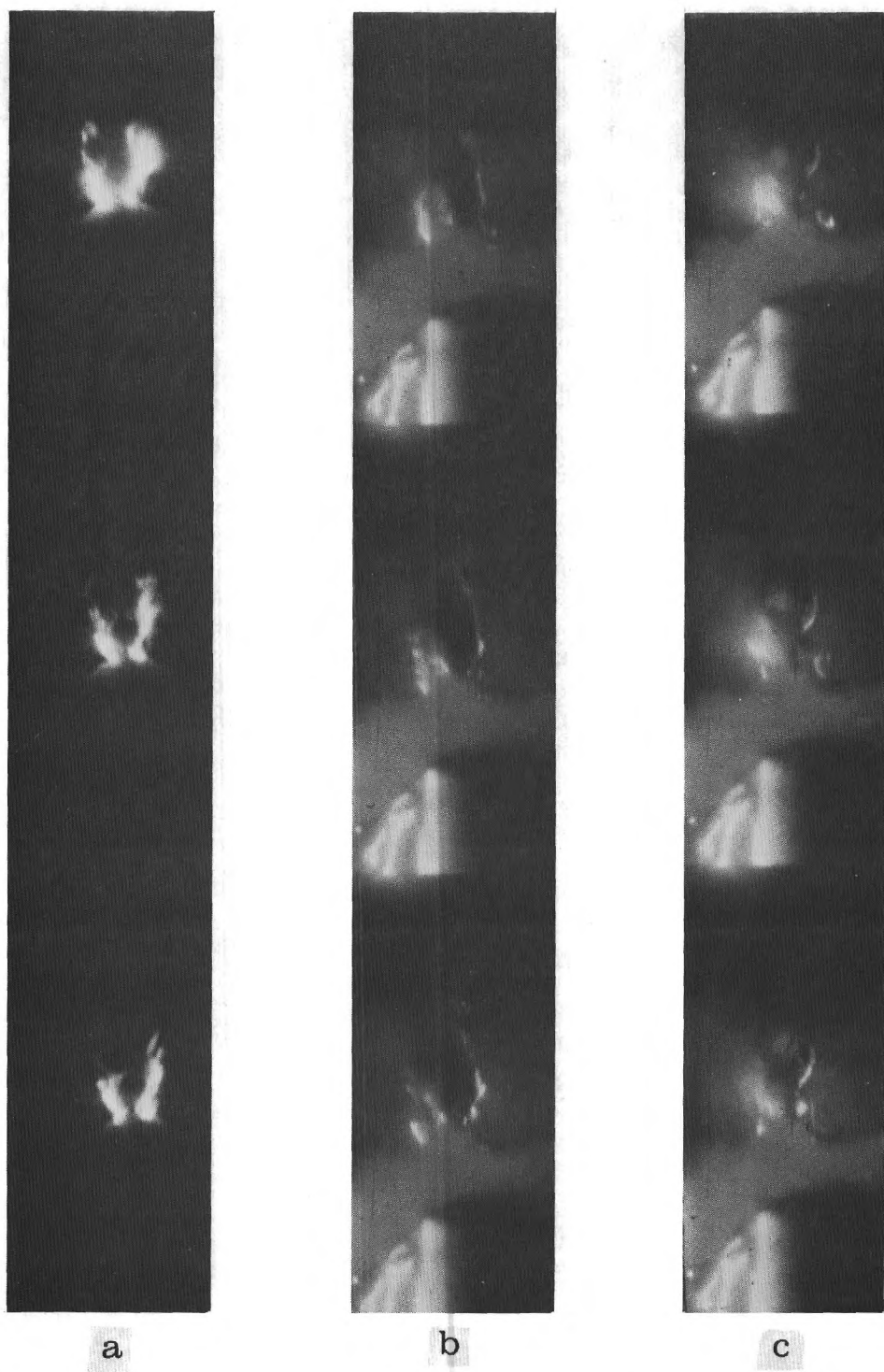


Figure 24. Picture sequences showing flame at the site of the "beads" (ridges) on the binder lamina.

- (a) No external illumination
- (b) and (c) Sequences with external illumination (in (b) and (c) the large light area below the flames is reflected external light) Pictures taken at 1000 frames per second.

This result suggests that the closed flame envelope may be more stable (or unstable at lower frequency) than a plane flame sheet. This is a speculative conclusion, because the geometry of the burning surface was too complex for interpretation of behavior. Further, there is usually a projecting char of binder inside the flame envelope and even with such a "flame holder", the flame envelope was not stationary, but simply fluctuated in a slower manner than the plane flame sheets of the conventional sandwiches.

The general surface character of the quenched beaded sandwiches was similar to other thin-binder sandwiches burned at the same pressure (6.9 MPa, 1000 psi), except near the sites of the binder beads. The binder was roughly 50  $\mu\text{m}$  thick at sites other than the beads. The AP surface sloped upward towards the AP-binder interface in a manner similar to regular sandwiches, and the binder laminae ranged from slightly recessed to slightly projecting relative to the interface oxidizer (Figure 25). The smaller beads of binder ( $\sim 125 \mu\text{m}$ ) generally projected above the adjoining AP, in a manner corresponding to behavior of conventional sandwiches with 125  $\mu\text{m}$  binder (Figure 25a). The samples with 250  $\mu\text{m}$  binder beads yielded recesses at the sites of the beads (Figure 25b), with evidence of melt behavior in the recesses. This result is not consistent with conventional sandwich behavior, but occurred consistently. There may be a problem of injection of molten binder during quench, a classic but never verified rationalization of unexplained features of  $\text{dp}/\text{dt}$  quenched samples (this point was not raised earlier in this report because recessed binders were noted primarily under conditions not conducive to injection of melt during quench, e.g., thin laminae, low pressures, and particularly with PS binder which shows minimal signs of melts).

Binder melt flow over the AP surface and "smooth band" effects were present but not conspicuous with the beaded sandwiches at the pressures tested. Samples were burned upside down and quenched, and gave nominally similar quenched surfaces, with some enhancement of the binder protrusion at the beads.

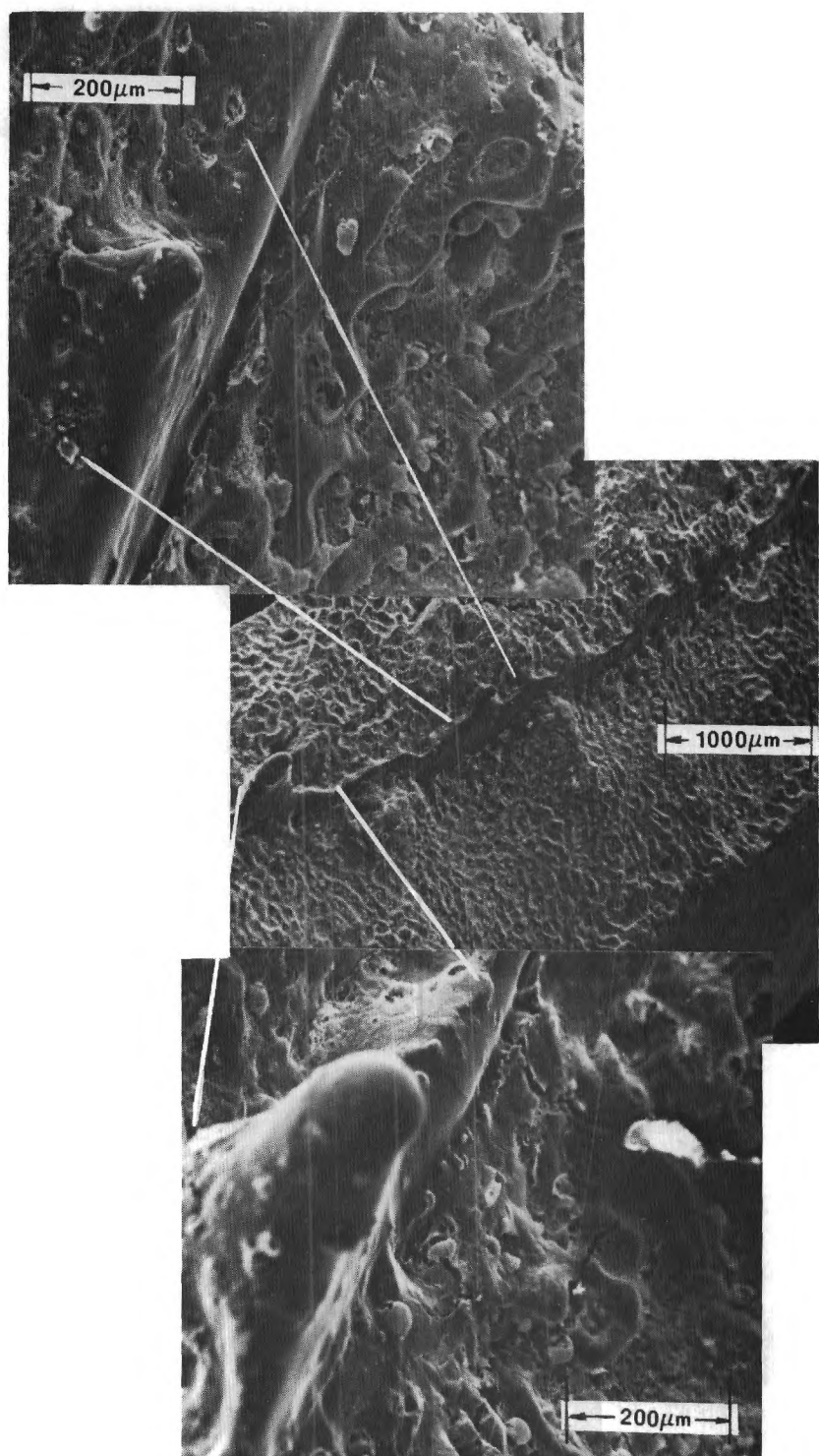


Figure 25. Surface of quenched beaded-binder sandwiches (6.9 MPa). (a) Small beads

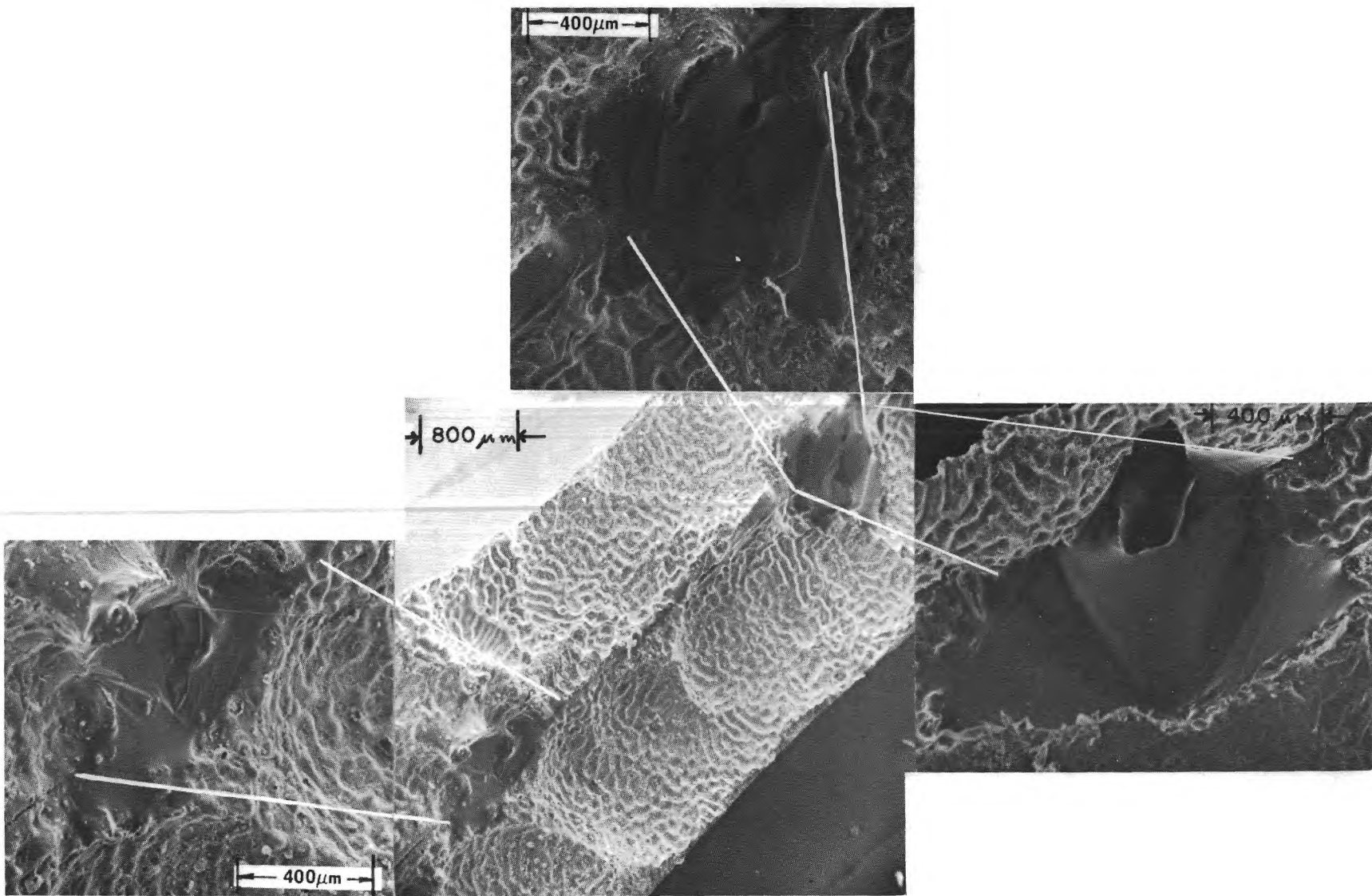


Figure 25. (Continued) Surface of quenched beaded-binder sandwiches (6.9 MPa). (b) Large beads .

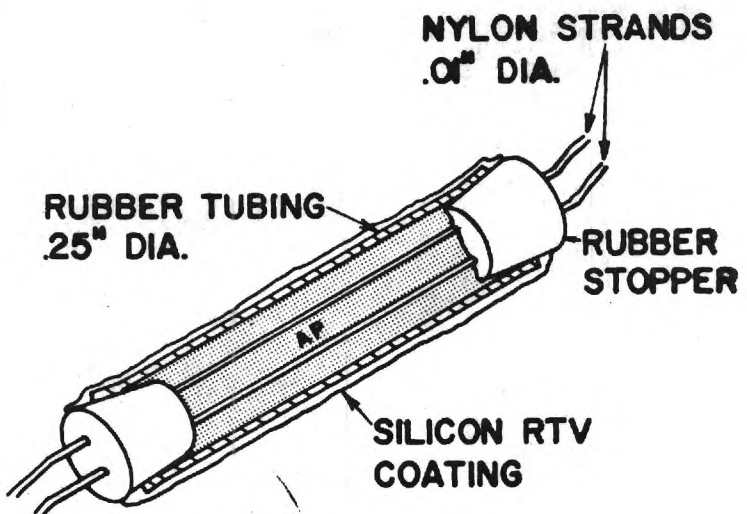


Figure 26. Arrangement for hydrostatic pressing AP samples with fuel filaments.

#### 4.4 Fuel Strands - Fuel Filaments

Another approach to fabrication of fuel strands in AP was to dry press powdered AP samples containing threads of polymer. For this purpose, samples of monofilament nylon fish line were used. The segments of thread were simply laid in the AP powder in the pressing die, covered by more AP, and pressed into wavers in the usual manner in the arbor press. In an alternate approach, samples were pressed in a hydrostatic press. These samples were prepared by filling a rubber tube (Figure 26) with AP powder, using rubber stoppers to seal the samples in the tube. Monofilament threads were supported through the sample by threading them through the stopper. This sample assemblage was subjected to 207 MPa hydrostatic pressure for 60 minutes. The pressed sample appeared to be well consolidated, but lacked the nearly translucent appearance of the die-pressed wafers. In a further adaptation of the method, samples were made by both the hydrostatic press and die-press methods with the polymer filament replaced by fine steel wires. After pressing, the steel wires were withdrawn and the holes were

filled with uncured propellant binder. This approach had the advantage of assuring a uniform polymer filament (not deformed by AP particle intrusion during pressing) and permitting use of conventional propellant binders. As noted below, test results on samples made by all methods suggested that voids and/or a gap between the binder and AP in the hole may have existed in many samples tested. However, further work seems to hold promise.

Actual tests on the fuel strand are listed in Table 2. Hydrostatically pressed samples tended to burn rapidly down the interface between the fuel strand and the AP. This was true of both HTPB-filled types and pressed-in-place nylon filament samples. Burning rate tests on samples prepared without the fuel strands were found to be much higher than with die-pressed samples of AP. These "suspicious" results led to abandonment of the hydrostatic pressure method. The behavior was not satisfactorily explained, but poor AP consolidation was suspected.

Fuel strand samples made by the more familiar die-pressing method also led to more rapid burning than expected down the interface, but the burning was even, and yielded quenched samples with axially symmetrical profiles about the axis of the fuel strand. An example of a quenched two-strand HTPB-filled sample quenched from 6.9 MPa (1000 psi) is shown in Figure 27. The high magnification part of the figure (part b) shows that the sample burned with the now-familiar "smooth band" in the AP near the binder interface. However combustion has proceeded much further down the AP surface there than in the rest of the AP. Similar behavior was observed at 4.15 MPa (600 psi), as shown in Figure 28. With nylon strands, the region of the fuel-oxidizer interface was similar to that with HTPB, and burning proceeded far ahead of the main AP surface as with HTPB strands. Results with nylon were inconclusive because the one die-pressed sample that was quench-tested was quenched so early in burning (Figure 29) that penetration of burning down the interface region may not have had sufficient time to yield a fully developed profile.

Although the number of tests on strands and beaded sandwiches was limited, the results pose a striking contrast (Figure 30). The beaded sandwiches yielded retarded regression of the AP in the region near the

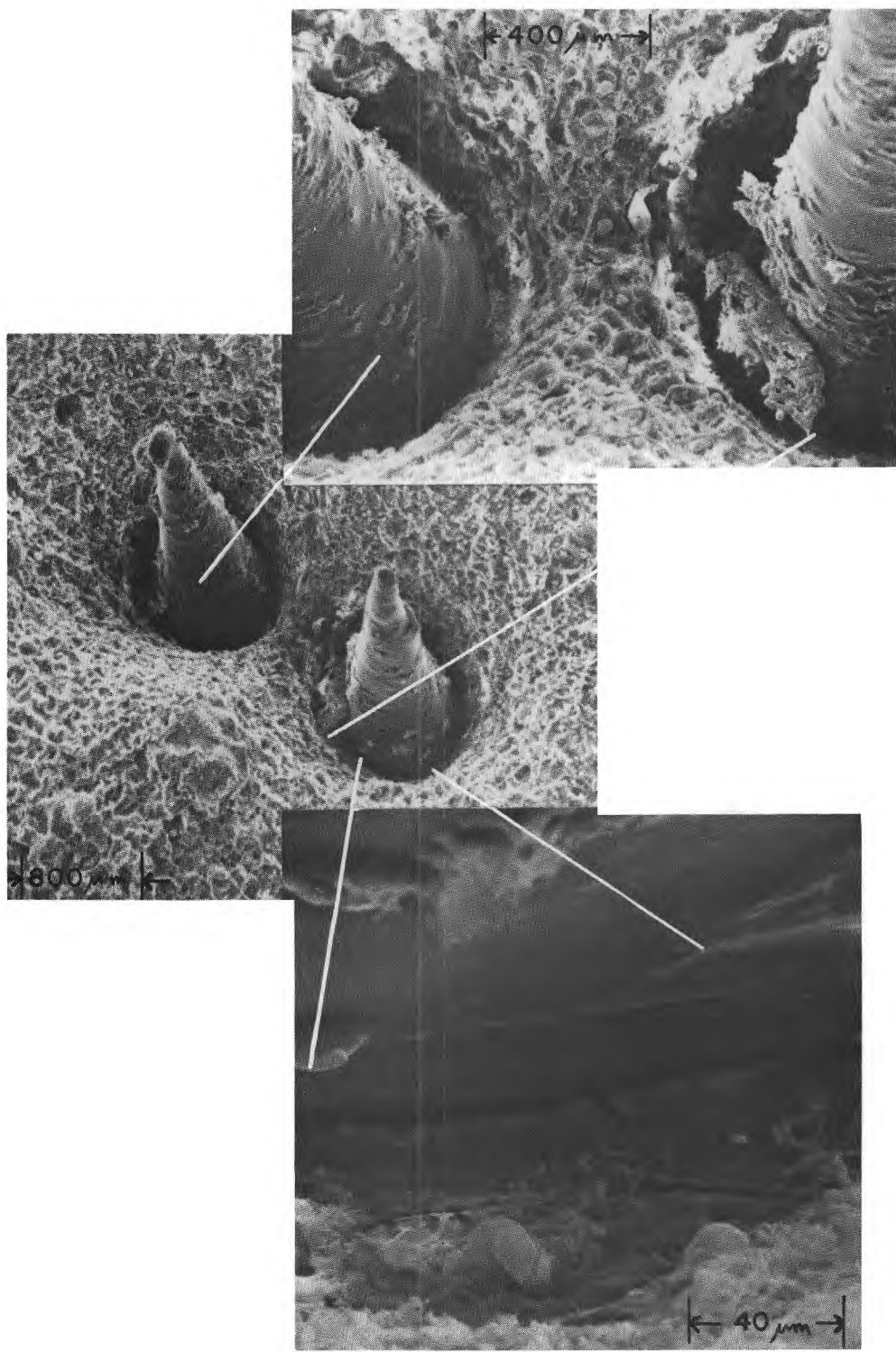


Figure 27. Surface of quenched AP sample having two cast HTPB filaments. Test run at 6.9 PMa. Sample was die-pressed.

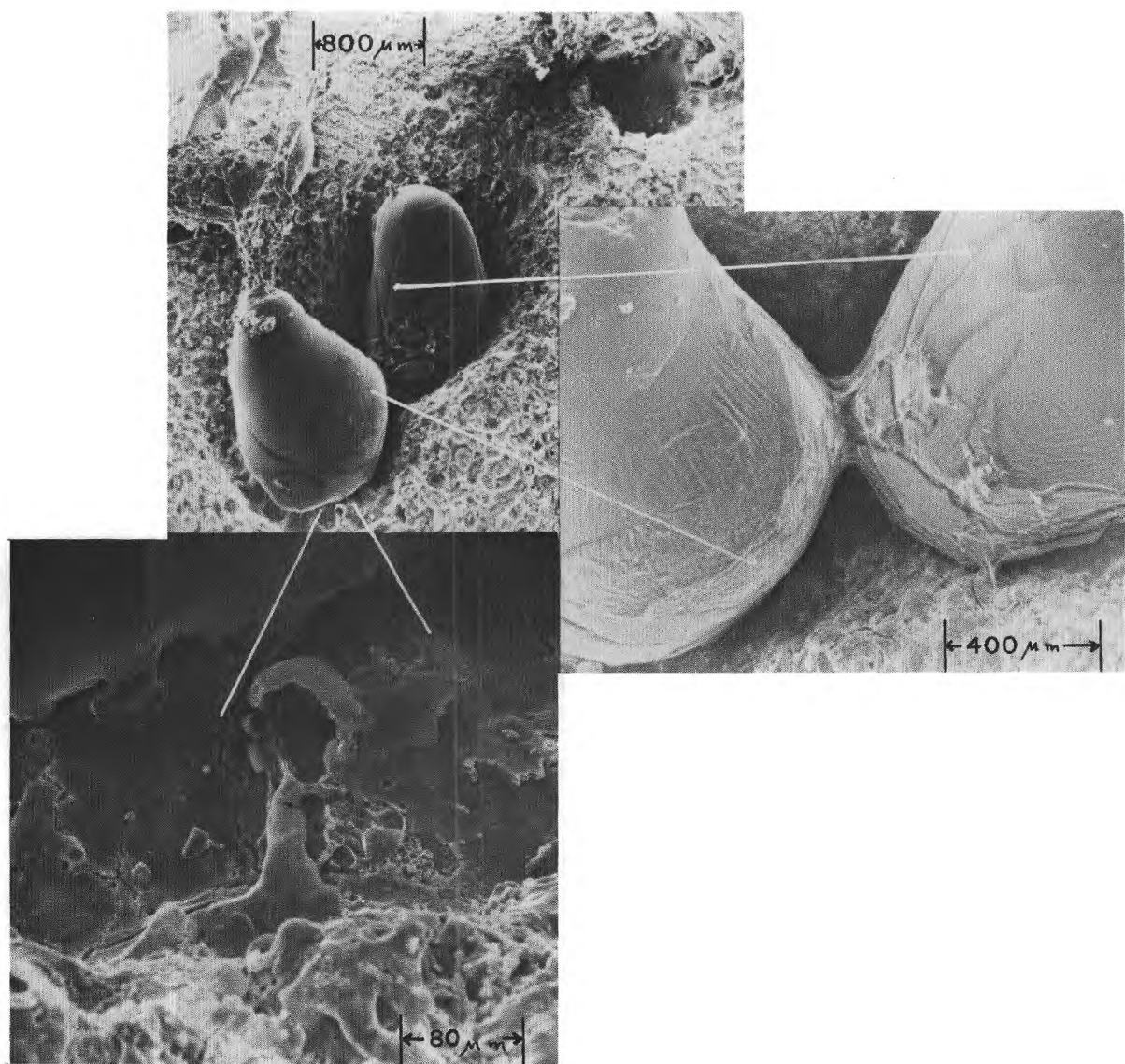


Figure 28. Surface of quenched AP sample having two cast HTPB filaments.  
Test run at 4.15 MPa. Sample was die-pressed.

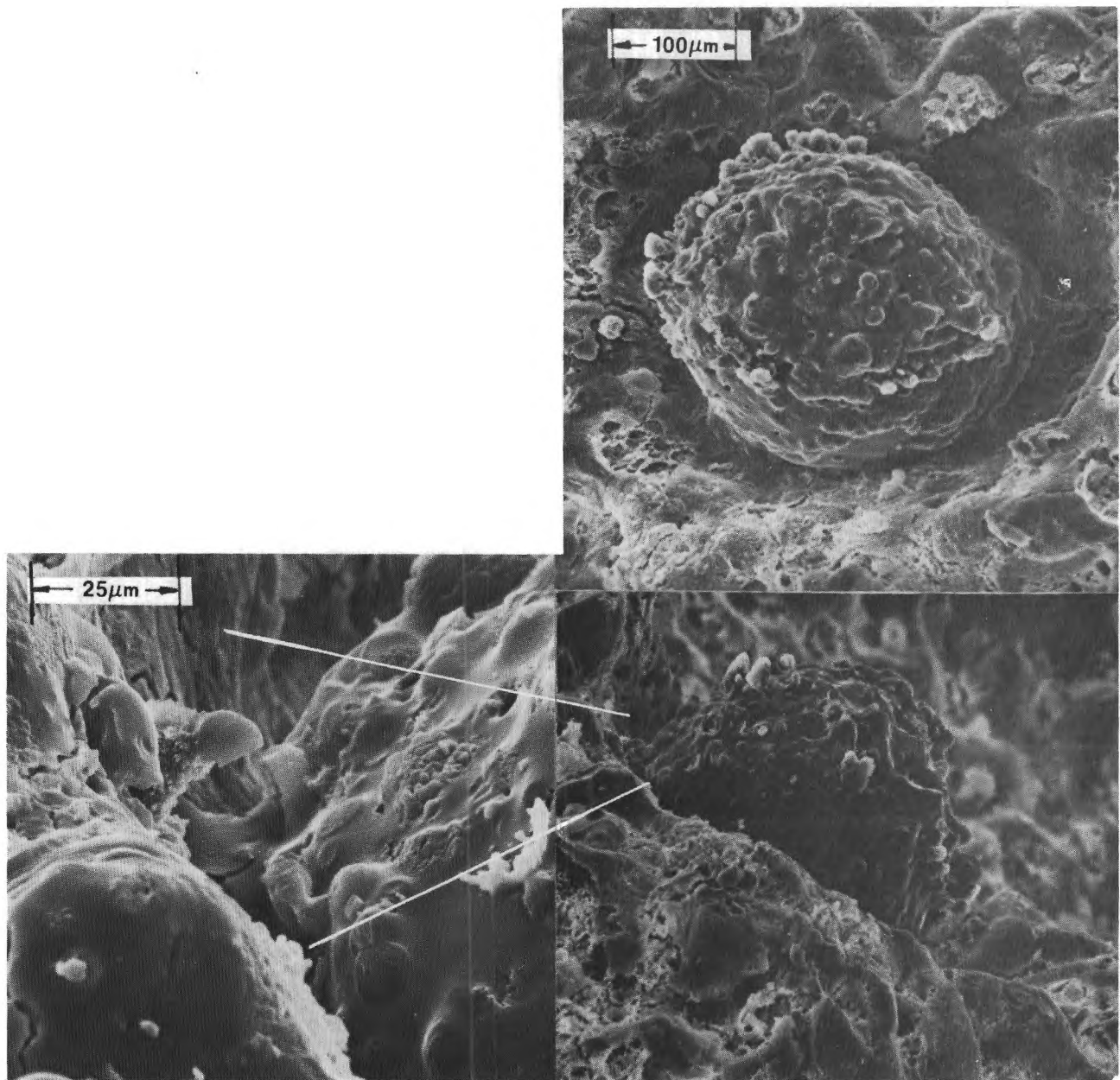


Figure 29. Surface of quenched AP sample having nylon filament die-pressed in the sample. Test at 6.9 MPa.

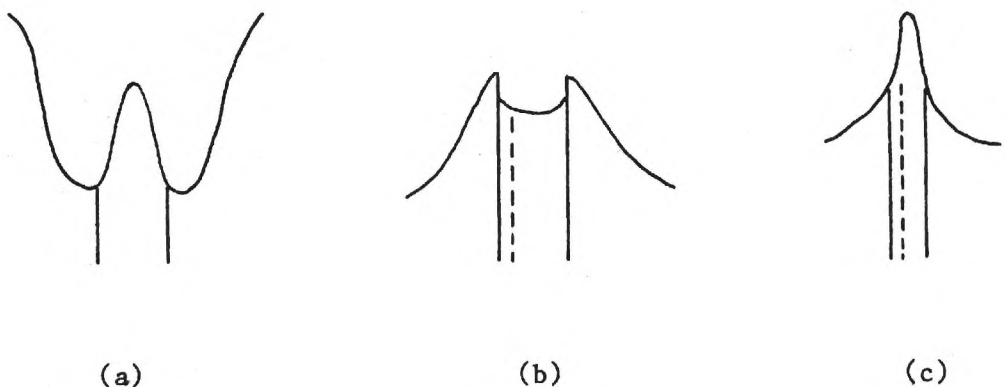


Figure 30. Comparison of quench profiles for HTPB strands in AP and HTPB beads (ridges) on sandwich laminae.

- (a) Profile of cast HTPB strand sample
- (b) Profile of beaded HTPB sandwich (section through bead, perpendicular to laminae), 250  $\mu\text{m}$  bead
- (c) Profile of beaded HTPB sandwich, 125  $\mu\text{m}$  bead

fuel beads, while the samples with pre-formed threads and with filled holes showed accelerated AP regression in the same region. However both showed the typical smooth band with retardation of rate immediately adjacent to the fuel. Both results are suspect because experience with sample preparation is limited and quality is suspect.

#### 4.5 Ordered Arrays of Spherical Oxidizer Particles

In order to study those aspects of propellant combustion that relate to the heterogeneity in the direction of surface regression, a microstructure consisting of ordered arrays of oxidizer particles is needed. Ammonium perchlorate spheres of uniform size would be desirable, because they can be arranged in a "lattice-like" array to give a determinate microstructure. However the nearest approximation to spheres that could be obtained was a commercial grade consisting of rounded particles of nominal 600  $\mu\text{m}$  size. These were not sufficiently uniform in shape and size to

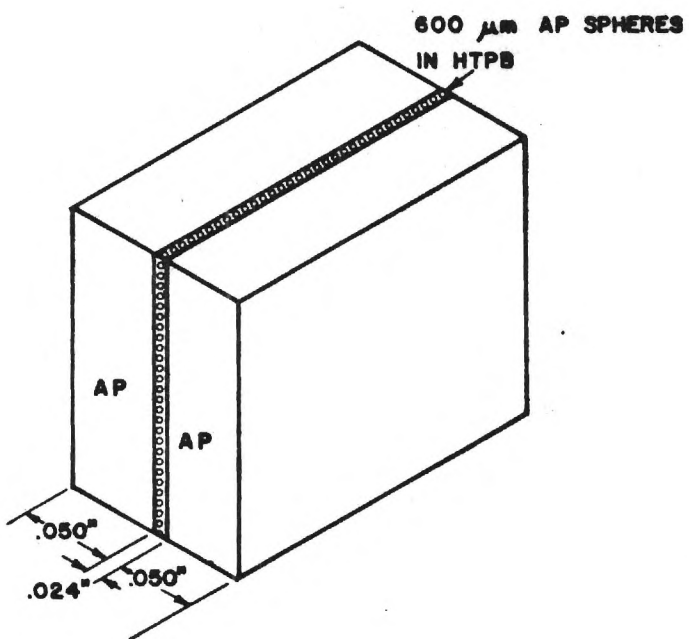


Figure 31. Idealized sandwich with ordered array of oxidizer spheres in the binder lamina.

yield a lattice-array packing. It was decided to test them in a conventional sandwich configuration with the particles in a binder layer of appropriate thickness to accomodate one layer of the AP particles (Figure 31). Four of these samples were prepared and tested, with inconclusive results. Motion pictures were obtained on one test, which showed the burning of the filled binder layer proceeding rapidly and unevenly ahead of the AP sheets. One quenched sample was obtained, which showed irregular burning had occurred with local penetration to the interior of the sample. These difficulties can no doubt be overcome, and further use of this configuration is anticipated.

#### 4.6 Stacked Cylinder Configuration

Propagation of the burning surface through a heterogeneous propellant involves not only deflagration of oxidizer surfaces and propagation down oxidizer-binder interfaces, but also burning through binder layers such as those separating oxidizer particles. In Section 6, this latter aspect

of interparticle burn-through is addressed as an integral part of a burning rate model. However it is recognized that very little is known about this interparticle burn-through process.

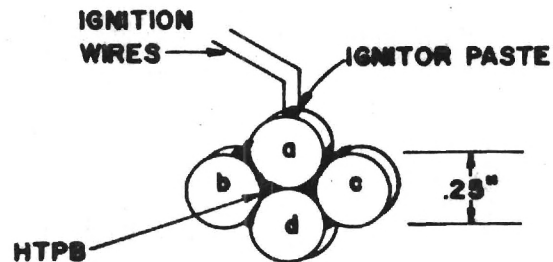
The process of interparticle burn-through was explored experimentally by preparing and burning samples (Table 2) of the form illustrated in part a of Figure 32. These samples were made by pressing cylindrical pellets of AP, 6.35 mm in diameter, and cementing them in the indicated array using HTPB binder. The samples were ignited at the top, and motion pictures were taken to observe how the deflagration proceeded through the sample. Figure 33 shows three frames from one of the motion pictures. Part b of Figure 32 shows the sequences of burn-through between cylinders from five tests. The numbers indicate the time sequence of burn-through. In 4 out of 5 cases, the bottom cylinder was ignited by a sequence of "diagonal" burn-throughs before a direct vertical burn-through occurred.

#### 4.7 Discussion

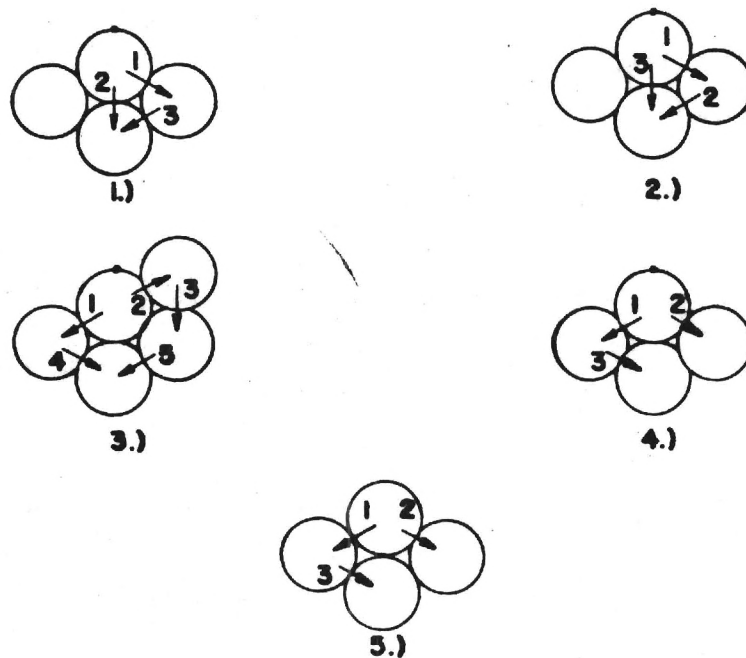
The investigations in this section were largely exploratory, and the results should be regarded accordingly. Of the methods used, some appeared to be amenable to control, some were not. Fuel strands by the beaded sandwich method resulted in regular burning, in a manner compatible with sandwich burning results. However the presence of a char on the binder strand invalidates the method as a test of flamelet stability. Further, it would be desirable to establish whether binder was ejected during quench of the sandwich with coarse binder beads. The objective of current testing with this type of sample is to determine the trend of behavior with pressure.

The results with nylon strands pressed in place suggest that dimensional changes after pressing are leaving a gap between oxidizer and fuel, and the method has been dropped. Results with samples prepared by filling holes in the oxidizer with binder after pressing are inconclusive, and the samples are difficult to prepare reproducibly. However the method holds promise.

The sandwiches with spherical oxidizer particles in the binder layer did not yield any reproducible results, but it is anticipated that useful



a) BEFORE IGNITION



b) RESULTS OF FIVE TESTS

Figure 32. Stacked array of AP cylinders.

- (a) Initial configuration with binder interfaces
- (b) Diagram showing order of burn-through between cylinders, for five tests

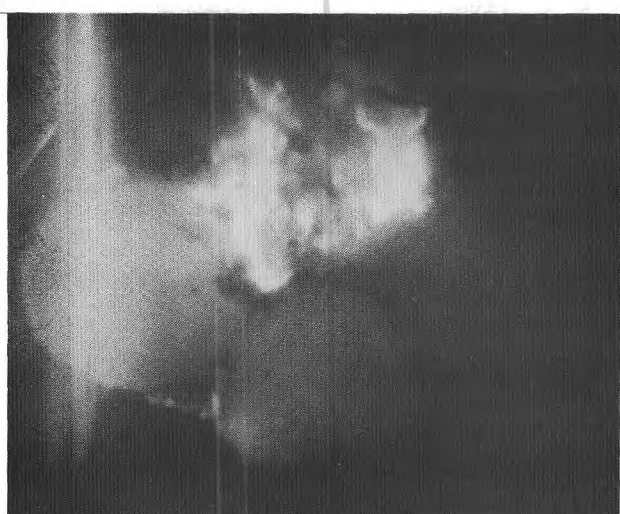
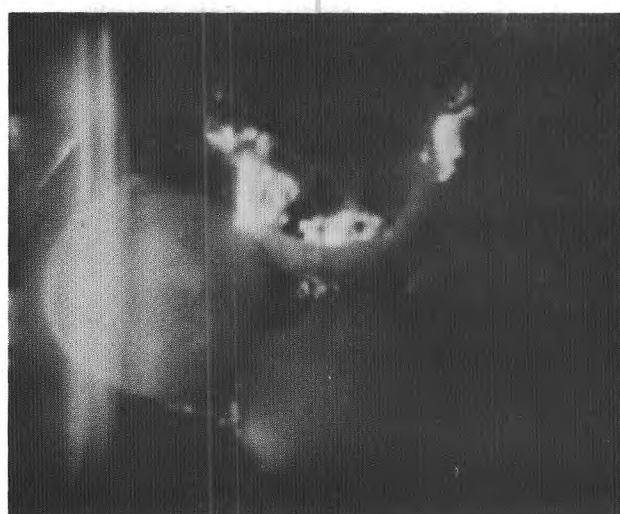
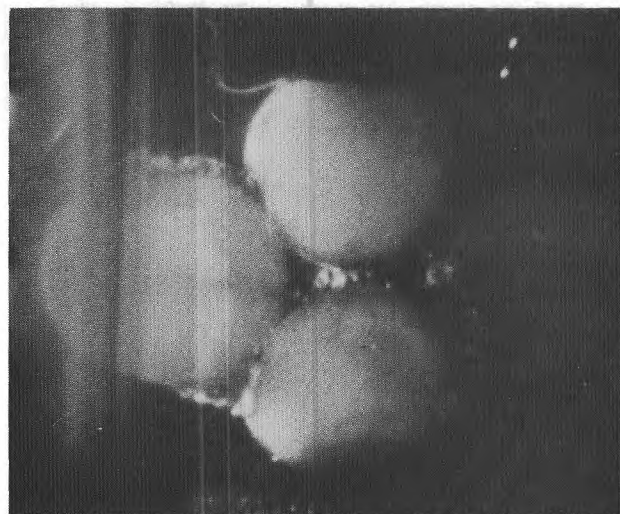


Figure 33. Photographic sequence of burn-through between stacked cylinders.

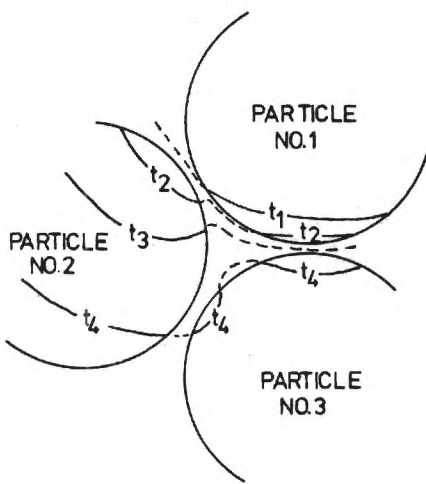


Figure 34. Sketch of propagation of burning surface through propellant microstructure. Example argues the least time path via particles 1 to 2 to 3, interpreting results of Figures 32 and 33.

At time  $t_1$ , interface between particle 1 and 2 is exposed to flame of particle 1, pyrolyzes binder and ignites particle 2 at nearest point.

At time  $t_2$ , particle 1 is burning out without igniting particle 3. Burning front in particle 2 has proceeded from the ignition point.

At time  $t_4$ , the deflagrators front in particle 2 has progressed past the nearest point to particle 3 and has burned through the binder to ignite particles 3 at that point. In the meantime, particle 3 may have ignited at the "top", but the results indicate that the delay causes the deflagration front from that point to lag the one originating at the particle 2-particle 3 point.

results concerning AP particle burning can be obtained by this method, and further tests are planned.

The tests with stacked oxidizer cylinders appeared to answer a fairly critical question concerning the least time path for propagation of the combustion front through the propellant microstructure. Specifically, burn-through of the binder layer between oxidizer particles appears to be a significant factor in propagation of the combustion front. Further, burn-through is apparently more rapid between particles adjoining each other at lateral surfaces than adjoining particles oriented in the direction of propagation of the macroscopic burning surface (Figure 34). This result

suggests that burn-through on lateral interfaces is supported by the sustained convection of hot oxidizer, which is absent when the interfacial binder is reached just as the oxidizer particle burns out. However this result is speculative because of the relatively large size of the oxidizer cylinders in the tests (compared to oxidizer particles in propellants).

Collectively, the various tests on ordered structures were not particularly rewarding, and relatively difficult to carry out. The results may be more revealing than they seem to be, but more testing is needed to distinguish between orderly combustion behavior and artifacts of the experimental methods.



Figure 37. Illustration of the "smooth band" on a quenched AP particle. T-81 propellant quenched from 6.9 MPa. Microscope technique for this picture shows the smooth band better than in previous quenched propellant figures.

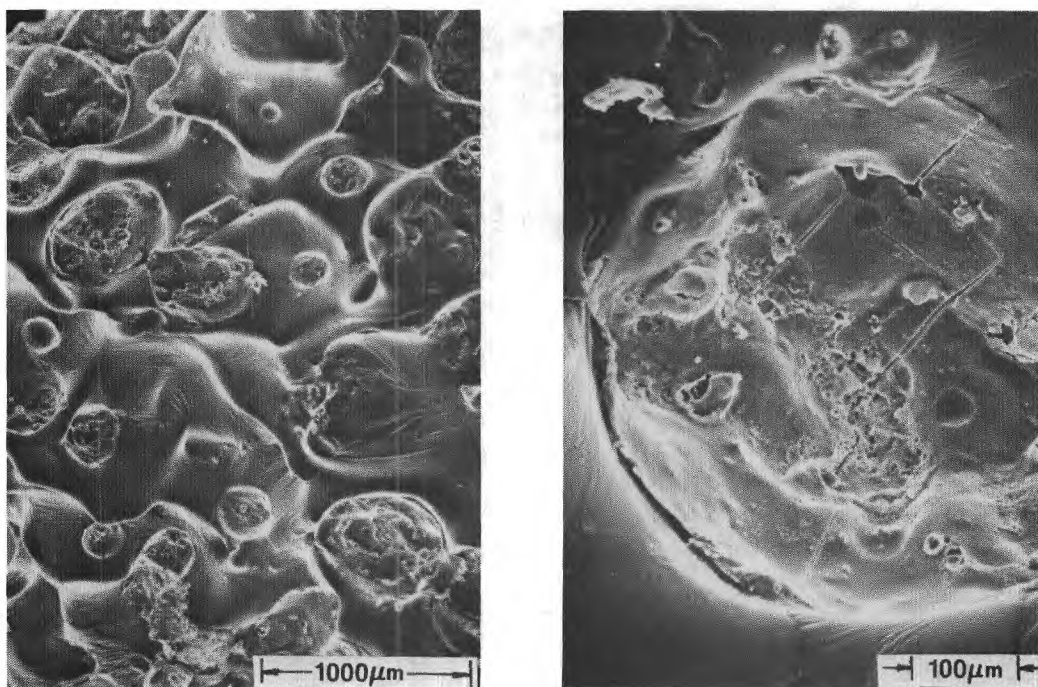


Figure 38. Quenched burning surfaces of AP-HTPB propellant with 600  $\mu$ m AP, 25% binder. Samples quenched from 6.9 MPa.

in the surface layer due to contraction upon cooling back through the cubic-orthorhombic phase transition after quench. Due to the pervasiveness of the binder, no generalizations about the surface profiles near the periphery of the AP surface are ventured here. However, it is notable that the nature and exposure of the AP surfaces is extremely varied. This appears to be due to the different extent of burning of the various particles, and suggests a complex and time-dependent role of the binder during the history of burning of each particle.

#### 5.4 Discussion

The results of this series of tests are similar to results reported by other investigators, and are useful here primarily in the context of the results of tests on ordered structures. As examples, the following analogies and contrasts help to determine what aspects of tests on ordered structures relate to conventional propellants, and what aspects do not:

1. The "smooth band", with apparent retardation of the AP burning rate is common to both propellants and ordered configurations. Whether the smooth surface and retarded rate are causally connected is not established. Further, it is not established whether the burning rate is actually retarded, or whether it simply adjoins a region of the AP surface that has abnormally high rate because of proximity to the diffusion flame.

2. Excess binder leads to accumulation and flow of binder melts, which can dominate the propellant surface. In sandwiches, this corresponds to thick binder laminae, which result in melt flow over the oxidizer. The "smooth band" was initially thought to be a result of binder melt flow over the AP surface, but the band has been evident in many tests under conditions where such flow is improbable, e.g., low pressure-thin binder sandwiches. Quench tests of sandwiches burned in an upside-down position have not shown conspicuous differences in either melt flow or smooth bands, indicating that intermolecular forces are dominant, i.e., the behavior is not fluid flow except possibly in the case of excess binder situations.

3. There is persistent evidence that the deflagration of AP oxidizer involves a very complex surface degradation. This is even more conspicuous

in propellants than with sandwiches, as evidenced by the porous raised areas near the center of the burning surfaces of particles in quenched propellants.

4. Given the complex interaction of binder and oxidizer, it seems likely that the role of the binder changes with time during the AP particle burning, and hence that the AP burning itself changes with time during particle burning. This is an unwelcome development from the standpoint of analytical modeling of propellant combustion, and merits further examination to estimate the range of behavior involved and the effect on burning rate and dynamic response of the combustion zone.

## 6.0 LEAST TIME PATH MODEL FOR BURNING RATE

The current generation of statistical models of heterogeneous propellant combustion stems from the original analyses of Hermance (Reference 14) and of Beckstead, Derr and Price (Reference 15). These models are "light on statistics" and heavy on mechanistic modeling of the combustion zone. The later developments involving more complete statistical description of the combustion were initiated by Glick (References 16, 17), and necessarily embodied relatively little mechanistic modeling (but used an ensemble assumption that drew from mechanistic models or experimental results for mechanistic inputs). These approaches avoid direct confrontation of the basic burning rate questions: "What is the quickest path through the propellant microstructure for burning to proceed to a given point that is distant from the burning surface (distant on the scale of ingredient particle size). How long does it take?" Without confronting these questions, one has not really directly confronted the processes that determine burning rate.

It is not clear that a direct confrontation of these questions would be successful, but at least it would help bring out the areas of ignorance that block progress on the burning rate problem. It was with this realization that efforts were undertaken to develop a "least time path model" for describing burning rate. To minimize the statistical complications in the first analysis, the model was based on a hypothetical propellant made up of oxidizer spheres arranged in a lattice array. The statistical aspect of the problem was introduced by allowing a limited range of variation of diameter of the spheres, which in turn resulted in a substantial percentage variation in thickness of the binder interface between particles. An analysis and computed results are presented in the journal reprint in Appendix A (Reference 18). An end result of the analysis was a realization that one must know more about the three-dimensional aspects of heat flow and surface regression in individual particles, before relevance of any model can be assured. Aside from these uncertainties, the model gave plausible burning rates.

## STABILITY ANALYSIS OF DIFFUSION FLAMES\*

### 7.1 Introduction

During experimental work on this program it was observed that the binder-oxidizer diffusion flame was rarely if ever steady. High speed photography of combustion of sandwiches showed the flame sheet to be more of a "brush" (as noted earlier by Boggs, et al, References 11, 12). In most cases the individual flamelets in the brush were of such short duration that they could not be identified in successive frames of movies at several thousand frames per second. While a variety of explanations were contrived for this unsteadiness relating it to unsteady behavior of binder melt or char accumulation, these explanations seemed to be of questionable relevance when applied to the time scale of unsteadiness observed in the movies. However the question arose as to the stability of the diffusion flame sheet itself. It was noted that steady state solutions to the analytical problem had been used in the past without verification that the solutions were stable, and it was decided to examine this question further. The following is a brief summary of that investigation.

### 7.2 Posing the Analytical Problem

Diffusion flames can arise when unmixed fuel and oxidizer flows come into contact.

Analytical modeling of steady state diffusion flames (e.g., the Burke-Schumann Problem, Reference 19) usually include the following assumptions:

1. Diffusion processes along the convective direction are ignored (boundary layer type assumption).
2. The region of chemical reaction is restricted to a geometrical surface.
3. The geometry of the problem is simple.
4. The flow is considered to be of low speed and assumptions are

---

\* A more detailed description of this work is in preparation as a thesis by T. S. Sheshadri.

made on the velocity and mass flux to either automatically satisfy or solve the mass and momentum conservation equations.

The problem is then solved by solving the energy and species conservation equations.

However, there arises the question of whether these flames are dynamically stable or not. That is to say, if disturbed from the steady state position, will the flame return to its steady state position or not. This, of course, depends in part on the nature of the disturbance. Since any arbitrary disturbance can be expanded in a Fourier series, it is sufficient to consider the stability of the flame with respect to a single general term in such a series. If such a general term grows, decays or remains constant with time the flame is unstable, stable or neutral respectively with respect to that general term. If a flame is to be stable for some arbitrary disturbance it must be stable for all the Fourier component terms that make up the disturbance. Thus, if the flame is shown to be unstable for a single component term it will be unstable for the disturbance as a whole.

### 7.3 Analysis

In order to answer the question of stability of the steady state, the unsteady mass, momentum, energy and species conservation equations are considered. All dependent variables are considered to be the sum of a steady state part (which is known from the steady state solution) and a time dependent perturbation about it. The conservation equations are then linearized in the perturbation quantities. This linearization is essential if all arbitrary disturbances are to be analyzed in a general way. In addition, there is the obvious advantage of simplification in the mathematics. As to the relevance of the linear theory, the following can be said. If the linear theory indicates instability, so will the non-linear theory. On the other hand if the linear theory indicates stability, there can still be finite amplitude unstable oscillations as a result of finite initiating disturbances.

The perturbation quantities are taken as a general Fourier component

term of the arbitrary disturbance. Their behavior in time can be obtained by solving the linearized conservation equations and this answers (within the scope of the linear theory), the question of the dynamic stability of the flame.

The above procedure was carried out for a diffusion flame problem whose geometry differs somewhat from that of the Burke-Schumann problem, and is illustrated below:

There are two concentric tubes, both of which terminate at  $z = 0$ . Oxidizer flows through the inner tube and outside the outer tube. Fuel flows between the inner and outer tubes. Diffusion flames can exist in the region  $z \geq 0$ .

#### 7.4 Results

The analysis shows that if perturbation solutions about the steady state exist at all, they must exist in conjugate pairs--one corresponding to an unstable solution, the other to a stable one. Both of these solutions are found to exist by computer analysis of the problem, thus establishing the instability of this class of diffusion flames.

The choice of geometry was motivated by the possibility of application to the combustion of composite solid propellants, where diffusion flames play a major role over certain pressure ranges. The results of the analysis suggest that the diffusion flame "sheets" from the individual oxidizer particles in a propellant may be inherently unstable. It is too much to infer from the analysis what the diffusion flamelets would be like, but the indicated inherent unsteadiness could be very important in low-pressure burning and in oscillatory burning. The results are consistent with the observation that the flame sheet in sandwich-burning tests is spatially discontinuous and temporally intermittent. More generally, the results indicate that the classical solution to a particular simple steady state flame problem represents a physically unattainable solution.

## STATISTICAL MODELING OF THE COMBUSTION ZONE

### 8.1 Introduction

Description of combustion zone behavior is very difficult when the combustion zone is a chaotic array of surfaces and flamelets. Since a detailed description over a representative surface area is virtually impossible, one resorts to statistical means of describing what is happening. Even in statistical descriptions, there is a need for severe assumptions in the interest of mathematical tractability (indeed, a statistical description of the propellant microstructure alone is a formidable task). Early approaches made severe assumptions about statistics of the surface microstructure in order to preserve some capacity to represent the flame structure (References 14, 15). This was followed by approaches that more fully describe the chaotic array of the burning surface, but contained no modeling of the flame structure (References 16, 17). Influence of flame structure was introduced with the aid of results from the earlier flame-structure-oriented models. In the course of the present studies, three efforts were carried out that pertained to statistical modeling. One was a review of current models, which was reported in Reference 5. A critique of models, based on Reference 5, is presented in the following Section (8.2). This is followed (Section 8.3) by a detailed description of the original surface-statistics-oriented analysis, carried out primarily to clarify the assumptions used.\* Finally, Section 6.0 presents a new statistical approach (published as Reference 18), which is designed to force consideration of mechanisms dominant in determining burning rate, even in the process of setting up the statistical approach (tractability is preserved in this approach by limiting the disorder in the propellant microstructure).

---

\* Since Section 8 was written, significant extension of statistical models has occurred, and the resulting models are reviewed in Reference 20. However, the following discussion remains relevant, and instructive to many readers. Accordingly, it is presented for "tutorial" purposes and to aid in perspective.

## 8.2 Critique of Statistical Models

For practical purposes, a description of combustion zone structure is of no interest, except to the extent that it is needed to describe or control macroscopic burning of the propellant. In problems of steady-state burning, the detailed behavior can be averaged in both space and time (i.e., we are concerned with regression of surfaces that are large compared to the scale of the propellant microstructure, and with times that are long compared to the burning time of elements of the microstructure). In transient problems we are concerned with the transient responses of large surfaces, but often on time scales comparable to (or shorter than) the burning time of elements of the microstructure. Thus it is natural that modelers would seek to describe the microscopic details of the combustion zone in statistical terms that allow surface-wise averaging of surface and flame elements. Of course the goal is to achieve surface-wise averaging of the behavior of elements. This usually starts with statistical descriptions of some classes of elements of the combustion zone that are considered to be important to macroscopic burning behavior. This presumes an a priori knowledge of what determines the surface average behavior. This last point is extraordinarily important, because a substantial body of analysis and "supporting" experiments has developed on this intuitive foundation. It is important that this intuitive foundation be strengthened by appropriate mechanistic studies; if this is not done the evolution of a relevant statistical model will be arrested.

The foregoing arguments are well illustrated by past work. The early work of Hermance (Reference 14) was done at a time when the idea of attack of oxidizer vapor on binder surface or fuel vapor on oxidizer surface was strongly advocated by some investigators. In the Hermance burning model, such reactions were assumed to cause burning to proceed down the interface between oxidizer and binder. This particular element of the combustion zone was found in the analysis to be the most important source of heat feedback to the solid, and hence the dominant factor in overall burning rate. However, concurrent experimental studies of burning of propellants and oxidizer-binder "sandwiches" (Reference 6) revealed that interfacial burning did not occur with conventional binders and oxidizers, thus casting

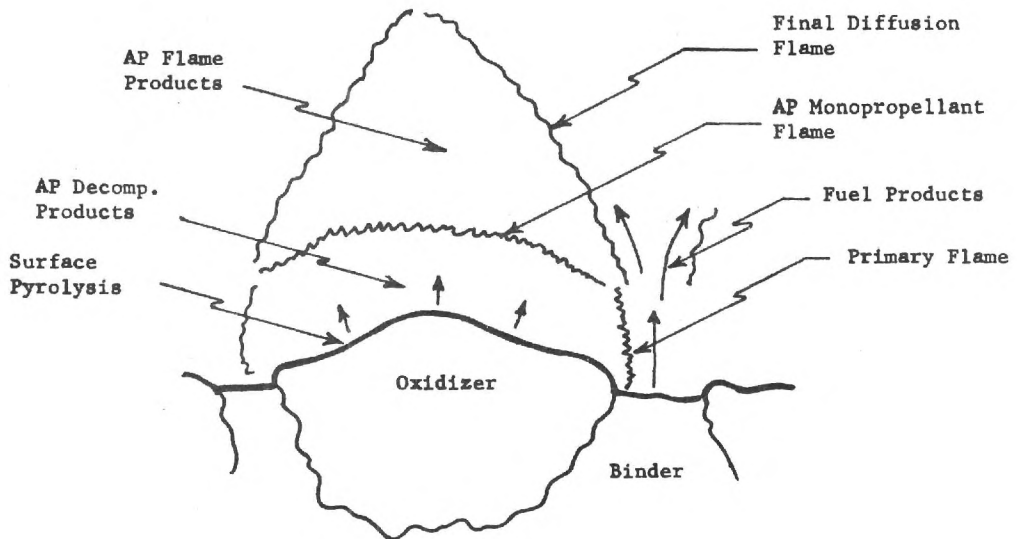


Figure 39. Combustion zone structure assumed in original Beckstead-Derr-Price model (Reference 15).

in doubt the foundation of the "heterogeneous" theory.

The statistical approach of the Hermance model was combined with a more relevant representation of the combustion zone structure by Beckstead, Derr and Price (Reference 15) and this "BDP" model has been moderately successful in describing the macroscopic steady state combustion behavior of nonaluminized ammonium perchlorate propellants with hydrocarbon binders. This model describes the combustion (Figure 39) in terms of four kinds of flame elements,

#### General Flame Structure Assumptions

1. Exothermic decomposition of AP at its surface
2. Exothermic gas phase flame of the AP
3. Primary diffusion flame between binder pyrolysis products and intermediate decomposition products of AP
4. Secondary diffusion flame between binder pyrolysis products

In the formulation of the original model, all flame elements were tied to the exposed surface size of the oxidizer particle by partly assumed, partly calculated flame structure. Thus the burning surface became a statistical array of oxidizer surface elements, each with its own independent oxidizer and diffusion flame structure. Further, it was assumed that the statistical array of oxidizer surface elements could be replaced by an equal number of elements of a single, "average" size, in the process replacing also the variety of flame structure by an array of identical flames. These assumptions are tabulated here because they will come up again.

#### Some Implicit Flame Structure Assumptions

1. A unique flame structure is determined for each size of exposed oxidizer surface (assumed circular).
2. The flame structure in 1 is independent of the time in the burning of the particle (except as the size of the exposed surface changes).
3. The flame structure in 1 is independent of the nature of surrounding (or preceding or underlying) microstructure.
4. The differences in flames of different sizes (insofar as their effect on macroscopic combustion behavior is concerned) averages in the same way as does oxidizer surface area.

These were perfectly appropriate strategies to use in the interest of mathematical tractability, but they represent further compromises with reality, the impact of which can only be assessed in retrospect, and then only if appropriate mechanistic studies are made to evaluate them and motivate further improvement in modeling. Efforts to correlate experimental burning rate trends with predictions of the model have suggested that the flames associated with small oxidizer surfaces must be "weighted" in the averaging process because they are more effective on a per unit area basis than large oxidizer surfaces, i.e., to an extent not balanced by the opposite effect for surfaces that are above the average size. This is a plausible approach within the constraints of present modeling, but the experimental trends the revised model seeks to accomodate may in fact be due to processes not encompassed in the present models at all.

A more general treatment of the statistical aspects of the combustion

zone was proposed by Glick (Reference 16) and developed further by Glick and Condon (Reference 17), and Cohen, et al (Reference 21). This treatment, as originally proposed, was concerned primarily with statistical description of the array of surfaces of oxidizer particles, so as to avoid settling for an average size. In this more general statistical description the implicit assumptions 1-3 above are still accepted, but the fourth is not. Instead it is assumed that the surface regression rate of the oxidizer particle is a unique function of the exposed particle surface area, and that the net oxidizer mass flow is the sum of that from the individual particle surfaces, each regressing according to its size. In a limited sense, this constitutes the "weighing" process called for in the last paragraph. In order to find the functional dependence of the oxidizer surface regression rate on the surface area, it is assumed that the rate for a given size oxidizer surface element is the same as the rate of a propellant containing only that size oxidizer particle areas, as calculated by a mechanistic model such as the BDP model. This scheme provides a computational procedure to calculate burning rate of the propellant as a function of oxidizer particle size distribution. Its validity is unknown, as it contains a logical inconsistency that prevents evaluation. The inconsistency is that small particles are supplied to the propellant burning surface only in the number present in the propellant. If they burn faster than the larger particles (i.e., higher surface regression rate), their population on the surface will be depleted until they contribute to the net oxidizer flow in the proportion corresponding to their mass proportion of total oxidizer in the propellant. Thus they cannot increase propellant burning rate simply by burning faster individually. They must in the process increase the rate of combustion of larger particles. At present the statistical models do not provide for this, as reflected in Implicit Assumption Number 3. The mechanistic models contain a potential for such effects, although it is by an indirect means relying on an aspect of the models discussed in the following.

In the mechanistic models, a second kind of averaging takes place, disguised in the use of "one dimensional" heat transfer to the propellant surface. The model seeks to determine the amount and average site of heat

release in the various reaction steps noted above. The "site" of heat release refers to distance from the burning surface, and an average distance is calculated in order to make a one dimensional heat transfer calculation to establish the effectiveness of that particular reaction step in supplying heat back to the surface to drive the combustion wave. In this kind of calculation, the concentrated sources are presumed to supply heat impartially to all of the surface. While current studies on this are seeking to deal with contributions from more than one oxidizer particle size (thus averaging contributions over the particle size range), they are not examining the significance of the three dimensionally local nature of reaction sites. Such an examination is necessary before a rational basis can be established for how the burning of small particles affects the burning of large particles, i.e., flame interaction (elimination of Implicit Assumption Number 3).

Some modifications of the original BDP mechanistic model have been made recently to accomodate for the inclusion of nitramine (HMX, RDX) particles (References 22 - 25) and exothermic binders (e.g., NG/NC) (Reference 26). These modifications have not received objective evaluation, so will not be examined here. Their nature is chosen to deal with differences in deflagration of the "new" particulate materials, and corresponding modification of flame structure resulting from the monopropellant nature of the binders, the melting properties of ingredients (and surface flow), and the different stoichiometry of nitramines and of NG/NC binders. Many of the difficulties with earlier models have been confronted in the more recent work by Beckstead (Reference 26), but a final report is not currently available. In general, the new work increases the flexibility of the model to deal with differences in ingredient characteristics, but of necessity deals superficially with detailed combustion steps and the statistics of "chaotic" surfaces.

As a matter of perspective, it should be understood that proper modeling of the transient behavior of composite propellants is an order of magnitude more difficult. Not only are the Implicit Flame Structure Assumptions of doubtful relevance, but time-wise averaging is no longer applicable.

The entire array of flame elements and local structure changes with time during a transient, in a manner that is largely unexplored. Recent efforts to adapt the statistical approach to description of transient response have not argued these points. Instead they have, in effect, determined the surface-averaged steady state burning and then used classical one dimensional theory to calculate transient response of a homogeneous propellant having those steady state burning characteristics. To take care of the fact of a spread of sizes of oxidizer areas in the surface, the one dimensional approach is applied over the size range, and a net transient response is calculated as the sum of the independent contributions of each particle size. It is extremely unlikely that this approach will give valid results, as none of the Implicit Assumptions are realistic, and any one-dimensionalization of heat feedback is also invalid when applied on a time-resolved basis. Further, there is not enough known about response of the individual flame structural elements to environmental disturbances (e.g. pressure oscillations) to know what to average in order to obtain the time resolved macroscopic combustion zone response.

Beyond these problems for experimentalists and modelers are the very real problems of how combustion characteristics are modified by certain low-concentration propellant additives, and how to model the role of ingredients such as aluminum, HMX, or nitroguanadine, ingredients whose behavior is either unknown, or known to be very complex.

### 8.3 Surface-Statistics-Model

As noted above, one line of endeavor in recent years is aimed at a more complete representation of the statistics of the propellant heterogeneity in the combustion models. The original approach by Glick is presented here with some elaboration and clarification of the assumptions used, or implied by the approach.

8.3.1 The burning surface of a propellant is revealed by examination of quenched samples, and shows a myriad of different size oxidizer surfaces, the different sizes reflecting different size oxidizer particles and different

times during burning of individual particles (Figure 20). For the present purposes, it is assumed that each exposed oxidizer particle can be characterized by a surface area,  $s_{ox}$  (i.e., there is a single well-defined continuous closed boundary between oxidizer and binder for each exposed oxidizer particle). Consequently there is a size distribution function  $F_{ox}$ , for surface area elements of oxidizer, defined by

$$\frac{dN}{N} = F_{ox} ds_{ox} \quad (1a)$$

In this expression, N represents the number of all exposed oxidizer surface elements in a large typical surface population of elements;  $dN$  is the number of those elements in the surface area range  $s_{ox}$  to  $s_{ox} + ds_{ox}$ ; and  $F_{ox}$  is that function of  $s_{ox}$  that satisfies the equation. As a matter of convenience it is assumed that these variables (N and  $F_{ox}$ ) refer to a unit of planar propellant surface area. This normalization and the use of differential notation imply that  $F_{ox}$  is continuous, i.e., based on an infinite population of surface elements, or derived from a "smoothed" fit to a finite population. By the same token, it is then necessarily assumed that there are no significant variations in  $F_{ox}$  on a macroscopic scale (if there were, a characteristic burning rate would not exist, a problem that sometimes occurs in practice when propellants are not properly mixed). It is appropriate to note here that  $F$  can be interpreted as a probability function, i.e.,  $F_{ox} ds_{ox}$  for a particular value of  $s_{ox}$  is the probability that a randomly chosen oxidizer surface element will fall in the size interval  $s_{ox}$  to  $s_{ox} + ds_{ox}$ .

Dealing with the oxidizer surface elements in statistical terms comes more naturally than with binder (fuel) surface elements, because the oxidizer elements are the more active contributors to combustion, are relatively defineable, and are related to the statistics of the original oxidizer particles used in the propellant. However, the binder plays a role in the burning rate of the propellant, and thus needs to be considered in the statistical modeling. Glick (Reference 16) suggests that the web of exposed binder (fuel) on the burning surface be viewed as an array of fuel surface elements, each associated with a particular oxidizer particle,

and having a particular surface area,  $s_f$ . At the moment, one might defer the exact procedure for identifying the fuel surface element or the pairing rule relating  $s_f$ 's to  $s_{ox}$ 's, and simply hypothesize a distribution (probability) function for fuel elements similar to that for oxidizer.

$$\frac{dN}{N} = F_f ds_f \quad (1b)$$

Since the fuel and oxidizer surface elements are paired, N is the same for both (every choice of an oxidizer particle brings a fuel particle). The distribution functions have the property that

$$\int \frac{dN}{N} = \int F_f ds_f = \int F_{ox} ds_{ox}$$

when the integration is over the full element size range. This implies simply that all N particles are in that range, or that the probability of a particle being in that range is one. Ultimately, one is interested in the fuel-oxidizer surface elements as pairs. The statistical distribution of size of pairs involves two size variables,  $s_{ox}$  and  $s_f$ . If one defines  $d^2N$  to mean the number of pairs (out of N total) with  $s_{ox}$  between  $s_{ox}$  and  $s_{ox} + ds_{ox}$  and  $s_f$  between  $s_f$  and  $s_f + ds_f$ , then a frequency distribution for pairs can be defined as

$$\frac{d^2N}{N} = \mathcal{F} ds_{ox} ds_f \quad (2)$$

where the script form of  $\mathcal{F}$  denotes a distribution function for pairs. This is depicted in Figure 40. In this definition, it is assumed that N and  $\mathcal{F}$  refer to the population per unit planar surface area, analogous with the definitions of  $F_{ox}$  and  $F_f$ . In the figure,  $d^2N/N$  is the volume under the surface element  $ds_{ox} ds_f$ , the probability that a randomly chosen pair will be in the particular interval  $ds_{ox} ds_f$ . Double integration over the entire size range present will give all the particle pairs, i.e., the integral of  $d^2N/N$  equals one; this corresponds to a volume of one under the surface (probability of one that a randomly selected pair from the population will be a member of the population).

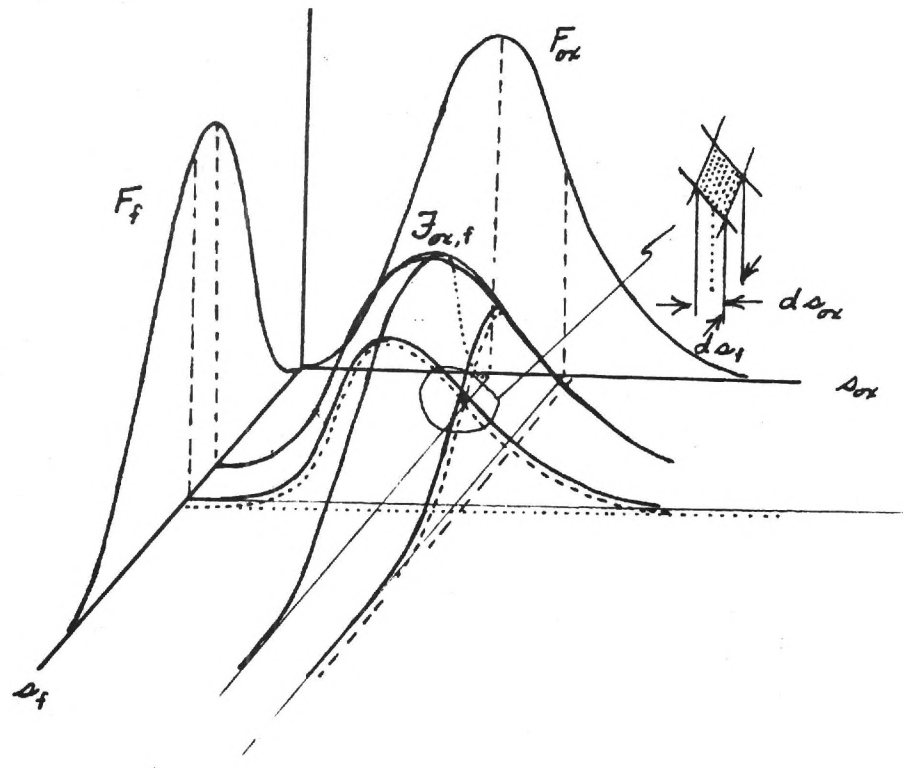


Figure 40. Combined distribution function for oxidizer and fuel elements (Equation 2).

The function  $\mathcal{F}$  is related to the functions  $F_{ox}$  and  $F_f$ . Thus if one considers a specific value of  $s_{ox}$ , it relates to a curve on the  $(s_{ox}, s_f)$  surface, parallel to the  $s_{ox} = 0$  coordinates plane (Figure 40). The volume under a differential slice of the  $\mathcal{F}$  surface based on the constant  $s_{ox}$  curve is the proportion of oxidizer particles,  $dN/N$  in the interval  $ds_{ox}$ . In other words

$$\frac{dN}{N} = (\int \mathcal{F} ds_f) ds_{ox} = F_{ox} ds_{ox} \quad (3a)$$

$$= (\int \mathcal{F} ds_{ox}) ds_f = F_f ds_f \quad (3b)$$

So  $\mathcal{J}ds_f$  is the probability that a random sample will have a value of  $s_{ox}$  between  $s_{ox} + ds_{ox}$  regardless of value of  $s_f$  (and analogous statement for  $\mathcal{J}ds_{ox}$ ).

The analytical form of the function  $\mathcal{J}$  is determined by the distribution functions of  $s_{ox}$  and  $s_f$ ; but any specific distribution function,  $\mathcal{J}$ , depends on a pairing rule for fuel and oxidizer surface elements. Do large oxidizer surface elements tend to occur in combination (pair) with correspondingly large fuel surface elements, and small  $s_{ox}$  with small  $s_f$ ?; large  $s_{ox}$  with small  $s_f$ ?; random combinations? To answer this question rationally, one would have to go back and define fuel surface elements, presumably in a manner based on the real issue, characterization of an element of the statistical flame population (References 16 and 26). For most propellants, the particulate content is so high that random packing of particles in the solid is impossible, so a valid rule for pairing of oxidizer and fuel surface area elements would have to reflect the fact that small particles pack in the "voids" among large particles. Thus fuel surface elements would have to reflect this fact in their definitions and in the resulting rules regarding how the elements pair with the oxidizer surface elements to give the distribution functions  $F_{ox}$ ,  $F_f$  and  $\mathcal{J}$ . This aspect of the statistical models has been circumvented almost without comment in most modeling work, simply by making unevaluated assumptions (see comments in Reference 26).

Continuing on the approach used by Glick (Reference 15), the pairing problem was "solved" by assuming that the pairing was a matter of pure chance; then for a particular increment,  $ds_{ox}$ , of the  $F_{ox}$  population, the number of those oxidizer elements that are paired with a particular increment,  $ds_f$ , of fuel elements is determined by the proportion,  $F_f$ , of the fuel elements in that particular  $ds_f$  increment.

Analytically the foregoing restrictive assumption, i.e., random pairing, means that all constant- $s_{ox}$  curves on the distribution surface are functionally alike and all the constant- $s_f$  curves are functionally alike, which implies that  $(s_{ox}, s_f)$  has the form (Reference 27)

$$\mathcal{J}(s_{ox}, s_f) = f(s_f) f(s_{ox}) \quad (4)$$

(in the following the functional notation will be dropped, leaving  $f$  with the subscript "f" referring to a function of  $s_f$ , or  $f$  with the subscript "ox" referring to a function of  $s_{ox}$ ). Thus, for any "random pairing" distribution surface,  $\mathcal{J}$ , the function  $f_f$  is a simple function of  $s_f$  only, and  $f_{ox}$  is a simple function of  $s_{ox}$  only.

For a distribution function of the form above (Equation 4), the distribution  $f_{ox}$  and  $f_f$  are simply related to  $F_{ox}$  and  $F_f$ . Thus

$$\frac{d^2N}{N} = \mathcal{J} ds_f ds_{ox} = f_f f_{ox} ds_f ds_{ox} \quad (5)$$

and following the form of Equation 3,

$$\frac{dN}{N} = (\int f_{ox} ds_{ox}) f_f ds_f = F_f ds_f \quad (6a)$$

$$\frac{dN}{N} = (\int f_f ds_f) f_{ox} ds_{ox} = F_{ox} ds_{ox} \quad (6b)$$

This implies that

$$f_f = F_f / \int f_{ox} ds_{ox} \quad (7a)$$

$$f_{ox} = F_{ox} / \int f_f ds_f \quad (7b)$$

and substituting in Equations 4 and 5

$$\mathcal{J} = F_f F_{ox} / [\int f_{ox} ds_{ox} \int f_f ds_f] \quad (8)$$

$$\frac{d^2N}{N} = [F_f F_{ox} / \int f_{ox} ds_{ox} \int f_f ds_f] ds_{ox} ds_f \quad (9)$$

Recalling that double integration of Equation 5 yields a volume of 1 under the surface  $\mathcal{J}$  (probability of 1), Equation 5 means that

$$\iint \mathcal{J} ds_f ds_{ox} = \iint f_f f_{ox} ds_f ds_{ox} = \int f_f ds_f \int f_{ox} ds_{ox} \quad (10)$$

Then the denominator in the bracket in Equation 9 has a value of one, and

$$\frac{d^2N}{N} = \mathcal{J} ds_f d\sigma_{ox} = f_f f_{ox} ds_f d\sigma_{ox} = F_f F_{ox} ds_f d\sigma_{ox} \quad (11)$$

In other words, for the special form of the distribution function in Equation 4,

$$\mathcal{J} = f_f f_{ox} = F_f F_{ox} \quad (12)$$

This is the form of the distribution function used originally by Glick (Reference 15). When the realities of defining and pairing of fuel and oxidizer surface elements are more thoroughly examined, and applied to situations such as bimodal oxidizer particle size distributions, this assumption of random pairing will need review and may have to be modified. However, it will be used for the present, and attention will be turned to other considerations.

8.3.2 Mass flow from the burning surface is the objective of most analytical models of solid propellant combustion. Indeed, the singular nature of the surface (as a boundary separating domains of physical and chemical states and of transitions of physical and chemical processes) traditionally leads to analytical formulation of conservation laws for the surface. These are used as boundary conditions for joining models of processes in the solid with processes in the gas. This convention is obviously jeopardized by presence of a chemically heterogeneous, geometrically complex surface, and the principal role of the statistical model is to represent the real process in some average form. Early approaches (References 14, 15) sought to achieve this by replacing the distribution of sizes of oxidizer surface elements by that resulting from some "effective" single size spherical particles. Since this still gave a distribution of oxidizer surface element areas (different times during burning of the "monodisperse" particles), a further approximation was made, i.e., all surface elements were the same size, that size being the time-average area for burning of a particle. This purely hypothetical surface was then used to write mass

conservation equations. The mass burning rate (per unit area) on the surface elements was considered to be a function of surface element size, but only after arriving at the hypothetical "equal circle" representation of the surface (i.e., only for different propellants). As noted by Glick, this does not take into account the fact that the mass burning rate per unit area actually is not expected to be the same for all surface elements because of actual size difference. If an average procedure is to be used in writing the conservation laws, the average must be an average of the quantity being conserved; in this case, mass flux, not area. Glick went to some lengths to stress this. However, the situation is complex, and successive studies will no doubt continue to reveal shortcomings in prior analyses. For example, the original analysis by Glick did not consider

1. The dependence of mass flux (flow per unit area) from surface elements of the same size at different stages in the particle burning ( $m_{ox}$  is assumed to be a function of  $s_{ox}$ , with reference to size of particle or stage of its burning).
2. The nonuniformity of mass flux as a function of location on the element surface.
3. The imprecise definition of the binder surface elements and corresponding difficulty of deciding anything about mass flux from them.

Regardless of these unresolved problems, it is no doubt worthwhile to pursue the formulation of mass conservation equations within this limited context, and generalize from there as familiarity with the analysis and advances in mechanistic knowledge subsequently permit. Thus, following the general approach of Glick, the mass flow rate per unit area of oxidizer produced from the  $d^2N$  surface elements in the size range  $s_{ox}$  to  $s_{ox} + ds_{ox}$  and  $s_f$  to  $s_f + ds_f$  is

$$d^2\bar{m}_{ox} = m_{ox} ds_{ox} d^2N = m_{ox} s_{ox} (N \mathcal{J} ds_{ox} ds_f) \quad (13)$$

Thus contributions to flux from pairs of surface elements in which the oxidizer surface elements are in the range  $s_{ox}$  to  $s_{ox} + ds_{ox}$  (but all  $s_f$

sizes) is

$$d\bar{m}_{ox} = N s_{ox} \left( \int m_{ox} f d\sigma_f \right) ds_{ox} \quad (14)$$

and the total oxidizer flux per unit planar surface area is

$$\bar{m}_{ox} = N \int s_{ox} \left( \int m_{ox} f d\sigma_f \right) ds_{ox} \quad (15)$$

In these integrations it should be noted that  $m_{ox}$  remains under the inner integral, reflecting its possible dependence not only on oxidizer surface element size, but also on fuel surface element size. In Equation 15, no use has been made of the random pairing assumption used by Glick. If the assumption is used, Equations 12 and 15 give Glick's equation 7 (Reference 15)

$$\bar{m}_{ox} = N \int s_{ox} F_{ox} \int m_{ox} F_f d\sigma_f ds_{ox} \quad (16)$$

Further, if the dependence of  $m_{ox}$  on fuel surface element size in the pair is neglected, this simplifies further to

$$\begin{aligned} \bar{m}_{ox} &= N \int m_{ox} s_{ox} F_{ox} \int F_f d\sigma_f ds_{ox} \\ \bar{m}_{ox} &= N \int m_{ox} s_{ox} F_{ox} ds_{ox} \end{aligned} \quad (17)$$

In a practical sense, this last assumption may not represent a serious further departure from reality, as the dependence of oxidizer product flux on fuel element size cannot be realistically accounted for in Equation 16 anyway, because the oxidizer surface elements have not been realistically paired with the fuel surface elements by the random pairing assumption used. All three of the forms 15 - 17 may merit future consideration, depending on the particular situation and application.

It should be noted that a parallel development can be made to obtain symmetrical equations for fuel product flux. If needed, those equations can be written from Equations 14-17 by interchanging subscripts ox and

f. As noted before, calculations based on fuel product flux are usually not used because of poor definition of the fuel surface elements and relatively passive role of the fuel surface. This may not always be so in future developments. However, it is necessary that the oxidizer and fuel product mass flows be in a ratio dictated by the mixture ratio of binder and oxidizer in the propellant. Thus if

$$\frac{\bar{m}_{ox}}{\bar{m}_T} = \alpha_{ox}; \quad \frac{\bar{m}_f}{\bar{m}_T} = \alpha_f; \quad \alpha_{ox} + \alpha_f = 1 \quad (18)$$

$$\bar{m}_T = \frac{\bar{m}_{ox}}{\alpha_{ox}} = \frac{\bar{m}_{ox}}{1-\alpha_f} = \frac{\bar{m}_f}{\alpha_f} = \frac{\bar{m}_f}{1-\alpha_{ox}} \quad (19)$$

The quantity  $\bar{m}_T$  is the net mass flow rate per unit planar burning surface area, the  $\alpha$ 's are a result of the propellant formulation, and suitable representation of  $\bar{m}_{ox}$  (or  $\bar{m}_f$ ) can be obtained from the foregoing (e.g., Equations 15-17).

8.3.3 Application of Equations 17 and 18 provides a scheme for calculating mass burning rate per unit planar surface area, and hence linear surface regression rate. The actual calculation is dependent on knowing the variables on the right in Equations 15-17. "Knowing the variables" means knowing the functional forms necessary to carry out the integrations. Using the results depends, of course, on knowing the dependence  $m_{ox}$  on other variables of interest, variables not explicitly shown in the equations, variables such as fuel-oxidizer pairing, propellant temperature, environmental pressure, and deflagration characteristics of the oxidizer. In short, Equations 15-17 and 19 constitute a statistical statement of the mass conservation at the burning surface. All other important aspects of the combustion process must be independently modeled in a form giving  $m_{ox}$  as a function of all relevant variables, including specifically those variables ( $s_{ox}$ ,  $s_f$ ) needed to carry out the indicated integrations.

In addition to knowing  $m_{ox}$  ( $s_{ox}$ ,  $s_f$ ) to evaluate  $\bar{m}_{ox}$  and  $\bar{m}_T$ , the

distribution function of surface element pairs must be determined. This is ordinarily thought of as deriving from the oxidizer particle size distribution, and has been based entirely on that in some analytical models (e.g., References 20-23). As evidenced by the foregoing (and the analysis of Glick), a more rigorous statistical model of the surface is not affected by the exact meaning of  $s_{ox}$  and  $s_f$ , at least up to Equation 19 inclusive. The "day of reckoning" comes when these vagaries focus into a determination of  $m_{ox}$  vs  $s_{ox}$ ,  $s_f$  pairs, a determination that cannot be made rigorously without reference to the complex micro-scale processes in the combustion zone that determine the surface details discussed in the present report. These pitfalls may be "boldly" circumvented by making direct assumptions about the surface geometry (all models to date do); and assumptions about dependence of  $m_{ox}$  on particle size, about pairing of  $s_{ox}$  and  $s_f$ , and about other variables such as pressure. It must be anticipated that such reckless appearing assumptions will be tried, in the interest of mathematical tractability. In a sense, they are a logical step in the search for understanding and useful results.

Those investigators who have use of the foregoing statistical approach have obtained the dependence of  $m_{ox}$  on pressure and temperature from the results of earlier published models (References 14, 15). This evades direct consideration of energy conservation and combustion processes in general, bringing instead a more visible treatment of the statistics of the burning surface.

In the interest of early progress towards realistic modeling, it is helpful to have clearly in mind the nature of the assumptions in present models. The following summarizes those assumptions explicitly. There is a growing awareness that some of these assumptions, e.g., assumptions 5-9 are unacceptable, and recent work has begun to provide more realistic representation of the detailed combustion process involved.

#### 8.3.4 Assumptions in the Surface Statistics Model

1. It is assumed that exposed oxidizer particles each exhibit a definable, connected burning surface area. No assumption of shape of surface is made. It is implied that the surface elements have areas related to particle size.

2. It is assumed that the exposed binder (fuel) surface area can be allocated in some manner into surface elements assignable one-on-one to the oxidizer surface elements (although no unique procedure is specified to do this).
3. It is assumed that the microscopic heterogeneity is macroscopically uniform, so that a regression rate of the surface (burning rate) can be assigned that is uniform on a macroscopic scale (i.e., when averaged over many particle diameters), and characteristic of the propellant.
4. Based on 3, it is assumed that the burning surface can be characterized by an average number,  $N$ , of oxidizer surface elements per unit burning surface area (the same number of fuel surface elements). In this assumption, the surface elements may be non-flat, but the number  $N$  is the average number of such elements per unit planar surface area, i.e., area projected on a plane perpendicular to the direction of the mean burning rate.
5. In certain instances, it is assumed that the pairing of oxidizer surface elements and fuel surface elements is uncorrelated with element sizes; i.e., the probability of a given size fuel surface element pairing with any particular oxidizer surface element depends only on the relative frequency of occurrence of that size in the oxidizer population.
6. The mass flow rate per unit real surface area (flux) of an oxidizer surface element is single valued over the surface of the element (at any moment).
7. The mass flux of oxidizer products may be different for different size oxidizer surface elements.
8. The mass flux of oxidizer products from a given size oxidizer surface element may depend on the size of the companion fuel surface element (Equation 16), or may not (Equation 17).
9. The mass flux of oxidizer products from a given size oxidizer surface element is not dependent on the circumstances leading to the element size (i.e., no distinction is made between particle size contribution

- to element size and time-during-burning contribution to element size). This implies that no consideration is given to the local microstructural details except as they are reflected in surface element area.
10. It is assumed that the dependence of burning rate on pressure, propellant temperature, and other variables not explicitly contained in the statistical model can be brought in as rate dependence of the oxidizer surface element.
  11. It is assumed that a surface element size distribution, , can be obtained for the oxidizer-fuel surface elements pairs, either by a more detailed theory, or by direct observation of burning surfaces, or by further simplifying assumptions.

Recent developments in modeling have sought to remedy (or evaluate) the limitations of assumptions, and these efforts were discussed in a JANNAF Workshop and reported in an excellent review by the chairman of the workshop (Reference 20). A very significant effort has been put into design of better physical and statistical models, with heavy reliance on rather extensive computer programs to extract burning rate predictions. The reader is referred to Reference 20 for the status of results. It is notable that "improvements" in the models (i.e., to conform to reality) are usually conceived on the basis of recognized deficiencies in representation of detailed physio-chemical processes operating at the microscopic level, but the adequacy of the improvements in the model are judged by the improved ability of the model to correlate measured average burning rates. This is not a particularly stringent test of the validity of the modified models, as they usually have greater flexibility in functional form and "free" parameters. As a result, a variety of models have emerged, but relatively little work has been done at the microscopic level to evaluate or guide the modeling.

### Notation

$dN$	average number of oxidizer surface elements (per unit planar surface area) having area in the interval $s_{ox}$ to $s_{ox} + ds_{ox}$ (see Eq. 6)
$d^2N$	average number of element pairs $s_{ox}, s_f$ (per unit planar surface area) having oxidizer element area between $s_{ox}$ and $s_{ox} + ds_{ox}$ and fuel element area between $s_f$ and $s_f + ds_f$ (see Eq. 5)
$F$	normalized frequency distribution of one variable
$F_{ox}$	normalized frequency distribution of oxidizer surface elements
$F_f$	normalized frequency distribution of $s_f$ (see Eq. 16)
$\mathcal{F}$	normalized frequency distribution of two variables, $s_{ox}$ and $s_f$ (see Eq. 2)
$f_{ox}$	a function of $s_{ox}$ , proportional to $F_{ox}$ (see Eq. 4)
$f_f$	a function of $s_f$ , proportional to $F_f$ (see Eq. 4)
$m$	mass flow rate per unit real area, mass flux
$\bar{m}$	mass flux averaged over a range of surface element sizes; per unit <u>planar</u> surface area
$m_{ox}$	mass flow rate per unit real area, of oxidizer products from oxidizer surface area (dependent on $s_{ox}, s_f$ , possibly other variables such as pressure)
$m_f$	mass flux from fuel surface
$\bar{m}_T$	mass flux from propellant surface mass flow per unit planar surface area
$N$	average number of surface element pairs per unit planar surface area
$\alpha$	ratio of mass of ingredients in the solid propellant
$\alpha_{ox}$	ratio of oxidizer mass to total mass in the solid propellant
$\alpha_f$	ratio of fuel mass to total mass in the solid propellant

## REFERENCES

1. Wimpress, R. N., "Internal Ballistics of Solid-Fuel Rockets," 1st Ed., McGraw-Hill, New York, 1950.
2. Journal of Physical and Colloid Chemistry, Vol. 54, No. 6, June 1950.
3. Office of the Director of Defense Research and Engineering, Ad Hoc Group on Solid-Propellant Instability of Combustion, Advisory Panel on Fuels and Lubricants, "Instability of Combustion of Solid Propellants," Final Report, June 1959. (Unclassified.)
4. The Committee on Standardization of the Combustion Instability Measurements in the T-Burner of the ICRPG Working Group on Solid Propellant Combustion, "T-Burner Manual," CPIA Publication No. 191, November 1969.
5. Price, E. W., W. C. Strahle, J. C. Handley, and T. S. Sheshadri, "Combustion of Nonaluminized Heterogeneous Ammonium Perchlorate Propellants," Thirteenth JANNAF Combustion Meeting, CPIA Publication No. 281, Vol. II, December 1976, p. 347.
6. Hightower, J. D., and E. W. Price, "Experimental Studies Relating to the Combustion Mechanism of Composite Propellants," Astronautica Acta, Vol. 14, No. 1, 1968, pp. 11-21.
7. Strahle, W. C., "Solid Propellant Sandwich Analysis," AIAA Journal, Vol. 13, No. 5, 1975.
8. Hightower, J. D., and E. W. Price, "Combustion of Ammonium Perchlorate," Eleventh Symposium (International) on Combustion, The Combustion Institute, Pittsburgh, 1967, pp. 463-72.
9. Boggs, T. L., Price, E. W., and D. E. Zurn, "The Deflagration of Pure and Isomorphously Doped Ammonium Perchlorate," Thirteenth Symposium (International) on Combustion, The Combustion Institute, 1971, pp. 995-1008.
10. Glazkova, A. P., "Effect of Catalytic Additives on the Burning of Ammonium Perchlorate and Certain of Its Mixtures," Fizika Gorenija i Vzryva, Vol. 2, No. 1, 1966, pp. 59-67.
11. Boggs, T. L., D. E. Zurn, W. C. Strahle, J. C. Handley, and T. T. Milkie, "Mechanisms of Combustion," Naval Weapons Center, NWC TP 5514, July 1973.
12. Boggs, T. L., and D. E. Zurn, "The Deflagration of Ammonium Perchlorate-Polymeric Binder Sandwich Models, Combustion Science and Technology, 1972, Vol. 4, pp. 279-292.

13. Boggs, T. L., R. L. Derr and M. W. Beckstead, "Surface Structure of Ammonium Perchlorate Composite Propellants, AIAA Journal, Vol. 8, No. 2, 1970.
14. Hermance, C. E., "A Model of Composite Propellant Combustion Including Surface Heterogeneity and Heat Generation, AIAA Journal, Vol. 4, No. 9, 1966.
15. Beckstead, M. W., R. L. Derr, and C. F. Price, "A Model of Solid Propellant Combustion Based on Multiple Flames, AIAA Journal, Vol. 8, No. 12, 1970.
16. Glick, R. L., "On Statistical Analysis of Composite Solid Propellant Combustion," AIAA Journal, Vol. 12, No. 3, 1974.
17. Glick, R. L., and J. A. Condon, "Statistical Analysis of Polydisperse, Heterogeneous Propellant Combustion: Steady-State," Thirteenth JANNAF Combustion Meeting, CPIA Publication No. 281, Vol. II, December 1976, pp. 313-345.
18. Strahle, W. C., "Some Statistical Considerations in the Burning of Composite Solid Propellants," AIAA Journal, Vol. 16, No. 8, 1978, p. 843.
19. Williams, F. A., "Combustion Theory," Addison-Wesley Publishing Co., 1965, p. 38.
20. Cohen, N. S., "Composite Propellant Burn Rate Modeling," AGARD-CP-259, July 1979, pp. 11-1 - 11-21. See also AIAA Preprint 79-0160, January 1979.
21. Cohen, N. S., R. L. Derr, and C. F. Price, "Extended Model of Solid Propellant Combustion Based on Multiple Flames," Ninth JANNAF Combustion Meeting, CPIA Publication No. 231, Vol. II, December 1972, pp. 25-42.
22. Cohen, N. S., and C. F. Price, "Combustion of Nitramine Propellants," Journal of Spacecraft and Rockets, Vol. 12, October 1975, pp. 608-612.
23. Cohen, N. S., C. F. Price, and L. D. Strand, "Analytical Model of the Combustion of Multicomponent Solid Propellants," AIAA Paper 77-927, AIAA/SAE Thirteenth Propulsion Conference, July 1977.
24. Cohen, N. S., "Combustion of Nitramine Propellants," Eleventh JANNAF Combustion Meeting, CPIA Publication No. 261, Vol. I, December 1974, pp. 267-283.
25. Beckstead, M. W., "Modeling Calculations for HMX Composite Propellants," Sixteenth JANNAF Combustion Meeting, CPIA Publication No. 308, Vol. III, December 1979, pp. 241-268.

26. Beckstead, M. W., "A Model for Solid Propellant Combustion," Fourteenth JANNAF Combustion Meeting, CPIA Publication 292, Vol. I, December 1977, pp. 281-306.
27. Miller, Irwin, and J. E. Freund, "Probability and Statistics for Engineers," Prentice-Hall, Inc., Englewood Cliffs, NJ, 1965, p. 28.

## APPENDIX A

# Some Statistical Considerations in the Burning of Composite Solid Propellants

Warren C. Strahle\*

*Georgia Institute of Technology, Atlanta, Ga.*

Propagation of a deflagration wave through a nearly ordered composite propellant is considered. The intent is to see some effects of the particle packing statistics on the propagation rate. A highly oversimplified model of the deflagration physics is considered, and only the statistics are emphasized. It is found that, for propellants of usual packing density, the least-time path of burning to a given point depends primarily on the packing statistics in a line parallel to the burn rate vector; there is little effect of particles only a few particle diameters to the side of this line. In a simplified model that may be solved analytically, there are clearly seen particle-size, pressure, and packing density effects on burn rate which are due to the statistics alone and not the deflagration physics.

## Introduction

THE heterogeneity of a composite solid propellant gives severe problems when it comes to modeling the combustion behavior. If one is positioned on a line parallel to the mean burn rate vector and follows the surface as it regresses, a time-dependent process is seen by the observer, involving alternate binder and oxidizer burnthrough (excluding metalized propellants) and other unsteady processes such as bubbling melts and melt flows. Alternatively, at any instant of time, if the observer looks over the surface, a spacewise heterogeneous process is involved. Precision in modeling, therefore, requires consideration of both time dependence and space heterogeneity.

Glick<sup>1</sup> and Glick and Condon<sup>2</sup> have tackled the space heterogeneity problem by application of a statistical method to the propellant structure. In their method, a combustion model is coupled with a statistical description of various fuel-oxidizer pair sizes to yield an average burn rate. The combustion model favored is the BDP<sup>3</sup> model, which is essentially a steady-state model and ignores the transients that would be found in an actual propellant burnthrough problem. There are also difficulties in the statistical description of the propellant surface. An early assumption in Ref. 1 is that for any particle of oxidizer the probability of a particular "size" of binder pocket being adjacent to the oxidizer is independent of the oxidizer size. This assumption is tantamount to assuming complete disorder to the propellant array. Furthermore, it is assumed that the existence of a particular oxidizer size at one point does not influence the allowable particle size at a neighboring point; this again is an assumption of complete disorder to the propellant structure.

These two difficulties, unsteadiness and a statistical description of the propellant surface, actually are coupled. The deflagration physics will, in fact, affect the surface configuration. It therefore would seem reasonable to actually track the deflagration front in time, using an appropriate deflagration model, to see how the surface details unfold with time. There are obvious difficulties with such an approach, however, because one still would need a combustion model and a statistical description of the propellant packing.

Concerning the propellant packing statistics, there is a real issue concerning the degree of disorder to the oxidizer particles imbedded in a binder matrix. For nonspherical particles with multimodal particle size distributions and wide cuts

Received Feb. 1, 1978; revision received May 1, 1978. Copyright © American Institute of Aeronautics and Astronautics, Inc., 1978. All rights reserved.

\*Index category: Combustion and Combustor Designs.

\*\*Regents' Professor, School of Aerospace Engineering. Associate Fellow AIAA.

about a nominal particle size, the observation of Ref. 2 that a propellant is a quite disordered structure is probably correct, even if the propellant is near the maximum possible solids loading. On the other hand, it is possible to conceive of a nearly ordered propellant structure if single-particle-size, spherical particles are packed at nearly the maximum solids loading. This becomes a completely ordered structure in the limit that the oxidizer loading is a maximum and the particle-size cut is of zero variance about the mean particle size (a delta-function size distribution). Such a packing is shown in Fig. 1. The lattice points of the array form an oblique parallelepiped. A perfectly ordered structure also would result with spherical particles in a multimodal distribution at the maximum solids loading if the particles had narrow cuts about each size in the distribution. The propellant of Fig. 1 is, in principle, possible to manufacture, although it would not be a practical propellant. If one now backs off slightly from the maximum packing density, a nearly ordered structure would result with particles near but randomly displaced from their ordered lattice points. This is the kind of propellant to be considered in this paper.

The motivation for considering the nearly ordered structure is twofold. First, it is a simple structure through which to track an unsteady deflagration wave. Second, the statistics of the packing are sufficiently simple to investigate the question of what is the lateral extent of influence of one point upon the other. Stated otherwise, given the deflagration arrival at a point, how was the time of arrival affected by particles above, but transversely separated from, the vertical axis running through the particle of interest?

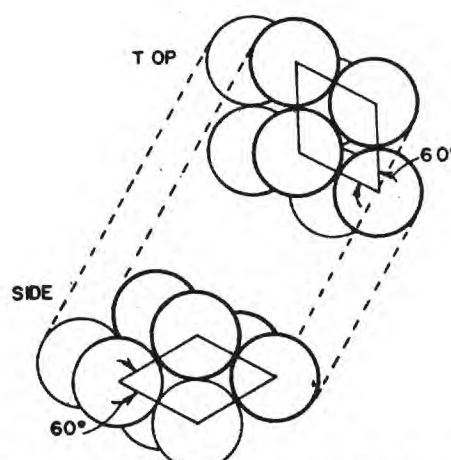


Fig. 1 Configuration of maximum packing density.

Although the propellant of Fig. 1 is clearly not a practical propellant, it is intended for use to see some statistical effects that are surely present in real propellants. The model to be employed for the deflagration process is also highly oversimplified and is selected not for its deflagration physics credibility but its demonstration of statistical effects.

This work should be considered complementary to the work of Refs. 1 and 2; this is intended to answer several questions that cannot be answered at the present time by their procedure. Although the analogy is not precise, the work here may be considered a Lagrangian approach to the problem where the deflagration front is tracked in time. The approach of Refs. 1 and 2 may be likened to an Eulerian view where a time-stationary average surface is under observation.

## Analysis

### Lattice Statistics

The lattice structure of Fig. 1 is the starting point and represents the maximum packing density for spherical particles. If  $V_0$  is any volume containing a large number of particles, the volume  $V$  of particulate material is given from elementary geometry as  $V/V_0 = 0.6981$ , which is the maximum packing density. Consider keeping the same lattice geometry, but shrinking each particle in size by an equal amount. Then each particle is in an ordered array with  $V/V_0 < 0.6981$ , and the particles are separated from each other by an equal amount at their points of closest approach. This perfectly ordered propellant actually would have a mild anisotropic burning behavior. In any principal lattice plane and along a direction parallel to a principal lattice axis, everything looks the same. But, by making planar cuts in an arbitrary plane and moving along an arbitrary line, the configuration changes to an observer, as compared with observations on the principal planes and directions. As an assumption of the analysis, observation will only be made on a principal plane and along a principal direction.

Now consider Fig. 2a, where a typical three-particle element is viewed, and consider small random displacements of the particles from their ordered lattice points. The particle radius is  $r$ , the distance between ordered lattice points is  $d$ , the displacement of the center of any particle from its ordered position is the vector  $\delta$  and the distance between two particles along the line of centers is  $x$ . The statistics to be employed consist of assigning a probability distribution to the  $\delta$ 's and then following the burn through the matrix.

To simplify things further, the "one-dimensional" approximation will be made that  $\delta$  has only a vertical component  $\delta$  and that all planes connecting particle centers which are parallel to the paper in Fig. 2 have the same set of  $\delta$ 's. Consequently, only events in the plane of the paper are of

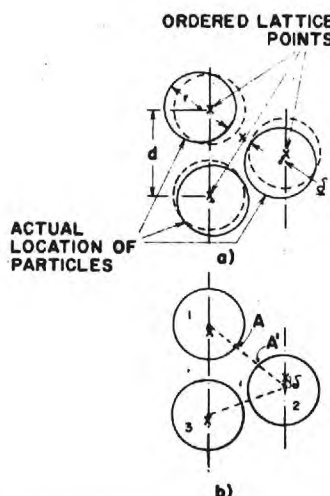


Fig. 2 Configuration of a nearly ordered array of spherical particles.

interest (there is no interaction between adjacent planes). One now has the situation of Fig. 1b. From elementary geometry, the distance  $A - A'$ , which is  $x$  for particles 1 and 2, is

$$x = \{ (3d^2/4) + [(d/2) - \delta_2 - \delta_1]^2 \}^{1/2} - 2r \quad (1)$$

An approximation to Eq. (1), which will be used and is valid if  $(d - 2r)/d \ll 1$ , is

$$x = d - 2r + [(\delta_1 - \delta_2)/2] \equiv \Delta + [(\delta_1 - \delta_2)/2] \quad (2)$$

Equation (2) is valid for well-packed propellants if the  $\delta$ 's are also restricted so that  $\delta_i/d \ll 1$ .

There is, in principle, no restriction on the magnitude of  $\delta$ . However, if one draws a sphere (circle) of influence about the ordered lattice center of  $r + \delta_m$ , where  $\delta_m$  is the maximum expected  $\delta$ , it is clear that these spheres will overlap if  $\delta_m > (d - 2r)/2$ . Consequently, if  $\delta_m > (d - 2r)/2$ , one particle will interfere with the allowable positions of an adjacent particle(s). This again would complicate the statistics, so it is required that  $\delta_m \leq (d - 2r)/2$ . This may be viewed physically as a "mixedness" assumption. That is, if the propellant is well mixed, no large voids of particles would be expected and each particle would be near its ordered lattice point.

For illustrative purposes, the probability distribution for the  $\delta$ 's will be the uniform distribution, whereby the differential probability  $dP$  of finding  $\delta$  between  $\delta$  and  $\delta + d\delta$  is

$$dP = d\delta / 2\delta_m \quad (3)$$

Obviously the particle must be somewhere between  $-\delta_m$  and  $+\delta_m$ , so that

$$P(-\delta_m \leq \delta \leq \delta_m) = \int_{-\delta_m}^{\delta_m} dP = 1 \quad (4)$$

Finally, two cases will be considered. The first, corresponding to Fig. 2b, will be periodic about two column

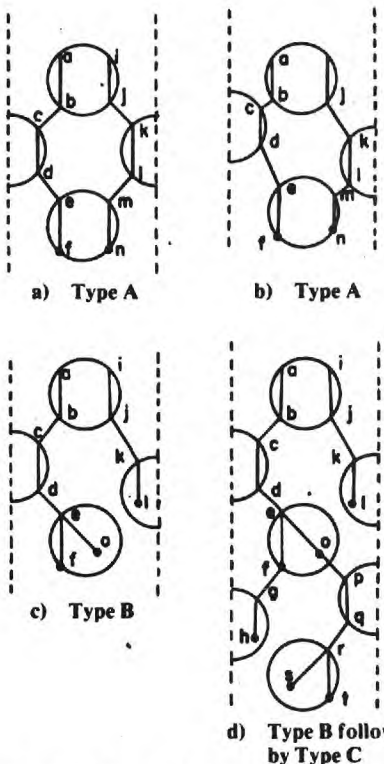


Fig. 3 Various situations in a three-column nearly ordered array of particles.

widths and will be symmetric about the left-hand centerline on Fig. 2b. This means that only the region between the two centerlines need be considered for burning calculations. The second case is shown in Fig. 3a. This case considers symmetry about the left-hand centerline and periodicity about three column widths. Thus, in case 1, only two columns can interact. In case 2, three columns can interact. In principle, one could continue this escalation to an infinite number of column widths which would be the limit of a truly heterogeneous, random propellant. It will be found that this is not necessary.

#### Mechanistic Model

It is assumed first that the oxidizer particles are monopropellants that have a planar deflagration rate of  $r_0$  at pressure  $p$  and cold temperature  $T$ . Second, it is assumed that the particles are ignited at the point of closest approach to a preceding adjacent particle. (The binder burns through at the thinnest point, and ignition of the oxidizer does not occur until the binder burnthrough has occurred.) Third, the consumption of the oxidizer is by a spherical outgoing deflagration wave at rate  $r_0$  which emanates from the ignition point or points. Fourth, after the deflagration wave has reached the point of closest approach to an adjacent oxidizer particle, there is a binder burnthrough time calculated by

$$t_b = Kx e^{\alpha x} \quad (5)$$

This law will be discussed later. Finally, it is assumed that oxidizer ignition is instantaneous after binder burnthrough.

Researchers and practitioners in this field will find this model unacceptable from the standpoint of reality. It is not presented, however, for its realism in deflagration physics. It has the necessary elements to test the statistics of the oxidizer matrix and to yield information of the effect of the statistics of the net propagation rate.

Equation (5) has the property that  $t_b \propto x$  for low  $\alpha$ , but, for general  $\alpha$ ,  $t_b$  is a nonlinear function of  $x$ . For large  $x$ , the binder burnthrough time increases at an increasingly fast pace

with the burnthrough distance. This behavior is expected to have its counterpart in reality. The self-deflagration wave in the oxidizer contains an advancing thermal wave in the solid phase which will precede the gas-phase reactions in arrival at the binder burnthrough point. This mechanism alone will provide energy for binder gasification. Following the gas-phase arrival, there is a convective flow of hot gases from the receding oxidizer which can provide more heat transfer to the binder. Moreover, a diffusion flame between the binder gases and oxidizer gases may form and will add further heat transfer for gasification. However, as the oxidizer surface recedes from the binder burnthrough point, there is a longer gas flow path, and a thicker heat-transfer "boundary layer" will exist at the burnthrough point. This will reduce the heat-transfer rate, making it more difficult to burn through the binder. Consequently, Eq. (5) embodies this expectation, although the exact analytical form probably is not correct.

The binder could, in principle, burn through to a particle adjacent and to the side or below a given oxidizer particle. However, the only heat source to a binder directly below the particle of interest is by an advancing thermal wave. It was shown in Ref. 4 that, although the energy in this thermal wave is often sufficient to pyrolyze the binder, the rate is often much too slow. This is so because the pyrolysis rate drops rapidly because the surface temperature drops rapidly as the initial pyrolysis carries away the initial portion of the binder. Binder burnthrough points to the side of a particle have additional convective, hot, and, perhaps, reacting gases to aid the burnthrough process. Consequently, it will be assumed in the analysis that burnthrough is only allowed sideways and not directly downward. This necessitates consideration of at least a two-particle column width for the analysis.

#### Case 1: Two-Column Model

It is first necessary to demonstrate that the ignition details will not alter the results to be presented. Consider Fig. 4, which is a two-column case at the maximum packing density. In this case, burnthrough at the bottom of particles can also occur. Equal time contours have been drawn on Fig. 4 assuming ignition in two different situations at time = -3 units. On the left is ignition on the tops of two particles, and on the right ignition is assumed on a plane cut through the propellant. By graphical construction, it is seen that the ignition transient disappears after only two particles in the columns have been consumed. After that, a surface profile that is periodic in time emerges. This indicates that the ignition will have no lasting effect or induce any wild oscillatory behavior in the sequence, and it is sufficient to consider an arbitrary set of particles in the interior of the propellant for analysis.

The two-column model is as shown in Fig. 3a but with the dotted line on the right moved one column width to the left, to exclude the third column. The propagation path for a typical element is ignition at point  $a$ , self-deflagration to  $b$ , binder burnthrough to point  $c$ , and then the process repeats. Considering a long column of length  $D$  containing  $N$  particles, the total time to burn through distance  $D$  is

$$t = t_{AP_1} + t_{b_{12}} + t_{AP_2} + t_{b_{23}} + t_{AP_3} + \dots + t_{b_{N-1,N}}$$

Since the individual binder burnthrough times depend upon the  $\delta_i$ ,

$$t = t(\delta_1, \delta_2, \dots, \delta_N)$$

and the  $\delta_i$  are random variables. The expected value of  $t$  is, using Eq. (3),

$$E(t) = \int_{-\delta_m}^{\delta_m} \dots \int_{-\delta_m}^{\delta_m} \frac{d\delta_1 d\delta_2 \dots d\delta_N}{(2\delta_m)^N} t(\delta_1, \delta_2, \dots, \delta_N) =$$

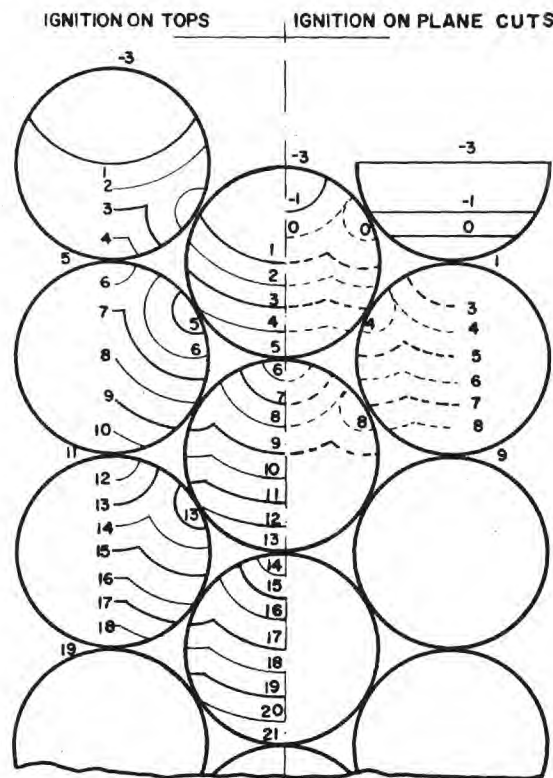


Fig. 4 Propagation through an ordered array of AP; labels are contours of constant times.

$$= N \int_{-\delta_m}^{\delta_m} \int_{-\delta_m}^{\delta_m} (t_{AP_1} + t_{b_{12}}) \frac{d\delta_1 d\delta_2}{4\delta_m^2} \quad (6)$$

For large  $N$ ,  $D=N d/2$ . Moreover, the burn rate is  $\dot{r}=D/E(t)$ , so that  $\dot{r}=d/2t$ , where, from Eq. (6),

$$\bar{t} = \int_{-\delta_m}^{\delta_m} \int_{-\delta_m}^{\delta_m} \frac{1}{4\delta_m^2} (t_{AP_1} + t_{b_{12}}) d\delta_1 d\delta_2$$

The distance between  $a$  and  $b$  on Fig. 3a is also slightly affected by the  $\delta$  values, but, under the previous approximation of close packing, it is only weakly dependent upon the  $\delta$  values. Approximately,  $t_{AP_1} = r/\dot{r}_0$ , and  $\bar{t}$  becomes

$$\bar{t} = \frac{r}{\dot{r}_0} + \frac{1}{4\delta_m^2} \int_{-\delta_m}^{\delta_m} \int_{-\delta_m}^{\delta_m} t_{b_{12}}(x) d\delta_1 d\delta_2 = \frac{r}{\dot{r}_0} + \bar{t}_b \quad (7)$$

The expression for  $t_{AP_1}$  is where the assumption of the close-packed hexagonal array enters. The final relation needed is  $t_{b_{12}}(x)$ . Using Eq. (5) for the burnthrough law, a rather important observation may be made. If  $t_{b_{12}} \propto x$ , then  $\bar{t}$  becomes the time taken for the AP to burn plus the time required for cookthrough to take place through the average binder thickness. That is, the statistics add nothing to the problem. Only when  $t_{b_{12}}$  is a nonlinear function of  $x$  does the statistical treatment give interesting results. The reason for this behavior, of course, is that if  $t_{b_{12}} \propto x$ , the burnthrough rate is a constant and the slowness of cookthrough of thick layers is canceled by cookthrough of an equal number of thin layers. When the function is nonlinear, however, the statistics will weight the slower burnthrough layers in a heavier manner. Placing Eq. (5) in Eq. (7) and carrying out the integration and forming the overall burn rate expression, there results

$$\frac{\dot{r}}{\dot{r}_0} = \frac{1}{(2r/d) + (\bar{t}_b/d) R \dot{r}_0} \quad (8a)$$

$$\bar{t}_b = K \Delta e^{\alpha \Delta} \quad (8b)$$

$$R = 2(\cosh \alpha \delta_m - 1) / (\alpha \delta_m)^2 \quad (8c)$$

In Eqs. (8),  $\bar{t}_b$  is the time to burnthrough of the average binder thickness.  $R \geq 1$ , depending upon the product of  $\alpha \delta_m$ ; this is the nonlinearity effect of the binder burnthrough law. If  $\bar{t}_b$  is short enough (if the binder on average burns at a faster linear rate than the oxidizer),  $\dot{r}/\dot{r}_0$  may be slightly greater than unity, according to this model, since  $2r/d \leq 1$ , depending solely on the oxidizer loading level.

Comparing with experiment, for example, with the polysulfide-AP work of Bastress,<sup>5</sup> it is known that the burn rate ratio of Eqs. (8) will increase with a decrease in AP particle size, decrease in pressure (the propellant has a lower exponent than does pure AP), and an increase in oxidizer loading. In Eqs. (8), the first term in the denominator of the burn rate expression depends solely on the oxidizer loading level, whereas the second term depends upon all parameters. The factor  $\bar{t}_b R/d$  will decrease with AP particle size at a rate depending on the magnitude of  $\alpha \Delta$  and  $\alpha \delta_m$ ; consequently, the particle-size effect is qualitatively predicted. If the binder burnthrough law is pressure-independent, as it is expected to nearly be, the pressure behavior is also qualitatively predicted properly, since  $\dot{r}_0$  increases with pressure in the second term of the denominator. Furthermore, the oxidizer loading effect is also properly predicted because  $\bar{t}_b R/d$  will decrease with an increase in oxidizer loading much faster than  $2r/d$  will decrease.

It should be mentioned that there is a serious limitation when compared with experiment. In the experiments cited,  $\dot{r}/\dot{r}_0$  was significantly greater than unity, except at suf-

ficiently large particle size. The current model cannot produce such results unless the pure AP rate is augmented, perhaps by consideration of an alternate heat source from oxidizer-binder reactions. On the other hand, there are several AP-binder systems that do exhibit burn rates less than that of pure AP over a significant pressure, particle-size, and oxidizer loading range.<sup>6</sup>

The major point is that some of the trends apparent in experiment are contained in the statistical treatment. The deflagration model is so naive that it was not expected to show the full picture with regard to various variables.

### Case 2: Three-Column Model

Returning to Fig. 3, consider the three-column model. The question now is whether or not there is significant interaction of the third column with the left two columns. In Fig. 3a, a perfectly ordered array is shown. Evidently the propagation path *abcdef* takes exactly the same time as path *ijklmn*. In this case, the same burn rate is obtained by considering either path, and the third column adds nothing to the problem. Consider next Fig. 3b, which is a somewhat disordered array. Here  $x_{bc} = x_{lm}$  and  $x_{de} = x_{jk}$ . Again path *abcdef* takes exactly the same time as path *ijklmn*, and there is no interaction between the third column and the left-hand two columns. This kind of event will be called one of "type A."

Figure 3c, on the other hand, shows a different type of event. Here, if the nonlinearity in the binder burnthrough law is strong enough,  $t_{jk} \gg t_{bc}$  or  $t_{de}$ . Consequently, path *abcdef* or *o* is faster than path *ijkl*. The bottom particle has been consumed solely by the left-hand path, and the right-hand path is stopped effectively at point *l*. This event will be called one of "type B," and the identical event with the left and right columns interchanged will be called one of "type C."

Neither type B or C events, if followed by the same type or one of type A, will alter a burn rate calculation as compared with a two-column calculation. All that is happening is that one column is being dragged along by the other. Since the burn rate is defined by the deepest penetration divided by the time, the left-hand column in the case of type B or A interaction is the sole determinant of the burn rate. Even a type B followed by type A followed by type C event does not increase the burn rate statistically. This is so because, immediately after the type A events, everything starts out "fresh" with the center column particle.

Consider now, however, Fig. 3d, where two opposite unusual events follow each other; in Fig. 3d, this is shown as type B followed by type C. Here, everything would start fresh at points *f* and *o*, but now  $t_{fg}$  is so long that the left-hand columns,  $t_{fg}$  would have had to be considered, and it would have decreased the expected burn rate. Here, however, path *opqrs* allows that long time interval to be bypassed. This is a clear interaction of all three columns which augments the burn rate. The question is, how frequent are such events? First of all, the event of Fig. 3d cannot happen unless the binder burnthrough law is nonlinear. Since the distance from *a* to *e* and *i* to *m* is always the same, the total time to burnthrough the binders would be the same if the law were linear; all events would be those of type A. Consequently, the nonlinearity is essential if the statistics are to give interesting effects. Second, the answer may be provided analytically, as in the two-column model, but the problem becomes so algebraically complex that it was done by computer.

A three-column array was set up on the computer with all  $\delta$ 's chosen by a standard FORTRAN random number generator. Again the uniform distribution of Eq. (3) should be reproduced if enough samples were taken. A baseline case where  $\bar{t}_b = 0.5 r/\dot{r}_0$  was chosen. An AP-binder propellant was assumed at 75% wt of AP with a binder specific gravity of 1.3. This yields  $d/2r = 1.015$ . If the mean binder burnthrough time were equal to the binder burnthrough time over the mean distance  $\bar{t}_b$ , this would yield  $\dot{r}/\dot{r}_0 = 0.677$ . The nonlinearity in

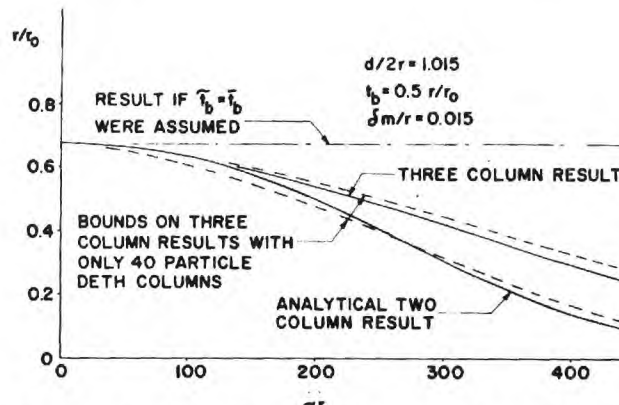


Fig. 5 Burn rate for the two- and three-column models as a function of the binder burnthrough nonlinearity parameter.

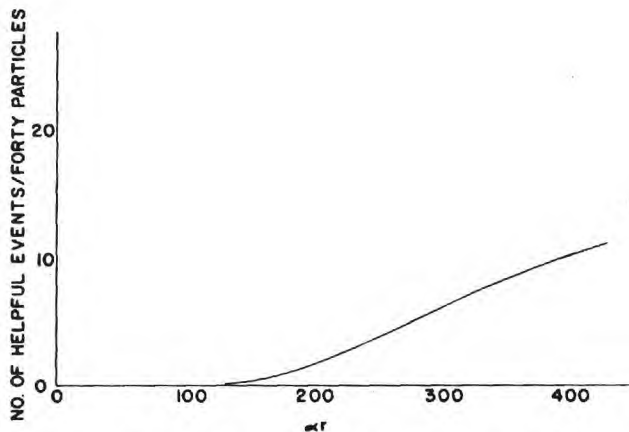


Fig. 6 Illustration of number of "helpful" events as a function of the binder burnthrough nonlinearity parameter.

the binder burnthrough law will, in general, reduce this value through Eqs. (8), but the three-column model will mitigate this drop.

The results are shown in Fig. 5. Shown is the analytical two-column result from Eqs. (8). This is a lower bound. An upper bound is the curve (constant) that would result if  $\bar{t}_b = \bar{t}_b$  were assumed. The three-column result lies in between and was obtained with a 120-particle column depth. With fewer particles, some severe scatter can occur, and approximate bounds on the results obtained with only a 40-particle depth column are shown. The scatter becomes worse at high  $\alpha$  (strong nonlinearity) because any deviation from perfection in the random number generator strongly weights the long binder burnthrough events. This is also the reason why the exact (120-particle) curve lies close to the upper bound of the 40-particle curve; deviation from perfect sampling heavily weights the long-time events.

The breakaway of the three-column result from the two-column result begins precisely with the onset of events shown in Fig. 3d. Figure 6 makes a count of the number of "helpful" events vs  $\alpha$ . Even at high  $\alpha$ , the number of helpful events is relatively small compared with the number of particles in the column, but the effects on rate are striking because an extremely long-time burnthrough has been avoided by the helpful event.

The three-column result makes a 100% augmentation in the two-column result for  $\alpha r \approx 400$ . The augmentation is shown to

about 25% at  $\alpha r \approx 275$ , where the burn rate is about half the zero- $\alpha$  value. This suggests that the two-column analytical result may be adequate for real propellants, since burn rate depressions from the monopropellant oxidizer rate often are not severe. That is, the effective  $\alpha$  is probably not very large. The major conclusion, therefore, is that a two-column model probably is not too bad; there is little influence of neighboring columns on the two-column situation. Another way of saying this is that the horizontal correlation length scale is only of the order of a couple of particle widths. From a practical standpoint, this says that, if the transient problem of combustion through a column that is about as wide as two of the largest oxidizer particles can be solved, an important breakthrough in burn rate modeling will have been achieved.

Considering more than three columns would elevate the result in Fig. 5 toward the  $\bar{t}_b = \bar{t}_b$  line, but not very much at moderate  $\alpha$ . There is a point of diminishing returns which is reached rapidly as the column width is expanded. The probability of a compound helpful event from extra columns becomes too small.

As  $\delta_m$  is reduced toward zero, all curves collapse to the  $\bar{t}_b = \bar{t}_b$  line. If  $\bar{t}_b$  is depressed by depressing  $K$  in Eq. (5), the curves all tend toward  $r/r_0 = 1.0$ . The other effects of oxidizer loading, particle size, and oxidizer size are the same with the three-column model as with the two-column case.

### Conclusions

1) Using a simplified deflagration model and a nearly ordered array of spherical oxidizer particles in a binder matrix, a simple model predicts known effects of oxidizer size, oxidizer loading, and pressure level through the statistics of the particle packing.

2) A nonlinearity in the binder burnthrough time vs distance law is required to obtain interesting results from the statistical treatment.

3) The transverse correlation length scale for burning through the matrix is relatively small. Hence, combustion modeling of a column of propellant only a couple of particle diameters wide would be a useful undertaking. This is probably the most important conclusion of the work.

### Acknowledgments

This work was supported by the Office of Naval Research under Contract N00014-67-A-0159-0016.

### References

- Glick, R. L., "On Statistical Analysis of Composite Propellant Combustion," *AIAA Journal*, Vol. 12, March 1974, pp. 384-385.
- Glick, R. L. and Condon, J. A., "Statistical Analysis of Polydisperse, Heterogeneous Propellant Combustion: Steady State," *13th JANNAF Combustion Meeting*, CPIA Publ. 281, 1976, pp. 313-345.
- Beckstead, M. W., Derr, R. L., and Price, C. F., "A Model of Composite Solid Propellant Combustion Based on Multiple Flames," *Vol. 8*, Dec. 1970, pp. 2200-2207.
- Price, E. W., Strahle, W. C., Handley, J. C., and Sheshadri, T. S., "Combustion of Nonaluminized Heterogeneous Ammonium Perchlorate Propellants," *13th JANNAF Combustion Meeting*, CPIA Publ. 281, 1976, pp. 347-365.
- Bastress, E. K., "Modifications of the Burning Rates of Ammonium Perchlorate Solid Propellants by Particle Size Control," Ph.D. Dissertation, Dept. of Aeronautical Engineering, Princeton Univ., 1961.
- Stein, J. A., Stang, P. L., and Summerfield, M., "The Burning Mechanism of Ammonium Perchlorate in Based Composite Solid Propellants," Princeton Univ., Aerospace and Mechanical Sciences Rept. 830, 1969.

## DISTRIBUTION LIST

	<u>No. Copies</u>		<u>No. Copies</u>		<u>No. Copies</u>		<u>No. Copies</u>
Assistant Secretary of the Navy (R, E, and S) Attn: Dr. R.E. Reichenbach Room 5E787 Pentagon Washington, DC 20350	1	AFATL Eglin AFB, FL 32542 Attn: Dr. Otto K. Heiney	1	Army Ballistic Research Labs Code DRDAR-BLP Aberdeen Proving Ground, MD 21005 Attn: Mr. L. A. Watermeier	1	Hercules Inc. Eglin AFATL/OLDL Eglin AFB, FL 32542 Attn: Dr. Ronald L. Simmons	1
Office of Naval Research Code 473 Arlington, VA 22217 Attn: Dr. R. Miller	10	AFRPL Code PACC Edwards AFB, CA 93523 Attn: Mr. W. C. Andrepon	1	Army Ballistic Research Labs ARRADCOM Code DRDAR-BLP Aberdeen Proving Ground, MD 21005 Attn: Dr. Ingo W. May	1	Hercules Inc. Magna Bacchus Works P.O. Box 98 Magna, UT 84044 Attn: Mr. E. H. DeButts	1
Office of Naval Research Code 2008 Arlington, VA 22217 Attn: Dr. J. Enig	1	AFRPL Code CA Edwards AFB, CA 93523 Attn: Dr. R. R. Weiss	1	Army Ballistic Research Labs ARRADCOM Code DRDAR-BLT Aberdeen Proving Ground, MD 21005 Attn: Dr. Philip Howe	1	Hercules Inc. Magna Bacchus Works P.O. Box 98 Magna, UT 84044 Attn: Dr. James H. Thacher	1
Office of Naval Research Code 260 Arlington, VA 22217 Attn: Mr. D. Siegel	1	Code AFRPL MKPA Edwards AFB, CA 93523 Attn: Dr. F. Roberto	1	Army Missle Command Code DRSMR-RK Redstone Arsenal, AL 35809 Attn: Dr. R. G. Rhoades Dr. W. W. Wharton	2	HQ US Army Material Development Readiness Command Code DRCDE-DW 5011 Eisenhower Avenue Room 8N42 Alexandria, VA 22333 Attn: Mr. S. R. Matos	1
Office of Naval Research Western Office 1030 East Green Street Pasadena, CA 91106 Attn: Dr. T. Hall	1	AFSC Andrews AFB, Code DLFP Washington, DC 20334 Attn: Mr. Richard Smith	1	Atlantic Research Corp. 5390 Cherokee Avenue Alexandria, VA 22314 Attn: Dr. C. B. Henderson	1	Johns Hopkins University APL Chemical Propulsion Information Agency Johns Hopkins Road Laurel, MD 20810 Attn: Mr Theodore M. Gilliland	1
Office of Naval Research Eastern Central Regional Office 495 Summer Street Boston, MA 02210 Attn: Dr. L. Peebles Dr. A. Wood	2	Air Force Office of Scientific Research Directorate of Chemical & Atmospheric Sciences Bolling Air Force Base Washington, DC 20332	1	Ballistic Missile Defense Advanced Technology Center P.O. Box 1500 Huntsville, AL 35807 Attn: Dr. David C. Sayles	1	Lawrence Livermore Laboratory University of California Livermore, CA 94550 Attn: Dr. M. Finger	1
Office of Naval Research San Francisco Area Office One Hallidie Plaza Suite 601 San Francisco, CA 94102 Attn: Dr. P. A. Miller	1	Air Force Office of Scientific Research Directorate of Aerospace Sciences Bolling Air Force Base Washington, DC 20332 Attn: Dr. L. H. Caveny	1	Ballistic Research Laboratory USA ARRADCOM DRDAR-BLP Aberdeen Proving Ground, MD 21005 Attn: Dr. A. W. Barrows	1	Lawrence Livermore Laboratory University of California Livermore, CA 94550 Attn: Dr. R. McGuire	1
Defense Technical Information Center DTIC-DDA-2 Cameron Station Alexandria, VA 22314	12	Anal-Syn Lab Inc. P.O. Box 547 Paoli, PA 19301 Attn: Dr. V. J. Keenan	1	Hercules Inc. Cumberland Aerospace Division Allegany Ballistics Lab P.O. Box 210 Cumberland, MD 21502 Attn: Dr. Rocco Musso	2	Lockheed Missiles and Space Co. P.O. Box 504 Sunnyvale, CA 94088 Attn: Dr. Jack Linsk Org. 63-10 Bldg. 154	1

## DISTRIBUTION LIST

<u>No. Copies</u>		<u>No. Copies</u>		<u>No. Copies</u>		<u>No. Copies</u>
Lockheed Missile & Space Co.	1	Naval Research Lab Code 6100 Washington, DC 20375	1	Naval Surface Weapons Center Code R101 Indian Head, MD 20640	1	Naval Weapons Center Code 388 China Lake, CA 93555
3251 Hanover Street Palo Alto, CA 94304 Attn: Dr. H. P. Marshall Dept. 52-35		Attn: Mr. G. L. MacKenzie		Attn: D. R. Derr		
Los Alamos Scientific Lab P.O. Box 1663 Los Alamos, NM 87545 Attn: Dr. R. Rogers, WX-2	1	Naval Sea Systems Command Washington, DC 20362 Attn: Mr. G. Edwards, Code 62R3 Mr. J. Murrin, Code 62R2 Mr. W. Blaine, Code 62R	1	Naval Surface Weapons Center Code R17 Indian Head, MD 20640 Attn: Dr. H. Haiss	1	Naval Weapons Center Code 388 China Lake, CA 93555 Attn: Dr. R. Reed Jr.
Los Alamos Scientific Lab P.O. Box 1663 Los Alamos, NM 87545 Attn: Dr. B. Craig, M Division	1	Naval Sea Systems Command Washington, DC 20362 Attn: Mr. R. Beauregard SEA 64E	1	Naval Surface Weapons Center Code R11 White Oak, Silver Spring, MD 20910 Attn: Dr. K. F. Mueller	1	Naval Weapons Center Code 385 China Lake, CA 93555 Attn: Dr. A. Nielsen
Naval Air Systems Command Code 330 Washington, DC 20360 Attn: Mr. R. Heitkotter Mr. R. Brown	1	Naval Surface Weapons Center Code R11 White Oak, Silver Spring, MD 20910 Attn: Dr. H. G. Adolph	1	Naval Surface Weapons Center Code R16 Indian Head, MD 20640 Attn: Dr. T. D. Austin	1	Naval Weapons Center Code 3858 China Lake, CA 93555 Attn: Mr. E. Martin
Naval Air Systems Command Code 310 Washington, DC 20360 Attn: Dr. H. Mueller Dr. H. Rosenwasser	1	Naval Surface Weapons Center Code R13 White Oak, Silver Spring, MD 20910 Attn: Dr. R. Bernecker	1	Naval Surface Weapons Center Code R122 White Oak, Silver Spring, MD 20910 Attn: Mr. L. Roslund	1	Naval Weapons Center China Lake, CA 93555 Attn: Mr. R. McCarten
Naval Explosive Ordnance Disposal Facility Indian Head, MD 20640 Attn: Lionel Dickinson Code D	1	Naval Surface Weapons Center Code R10 White Oak, Silver Spring, MD 20910 Attn: Dr. S. J. Jacobs	1	Naval Surface Weapons Center Code R121 White Oak, Silver Spring, MD 20910 Attn: Mr. M. Stosz	1	Naval Weapons Support Center Code 5042 Crane, Indiana 47522 Attn: Dr. B. Douda
Naval Ordnance Station Code 5034 Indian Head, MD 20640 Attn: Mr. S. Mitchell	1	Naval Surface Weapons Center Code R11 White Oak, Silver Spring, MD 20910 Attn: Dr. M. J. Kamlet	1	Naval Weapons Center Code 3853 China Lake, CA 93555 Attn: Dr. R. Atkins	1	Rohm and Haas Company 723-A Arcadia Circle Huntsville, Alabama 35801 Attn: Dr. H. Shuey
Naval Ordnance Station Code PM4 Indian Head, MD 20640 Attn: Mr. C. L. Adams	1	Naval Surface Weapons Center Code R04 White Oak, Silver Spring, MD 20910	1	Naval Weapons Center Code 3205 China Lake, CA 93555 Attn: Dr. L. Smith	1	Strategic Systems Project Office 1 Dept. of the Navy Room 901 Washington, DC 20376 Attn: Dr. J. F. Kincaid
Dean of Research Naval Postgraduate School Monterey, CA 93940 Attn: Dr. William Tolles	1	Attn: Dr. D. J. Pastine	1	Naval Weapons Center Code 3205 China Lake, CA 93555 Attn: Dr. C. Thelen	1	Strategic Systems Project Office 2 Dept. of the Navy Room 1048 Washington, DC 20376 Attn: Mr. E. L. Throckmorton Mr. R. Kinet
Naval Research Lab Code 6510 Washington, DC 20375 Attn: Dr. J. Schnur	1	Naval Surface Weapons Center Code R13 White Oak, Silver Spring, MD 20910 Attn: Dr. E. Zimet	1	Naval Weapons Center Code 385 China Lake, CA 93555 Attn: Dr. A. Amster	1	Thiokol Chemical Corp. Brigham City Wasatch Division Brigham City, UT 84302 Attn: Dr. G. Thompson

## DISTRIBUTION LIST

<u>No. Copies</u>	<u>No. Copies</u>	<u>No. Copies</u>	<u>No. Copies</u>
USA ARRADCOM DRDAR-LCE Dover, NJ 07801 Attn: Dr. R. F. Walker	1 Georgia Institute of Technology Office of Research Administration Atlanta, Georgia 30332 Attn: Professor Edward Price	1 University of California Dept. of Chemistry 405 Hilgard Avenue Los Angeles, CA 90024 Attn: Prof. M. F. Nicol	1 Director Army Ballistic Research Laboratory Aberdeen Proving Ground, MD 21005 Attn: Austin W. Barrows/DRDAR-BLP
USA ARRADCOM DRDAR-LCE Dover, NJ 07801 Attn: Dr. N. Slagg	1 Univ. of Utah Dept. of Mech. & Industrial Engineering MEB 3008 Salt Lake City, Utah 84112 Attn: Dr. Stephen Swanson	1 Office of Naval Research Structural Mechanics Program Arlington, VA 22217 Attn: Dr. N. L. Basdekas, Code 474	1 Commander Army Material Development & Readiness Command (DARCOM) 5001 Eisenhower Ave. Alexandria, VA 22333 Attn: Stephen R. Matos/DRCDE-DW
U.S. Army Research Office Chemistry Division P.O. Box 12211 Research Triangle Park, NC 27709	1 Space Sciences, Inc. 135 Maple Avenue Monrovia, CA 91016 Attn: Dr. M. Farber	1 University of California Berkeley, CA 94720 Attn: Prof. A. G. Evans	1 Commander Army Missile Research & Development Command (MIRADCOM) Redstone Arsenal, AL 35809 Attn: Dr. R. G. Rhoades/DRDMI-RK
Institute of Polymer Science University of Akron Akron, OH 44325 Attn: Professor Alan N. Gent	1 Washington State University Dept. of Physics Pullman, WA 99163 Attn: Professor G.D. Duvall	1 Texas A & M University Dept. of Civil Engineering College Station, TX 77843 Attn: Prof. Richard A. Schapery	1 Commanding Officer Army Research & Development Command (ARRADCOM) Dover, NJ 07802 Attn: C. Lenchitz/LCWSL
SRI International 333 Ravenswood Avenue Menlo Park, CA 94025 Attn: Dr. Y.M. Gupta	1 Univ. of Maryland Department of Mechanical Eng. College Park, MD 20742 Attn: Professor R.W. Armstrong	1 SRI International 333 Ravenswood Ave. Menlo Park, CA 94025 Attn: Mr. M. Hill	1 Commanding Officer Army Research & Development Command (ARRADCOM) Dover, NJ 07802 Attn: L. Stiefel/DRDAR-SCA-PE
Graduate Aeronautical Lab. California Institute of Technology Pasadena, CA 91125 Attn: Professor W.G. Knauss	1 The Catholic University of America Physics Department 520 Michigan Ave., N.E. Washington, D.C. 20017 Attn: Professor T. Litovitz	1 Los Alamos Scientific Laboratory Los Alamos, NM 87545 Attn: Dr. J. M. Walsh	1 Atlantic Research Corporation 5390 Cherokee Ave. Alexandria, VA 22314 Attn: Merrill K. King
Pennsylvania State University Dept. of Mechanical Engineering University Park, PA 16802 Attn: Professor Kenneth Kuo	1 Sandia Laboratories Division 2513 P.O. Box 5800 Albuquerque, N.M. 87185 Attn: Dr. S. Sheffield	1 Aeronautical Research Associates of Princeton, Inc. 50 Washington Road Princeton, NJ 08540 Attn: E. S. Fishburne	1 AVCO Corporation AVCO Everett Research Lab Div. 2385 Revere Beach Parkway Everett, MA 02149 Attn: D. Stickler
Office of Naval Research 800 N. Quincy St. Arlington, VA 22217 Attn: Dr. G. Neece Code 472	1 IBM Research Lab. K42.282 San Jose, CA 95193 Attn: Dr. Thor L. Smith	1 Aerospace Corporation P.O. Box 92957 Los Angeles, CA 90045 Attn: Ellis M. Landsbaum	1 Battelle Memorial Institute 505 King Ave. Columbus, OH 43201 Attn: Abbott A. Putnam
Thiokol Corp. Huntsville Huntsville Div. Huntsville, AL 35807 Attn: Mr. J.D. Byrd	1 California Institute of Tech. Dept. of Chemical Engineering Pasadena, CA 91125 Attn: Professor N.W. Tschoegl	1 Commander AFRPL/DYSC Edwards, CA 93523 Attn: Daweel George	1 Brigham Young University Provo, UT 84601 Attn: Merrill W. Beckstead
Washington State University Dept. of Physics Pullman, WA 99163 Attn: Prof. T. Dickinson	1 Northwestern University Dept. of Civil Engineering Evanston, IL 60201 Attn: Professor J.D. Achenbach		

## DISTRIBUTION LIST

No. Copies	No. Copies	No. Copies	No. Copies				
California Institute of Technology 204 Karman Lab 1201 E. California St. Pasadena, CA 91109 Attn: Fred E. C. Culick	1	NASA/Lewis Research Center 21000 Brookpark Road Cleveland, OH 44135 Attn: Richard J. Priem, MS-500-204	1	Commander Naval Weapons Center China Lake, CA 93555 Attn: James A. Loundagin/Code 4576	1	Thiokol Corporation Wasatch Division P.O. Box 524 Brigham City, UT 84302 Attn: John A. Peterson	1
California Institute of Technology Jet Propulsion Laboratory 4800 Oak Grove Drive Pasadena, CA 91103 Attn: Leon D. Strand	1	NASA/Lyndon B. Johnson Space Center Houston, TX 77058 Attn: Joseph G. Thibodaux, EP	1	Princeton University Forrestal Campus Library P. O. Box 710 Princeton, NJ 08540 Attn: Martin Summerfield	1	TRW, Inc. TRW Systems Group One Space Park Redondo Beach, CA 90278 Attn: A. C. Ellings	1
California State University Sacramento School of Engineering 6000 J Street Sacramento, CA 95819 Attn: Frederick H. Reardon	1	NASA/George C. Marshall Space Flight Center Huntsville, AL 35812 Attn: J. Q. Miller /EP 25	1	Propulsion Sciences, Inc. P. O. Box 814 Melville, NY 11746 Attn: Vito Agosta	1	United Technologies Research Center 400 Main Street East Hartford, CT 06108 Attn: R. H. W. Waesche/MS 20	1
Calspan Corporation P. O. Box 235 Buffalo, NY 14221 Attn: Edward B. Fisher	1	NASA/George C. Marshall Space Flight Center Huntsville, AL 35812 Attn: Robert J. Richmond/EP24	1	Purdue University School of Mechanical Engineering TSPC Chaffee Hall West Lafayette, IN 47906 Attn: John R. Osborn	1	United Technologies Corporation Chemical Systems Division 1050 E. Argus Ave. Sunnyvale, CA 94088 Attn: Robert S. Brown	1
Commanding Officer Frankford Arsenal Bridge & Tacony Streets Philadelphia, PA 19137 Attn: J. Lannon	1	NASA HQ 600 Independence Ave., SW, Rm. 625 Washington, DC 20546 Attn: Frank W. Stephenson, Jr./Code RP	1	Rockwell International Corp. Rocketdyne Division 6633 Canoga Ave. Canoga Park, CA 91304 Attn: Joseph E. Flanagan/BA08	1	Universal Propulsion Co. P. O. Box 546 Riverside, CA 92502 Attn: H. J. McSpadden	1
General Applied Science Labs Merrick & Stewart Avenues Westbury, Long Island, NY 11590 Attn: John Erdos	1	Commanding Officer Naval Ordnance Station Indian Head, MD 20640 Attn: Peter L. Stang	1	Rockwell International Corp. Rocketdyne Division P. O. Box 548 McGregor, TX 76657 Attn: William G. Haymes	1	University of California, San Diego AMES Dept. P. O. Box 109 LaJolla, CA 92037 Attn: Forman A. Williams	1
General Dynamics Corporation Pomona Division P. O. Box 2507 Pomona, CA 91766 Attn: Paul L. Boettcher	1	Superintendent Naval Postgraduate School Department of Aeronautics Monterey, CA 93940 Attn: David W. Netzer	1	Science Applications, Inc. 20335 Ventura Blvd. Woodland Hills, CA 91364 Attn: R. B. Edelman/Suite423	1	University of Delaware Department of Chemistry Newark, DE 19711 Attn: T. C. Brill	1
Institute for Defense Analyses 400 Army-Navy Drive Arlington, VA 22202 Attn: R. C. Oliver	1	Commander Naval Surface Weapons Center Silver Spring, MD 20910 Attn: G. B. Wilmot	1	Southwest Research Institute Institute Scientist P. O. Drawer 28510 San Antonio, TX 78228 Attn: William H. McLain	1	University of Illinois AAE Dept. Transportation Building, Room 105 Urbana, IL 61801 Attn: Herman Krier	1
Johns Hopkins Univ/APL Chemical Propulsion Information Agency Johns Hopkins Road Laurel, MD 20810 Attn: Thomas W. Christian	1	Commanding Officer Naval Underwater Systems Center Energy Conversion Dept. Newport, RI 02840 Attn: Robert S. Lazar/Code 5B33I	1	Thiokol Corporation Huntsville Division Huntsville, AL 35807 Attn: David A. Flanigan	1	University of Massachusetts Dept. of Mechanical Engineering Amherst, MA 01002 Attn: Karl Jakus	1
University of Utah Salt Lake City, UT 84112 Attn: G. A. Flandro	1	University of Southern California Mechanical Engineering Dept./OHE200 Los Angeles, CA 90007 Attn: M. Gerstein	1	Whittaker Corporation Bermite Div. 2216 W. Soledad Canyon Road Saugus, CA 90024 Attn: L. Bloom	1	University of Waterloo Dept. of Mechanical Engineering Waterloo, Ontario CANADA Attn: Clarke E. Hermance	1